Effects of Cellular and Tissue Pharmacokinetics on Control Released Growth Factors

by

David Wu

B.S. Chemical Engineering and B.S. Biochemistry
University of Illinois at Urbana-Champaign, 1995

SUBMITTED TO THE HARVARD-M.I.T. DIVISION OF HEALTH SCIENCES AND TECHNOLOGY
IN PARTIAL FULFILLMENT OF THE REQUIREMENTS FOR THE DEGREE OF

DOCTOR OF PHILOSOPHY IN
MEDICAL ENGINEERING AND MEDICAL PHYSICS
AT THE
MASSACHUSETTS INSTITUTE OF TECHNOLOGY

JUNE 2001

Signature of author: _____
Division of Health Sciences and Technology
May 4, 2001

Certified by: _____
Elazer R. Edelman
Thomas D. and Virginia W. Cabot Professor of
Health Sciences and Technology
Thesis Supervisor

Certified by: _____
Martha L. Gray
Edward Hood Taplin Professor of
Medical Engineering and Electrical Engineering
Director, Health Sciences and Technology

Effects of Cellular and Tissue Pharmacokinetics on Control Released Growth Factors

by

David Wu

Submitted to the Harvard-M.I.T. Division of Health Sciences and Technology on May 4, 2001 in Partial Fulfillment of the Requirements for the Degree of Doctor of Philosophy in Medical Engineering

ABSTRACT

Aim: To examine the effects of cellular and tissue pharmacokinetics on control released growth factors.

Motivation: The resurgence of interest in controlled drug delivery reflects the increasing appreciation of the importance of local pharmacokinetics in defining the efficacy and potency of bioactive compounds. Despite promising data in vitro, growth factor use in vivo has generally failed to live up to its full potential. Without a theoretical framework to consider local pharmacology, there remains no consensus approach for improving the clinical outcomes of control released growth factors. As a result, a series of experiments incorporating cellular pharmacokinetics, computational modeling, and tissue pharmacokinetics were conducted.

CellularPharmacokinetics: The effect of ligand-receptor trafficking was examined on the potency of sustained release versus bolus administration of two growth factors that differed by intracellular trafficking kinetics. Sustained delivery potency was demonstrated to be dependent on both ligand and receptor trafficking and could be predicted based on trafficking considerations.

Computational Models: Computational models were conceptualized to describe the relationship between controlled-delivery, transport, receptor ligand pharmacokinetics, and tissue response. Theoretical predictions were made about potential approaches for optimizing local delivery and about the spatial correlation of tissue concentrations with tissue response.

Tissue Pharmacokinetics: The roles of physiological transport forces and proteolytic constraints on control released growth factor were examined. Partitioning and convection were shown to be dominant forces in governing drug distribution. A novel method based on intramolecular fluorescence quenching was implemented to describe the proteolytic constraints of local fibroblast growth factor delivery in an ex vivo carotid explant model.

Conclusion: Both experimental and theoretical models of cellular and tissue interactions of growth factors have suggested concepts that may be relevant for local growth factor delivery.

Thesis Committee: Prof. Elazer R. Edelman, (Thesis Supervisor)
Prof. Robert S. Langer
Prof. Matthew A. Nugent
Prof. Peter C. So

Dedicated to

my parents,

Dr. and Mrs. Susan and Yeongchi Wu

ACKNOWLEDGEMENTS

I wish to thank first and foremost my thesis advisor, physician-scientist, teacher, mentor, and friend, Prof. Elazer R. Edelman. Without his guidance, generosity, and faith in me, this work would not have been completed. He provided for me not only the environment in which to thrive, but also the leadership and insight for much of my work. I learned to think, analyze, and communicate, because he gave himself wholly as an excellent mentor and teacher.

I would like to pay special tribute to my thesis committee members, Profs. Robert S. Langer, Matthew A. Nugent, and Peter T. So. I am thankful to have had each of their attention, interest, support, and guidance, as experts in controlled delivery, growth factor biochemistry, and fluorescence imaging respectively. I thank Prof. Langer for insightful discussions and for sharing with me all of the resources of his laboratory. I thank Prof. Nugent for critically and carefully examining my work and providing great inspiration and encouragement. I thank Prof. So equally for his wisdom, insight, encouragement, and generous sharing of his time and facilities. Each of the members has been wholeheartedly supportive of my endeavors, and I am thankful for his comments and guidance. My doctoral experience has been greatly enhanced because of their collective input and suggestions.

I owe a great debt of gratitude to many in the Edelman Laboratory. I thank Dr. David Ettenson for being a tremendously resourceful, generous, and supportive friend and colleague. I thank Chao-Wei Hwang for many enjoyable collaborative projects, some partially included in Chapter 4 on physiological transport forces. I thank Drs. Mark Lovich and James Squire as my predecessors for their guidance and insight into this whole process. I thank Drs. Mercedes Balcells, Larry Brown, Iveta Dinbergs, Haim Danenberg, Anthony English, Elle Nugent, Edward Koo, Matthew Walker III, and Chun Yu for their encouragement, wisdom, and friendship. I thank my colleagues, Aaron, Alisa, Andrew, Fardad, Jeff, Kha, Kumaran, Marta, Neda, Peter, Rosanne, Vishal, Wade, and Yoram, for making this experience enjoyable, fun, and complete. Lastly, I thank Chad Blystone, Anna Browne, Carol Gibbs-Henderson for literally making all my studies possible.

I acknowledge the guidance of Prof. Douglas A. Lauffenburger as my academic advisor and one who initially steered me towards Prof. Edelman's laboratory. I thank him also for generously sharing with me all resources of his lab and time. I thank Dr. Roger Mark for wisdom and guidance as an informal advisor. I thank Dr. Campbell Rogers for mentoring me as

a student for my HST.203 Clerkship. I thank Dr. David Schaffer for guidance in my early years at the University of Illinois and later at MIT. I thank Dr. Andrew Protter for research materials used in Chapter 4 on proteolytic tissue constraints. I thank Lippincott Williams & Wilkins for granting me permission to reproduce in part the copyrighted text and figures included in Chapter 4 on physiological transport forces. I thank the Whitaker Foundation for Graduate Fellowship support from 1996-2001.

All of my friends outside of lab deserve much thanks and gratitude for helping me reach this goal in sound mind. I am grateful for the enduring friendships of Gary Tsai, James Lin, George and Patricia Lin, Frank Kofron, Dr. Ellen Omi, Portia Eleveld, Sang-Hyuck Ahn, Joy Rebecca Meek, Kathy Lo, Shon Yim, Dr. Melissa Lee, Dr. Jeff Kuo, Dr. Bryant Yang, Dr. Philip Soo, Vince Lau, Dr. Kevin Chen-- each for sharing with me their unconditional friendship and support.

I thank my wife, Grace, whom without her help, encouragement, guidance, and love, I would have fallen well short of this goal. I am grateful for her hard work and patience in supporting me wholeheartedly throughout my studies. I thank my brother Jesse and his wife Rochelle for being in Boston just around the corner and for making life outside of lab fun and memorable. I thank my brother Mark for reminding me that life is indeed quite simple. I am forever grateful to my parents, Dr. Yeongchi and Susan Wu, who through their endless love and patience made it possible that I might have the chance and ability to succeed. Last, but not least, I thank God for patiently showing me that green pastures and quiet waters are not always apparent at first, Psalm 23.

1 BACKGROUND AND INTRODUCTION

1.1 Local Delivery

The resurgence of interest in controlled drug delivery reflects not only a fascination with the challenges of delivering therapeutics more precisely, more biocompatibly and more stably, but an increased appreciation of the importance of pharmacokinetics and pharmacodynamics in the activities of therapeutic compounds [1-5]. As a result, there has been intense interest in defining optimal approaches for administrating therapeutic agents in a site-specific manner through the use of controlled-release technologies— an approach known as local delivery. Through strategic placement of polymeric devices loaded with drug near pathological sites, local delivery seeks to achieve maximal drug targeting and at the same time minimal whole-body, systemic dosing. Local delivery therefore attempts to maximize biological efficacy with high local drug concentrations and to minimize systemic toxicity with low systemic concentrations. As a consequence, significant enhancements in both potency and efficiacy can potentially be achieved.

While local delivery has proven to be advantageous and successful in several applications, the lack of a framework in which to understand the mechanisms of drug delivery, drug transport, and drug-tissue interactions has prevented explanations for clinical situations in which this particular approach has failed. This issue is most profound for the local delivery of growth factors in general, and in the cardiovascular system in particular, because while cardiovascular diseases account for more morbidity and mortality than all of the remaining top 10 disease states combined worldwide, only limited pharmacological therapies have proven especially clinically robust. In therapeutic angiogenesis, the local delivery of angiogenic growth factors has been reasonably attempted as a viable therapeutic option. Experimentally however, only few clinical trials have demonstrated any convincing results. In many of these attempts, it is obvious that there is an inability to describe the relationship between the tissue distribution and biological effects of these therapeutic molecules [6]. As standard, compartmental pharmacological approaches do not suffice in describing the pharmacokinetics of sustained local drug delivery, little is known about the optimal methods to deliver these agents. Moreover, as even less is known about the transport mechanisms within vessel walls and myocardial tissue, it

remains unclear where such agents should be delivered, how long their load should be maintained, what drug distribution can be expected, and lastly what tissue response can be anticipated. In short the lack of a theoretical framework in which to consider transport mechanisms and drug tissue interactions has prevented rational approaches for resolving confounding technical issues.

Traditionally, pharmacokinetics has considered the entire organism as a limited number of homogeneous compartments between which drugs flow with definable rate constants, and from which drug is eventually cleared by way of the kidney, and/or liver [7-10]. Such models are sufficient to describe the time-varying concentration of drug in the compartments representing plasma, fat, solid, tissues, etc., so that experimental pharmacokinetic analysis might involve sampling a large piece of target tissue and assaying for tissue average drug content. However, this analysis is insufficient for local delivery. Unequivocally in local delivery, the target tissue must be treated as a continuum wherein drug concentration varies continuously rather than in discontinuous, discrete steps. As various therapeutic agents are locally delivered from controlled-release devices, diffusion, convection, and diverse tissue interactions including binding, metabolism, and sequestration govern their transport to the surrounding tissues [11]. Drugs interact with extracellular tissue proteases, enzymes, carrier proteins, and non-specific binding sites. In addition, they may interact with specific cellular entities such as receptors and membrane processes that involve fluid-phase phagocytosis or transcytosis. Receptor trafficking events including intracellular endosomal sorting and endocytic regulation, further complicate issues [12, 13]. At the cellular level, ligand depletion, receptor regulation and extracellular matrix interactions may be involved [12-14]. Together, these interactions distribute and disperse compounds, and can degrade, denature, partition and/or sequester them as well. As a consequence of these diverse interactions, drugs that are locally delivered result in concentration gradients in tissues due to physiological transport forces such as diffusion and convection. Moreover, as these gradients evolve with time and are governed by idiosyncratic physicochemical and transport properties, local tissue concentrations can therefore be either toxic or sub-therapeutic and the resultant tissue response can be less than optimal. Theoretical and experimental paradigms for these scenarios would potentially, immensely aid in optimizing the clinical usage of locally delivered growth factors. Without in-depth study of these and other

processes, and the mechanisms of drug transport and resulting deposition, the success of local delivery becomes phenomenological trial and error.

1.2 Spatial-Temporal Gradients: Intrinsic to Nature

The importance of local pharmacology is profound and exemplified when the fact that local drug concentrations in tissues are both spatially and temporally correlated with the subsequent pharmacodynamic effects is appreciated. This notion is intrinsic in nature. Spatially, local concentrations and gradients of various proteins are known to guide the discrete formation of specific structural and functional tissues in developing organisms [15-25]. For example, morphogens establish patterns in early embryos by specifying several cell fates along a gradient of concentration. Bone morphogenic protein 4, (BMP4), controls the fundamental choice between neural and epidermal fates in the vertebrate ectoderm, under the control of the mesoderm [15]. BMP4 can evoke distinct responses in Xenopus ectodermal cells at high or low concentrations and its extracellular concentration is translated directly into transcription factor activity via the signal transduction molecule Smad1. Thus, a graded distribution of BMP4 activity controls the specification of several cell types in the gastrula ectoderm by establishing an intracellular and then nuclear gradient of Smad1 activity. Similarly, the patterned formation of embryonic limbs is guided by spatial concentrations of molecules [26]. For example, here retinoids are implicated in pattern formation processes in both developing chick limbs and in the regenerating limbs of urodele amphibians. As measured by HPLC, the concentration of retinoic acid (RA) is about five times higher in posterior quarters of the limb regeneration blastema compared to anterior quarters. In addition, levels of RA are about two and a half times higher in blastemas from the radius-ulna level of the limb, compared to those from the humerus level [26]. As another relevant example, neurons appear to rely on diffusible factors to guide their outgrowing process during development. Recent experiments suggest that concentration gradients of these factors released from denervated peripheral neurons direct the outgrowth of sensory and motor neuron growth over length scales of several hundred microns [27]. Similarly, local concentrations of various biomolecules including chemokines and cytokines lead to the directed recruitment of various inflammatory cells [28-32]. By establishing steep concentration gradients, appropriate immune cell types are recruited to sites of injury, thus minimizing

activation elsewhere. Taken together, these examples reveal that local concentrations and gradients of biomolecules correlate almost identically with their subsequent biological effects.

While the spatial correlation of drug concentrations with biological responses is clear, it is also as apparent that local concentrations are temporally correlated with biological responses. Release of various biomolecules such as growth hormone, insulin, melatonin, gonadotrophin releasing hormone and oxytocin are naturally pulsatile [33-49]. Enhanced biological effects are achieved in all of these cases with pulsatile versus sustained presentation. The natural physiology of these molecule must therefore be distinguished temporally in some yet to be defined manner.

In local delivery, these spatio-temporal relationships between molecular concentration and biological effects are becoming clearer. Using a combination of experimental and computational methods, Lovich et al. recently demonstrated in vivo that the spatial distribution of heparin in the rat arterial wall when delivered perivascularly from polymeric matrices correlates with arterial responses to treatment [50]. When theoretical profiles of heparin concentrations were spatially integrated across the arterial wall, the response to heparin could be defined as a sigmoidal plot with an apparent potency nearly two orders of magnitude larger than that seen in tissue culture. This dramatic right shift of the in vivo dose response curve from the in vitro case suggests that tissue pharmacokinetics appear to effectively govern the therapeutic efficacy of locally delivered heparin. Thus, one can begin to see how actual tissue concentrations correlate with tissue dose responses. In an analogous study, Mahoney and Saltzman correlated the brain tissue concentration gradient of nerve growth factor, NGF, as delivered from a polymeric matrix, to the biological response gradient of NGF-induced enhancement in choline acetyltransferase, ChAT, immunoreactivity [51]. They found that because of significant degradation of NGF by brain tissue, concentrations of local growth factor, as assessed by enzyme-linked immunosorbent assay, ELISA, dropped two orders of magnitude within 1-2 millimeters of the implant surface. More significantly, they found that this drop in concentration correlated spatially with the drop in ChAT immunoreactivity. This suggests that the functional penetration of NGF is limited by pharmacokinetic degradation and metabolism, so that its distribution and range of effect is localized to the delivery site. Similar studies in vitro also suggest intimate relationships between local concentrations and biologic effect. Beaty and Saltzman correlated NGF concentrations to neurite differentiation by quantitatively measuring

NGF concentrations with ELISA and qualitatively measuring neurite sprouting in a model tissue composed of rat pheochromocytoma cells suspended in collagen gel [52]. Specifically, they found that the concentration profile of NGF after one day of release from a polymeric device correlated identically with the cellular response on Day 7. Flaumenhaft et al. described a similar coupling with a different growth factor and cell system [53]. They observed that the extent of diffusion of fibroblast growth factor, FGF-2, from a centrally placed source corresponded identically with the spatial localization of endothelial morphologic transformation. Endothelial cells closest to the source of FGF-2 morphologically transformed from their native, cobblestone state, whereas cells several centimeters away remained cobblestone. Upon the introduction of soluble heparin, which binds FGF-2 and prevents its interaction with immobile extracellular matrix, the transport of FGF-2 was significantly increased. In parallel, the extent of endothelial transformation was increased. These examples together suggest that spatial gradients imposed by local delivery devices will affect tissue responses in a manner that is consistent with their local concentrations.

Temporally, this causal relationship between drug concentration and biological response is also true. For example, the physiological delivery of growth hormone, insulin, melatonin, gonadotrophin releasing factor, and oxytocin in a pulsatile manner elicits enhanced biological effects. Not surprisingly, various studies have demonstrated that comparable biological responses can be achieved with pulsatile delivery at doses significantly lower than sustained administration [36, 37, 39, 41, 42, 45, 47, 54-58]. These studies suggest that not only are the spatio-temporal concentrations of natural, endogenous molecules correlated intimately with biologic effects, so too are the spatio-temporal concentrations of therapeutic agents introduced for local delivery.

1.3 Transport

To begin to understand how local concentrations are established, it is important to appreciate the mechanisms by which drugs transport and distribute in tissues. Theoretical predictions in local pharmacokinetics were first generally devoted to understanding monoclonal antibody distribution across tumors and lipoprotein distribution in the native and atherosclerotic arterial wall [59-66]. Simultaneously, studies of substrate diffusion with chemical reactions also arose from the study of immobilized enzyme and cell systems for use in the chemical processing

industry [67]. Saltzman and Radomsky, however, presented the earliest generalized formalism specific for drug delivery from polymeric devices and noted that spatially averaged concentrations approach maximal concentrations, a virtual steady-state condition, when degradation is less dominant than diffusion [68]. In contrast, when diffusion is overshadowed by degradation, significant concentration gradients exist. Such gradients mean that tissues closest to the source receive high, perhaps toxic, doses of drug, whereas tissues furthest from the source receive little or none. For peptides and proteins, Saltzman and Radomsky determined the ratio of degradation to diffusion to be approximately between ~1 to 100. Within this critical range, the influence of chemical reactions such as degradation/metabolism are comparable or greater than that of diffusion, and can lead to significant deviations in local concentration from uncomplicated, steady-state Fickian diffusion profiles.

Other detailed models that include specific interactions with binding sites, molecular size, intracellular receptor-ligand trafficking processes, also support the importance of local pharmacokinetics on effective drug distribution. Rippley and Stokes presented a model of transferrin diffusion through tissue, incorporating the potential for intracellular receptor-ligand trafficking events, such as endosomal sorting and receptor ligand recycling, as modulators of effective drug distribution [13]. Their simulations demonstrated the importance of cellular pharmacology as they predicted more drug to be sequestered near the drug source, resulting from drug-cell interactions, than the amount localized there by either diffusion alone or diffusion with binding. Variations in kinetic processes such as binding or internalization can thus conceivably translate into significant differences in drug distribution in tissues. Similarly, Chu and Lauffenburger presented an alternative generalized model for receptor-mediated trafficking to analyze the effect of specific cell interactions on growth factor transport [12]. In their model, they included the potential for both intracellular diffusion and extracellular proteolysis of growth factor, events that were excluded in previous work [13]. They found that while receptor-mediated trafficking can hinder mass transfer of some growth factors, in some cases such trafficking could surprisingly enhance it. Three variables, the ratio of intracellular to extracellular diffusivities, the fractional extent of intracellular receptor recycling to the cell surface, and extracellular proteolytic rates govern whether enhancement or retardation of growth factor transport occurs. Computational work from the Edelman laboratory has also demonstrated the importance of tissue pharmacokinetics. Lovich and Edelman showed that heparin is poorly

localized to arterial tissue and diffuses away within one hour of a hypothetical uniform loading as a result of local convective and diffusive forces and minimal endothelial resistances [69]. Furthermore, their model predicted that most of the residual heparin distributed in the arterial wall was internalized and sequestered, an insight that is experimentally unattainable. Through the use of robust computational models, it has been possible to elucidate key parameters and mechanisms that define important biological responses that should aid in defining dominating pharmacokinetic issues.

Experimentally, considerable evidence supports the importance of local pharmacokinetics in determining drug targeting and effect. For example, Juweid et al. demonstrated the existence of a "binding-site barrier," the scenario in which specific antigen-antibody binding establishes an effective barrier that prevents deep penetration of therapeutic antibodies into a tumor [70, 71]. In their work they observed an inverse relationship between tissue penetration and antibody affinity for antigen. Antibodies that bound more tightly to an antigen were less able to penetrate a tumor in comparison to antibodies that bound the same antigen less tightly. Shockley et al. similarly demonstrated such phenomena in melanoma xenografts [72]. In other notable work, Chu and Lauffenburger observed predictable differences in the flux of intact growth factor through cellular matrices dependent on ligand-receptor trafficking differences [73]. Fibroblasts, transfected with either wild-type receptors or mutant trafficking receptors, were embedded into agarose gels and the transport of both wild-type ligands and various trafficking mutants thereof were measured. To a reasonable extent, growth factor flux predictably correlated with various alterations in receptor trafficking processes. Transport experiments across simple, cellular monolayers have also suggested the potential for cellular trafficking to effect drug targeting [74, 75]. Cell monolayer-drug interactions can cause the drug to be metabolized and/or sequestered by both specific and non-specific mechanisms and hinder transport [76-80]. Taken together, these and many other studies have demoonstrated clearly the role of tissue and cellular level pharamcokinetics in defining efficacy.

1.4 Previous work and work in this thesis

Over the course of several years, work from the Edelman laboratory has formulated in part a framework for understanding local pharmacology to describe the delivery, transport, and tissue-interactions of various therapeutic agents within the arterial wall. For example, work by

Lovich et al. has suggested that the in vivo failure of heparin, a model vasoactive compound in vitro, in controlling clinical restenosis is likely from deficiencies in targeted delivery and localization—a pharmacokinetic versus a pharmacodynamic limitation [81-83]. In these studies, the researchers administered heparin either systemically or locally perivascularly from polymeric devices to treat a rat model of restenosis, and found far better control of the tissue and cellular effects with local rather than systemic heparin administration. In subsequent work, they found in a rabbit iliac injury model that this control intimately dependent on the site and mode of heparin administration [82]. Delivery of heparin via stent-based polymers was insufficient to control long-term restenosis. In contrast, perivascular delivery of heparin from polymeric matrices was sufficient to control long-term restenosis. Thus, despite the fact that both delivery devices were juxtaposed to the lesion site, only the perivascular matrix was effective in controlling restenosis. Subsequent ex vivo transport experiments further demonstrated that rapid washout of heparin from the arterial wall minimized its potential to control the tissue hyperplasia [84-86]. These studies, taken as a whole, suggest that tissue pharmacokinetics can explain reasonably well the poor efficacy and potency of heparin in human clinical trials.

In comparable studies, others in this laboratory have also demonstrated the importance of cellular pharmacokinetics in defining the potency and efficacy of anti-sense oligonucleotides [87-89]. In these experiments, Edelman et al. compared two approaches for the delivery of antisense oligonucleotides to genes central to cellular proliferation in the arterial wall to control restenosis. Antisense c-myb and c-myc oligonucleotides were delivered rapidly (τ~12 hrs) from Pluronic gels or in a sustained fashion (τ~7 days) from EVAc matrices. These two proto-oncogenes are essential cell cycle promoters, and yet while either modes of release of antisense c-myb oligonucleotide was sufficient to control tissue hyperplasia, only the sustained-release of antisense c-myc oligonucleotide demonstrated efficacy [88]. Short time-course delivery of c-myc had an early effect in c-myc suppression, but was subsequently ineffective one week later. Most noticeably though, cell culture experiments demonstrated that the temporal expression of these early-response genes dictated the time course of antisense oligonucleotide delivery [90]. Thus, the efficacy of the antisense delivery was found to be dependent on the time course of gene expression as well as the kinetics of delivery. Together, these data argued that a detailed appreciation for cellular pharmacokinetics is especially meaningful and relevant.

In these two studies, appreciation of tissue level and cellular level pharmacokinetics and pharmacodynamics has allowed one to derive insight into the optimal means of delivering such agents. This approach effectively aided in elucidating the close relationship between cellular and tissue pharmacology and local delivery efficacy. A generalized theoretical and experimental framework for local pharmacokinetics would greatly aid in improving the clinical delivery of therapeutic agents.

1.5 Clinical use of growth factors and limitations

Perhaps the most intriguing observation about the use of growth factors in the treatment of diseases from wound healing to angiogenesis is the sheer number of failures of these molecules in clinical trials. Despite usually outstanding in vitro data, most of these molecules perform inconsistently in the clinical situation. As it stands, only one growth factor, platelet derived growth factor, has become a successful clinical product (Regranex Gel® by Johnson & Johnson). In contrast, a handful of cytokines, which are growth factor like compounds, has become successful products in clinical use, for examples, GCSF (NUEOPOGEN®), erythropoeitin (EPOGEN®), and type 1 interferon (INFERGEN®). The reason for the dichotomy of clinical responses perhaps lies in the fact that most, if not all, of these cytokines target cell populations that circulate in the blood or that reside in highly vascularized tissues such as bone marrow, whereas growth factors target cell populations that reside in tissues. As such, cytokines are not limited by tissue pharmacokinetic concerns such as transport, binding, and metabolism that concern growth factors. As the optimal delivery of therapeutic growth factors is poorly understood, it is perhaps not surprising that these pluoripotent molecules have not lived up to their therapeutic potential.

1.6 Summary of Analysis

Since the success of any potential therapeutic agent is equally dependent on its intrinsic biochemical mechanism and targeted delivery, this thesis proposes as a central hypothesis that cellular and tissue level pharmacokinetics intimately govern the therapeutic potential of control-released growth factors. This thesis has therefore attempted to define experimental and computational approaches for examining this hypothesis, and used them to bring insight into optimizing the delivery of growth factors. Through the combination of cell culture studies, mathematical modeling, protein chemistry, and fluorescent imaging, an attempt was made to

identify and define novel concepts relevant for the local delivery of growth factors. With the coming of the proteomic revolution and the anticipated interest in the delivery of novel therapeutic proteins, insights from this work should be relevant and timely.

The following chapters in this thesis describe the experimental and computational studies that were conducted to examine the relationship between cellular and tissue pharmacologies and biological response of growth factors:

Chapter 2. Cellular Pharmacology - The roles of ligand depletion and cellular trafficking were examined in governing the efficacy of sustained released growth factors.

Chapter 3. Computational Models - Mathematical models were conceptualized based on cellular trafficking kinetics to enable a priori predictions of optimal delivery approaches and an understanding of the correlation between drug penetration and tissue response.

Chapter 4. Tissue Pharmacology - The roles of physiological transport forces, including convection, diffusion, and partitioning, and proteolytic constraints on growth factor delivery were examined.

Chapter 5. Next steps

Chapter 6. Concluding Remarks

Chapter 7. Appendices

Chapter 8. Nomenclature

Chapter 9. References

2 CELLULAR PHARMACOLOGY

2.1 Background

Growth factors are polypeptide molecules that influence cellular biology through the stimulation and inhibition of proliferation, migration, differentiation, apoptosis, and metabolism [91, 92]. With maximal activity at pico- to nanomolar concentrations, they are potent therapeutic agents that have diverse applications in wound healing, tissue engineering, angiogenesis, vascular repair, bone and cartilage regeneration, cancer therapy, and organogenesis [91]. However, their ability to function effectively in therapeutic applications has been limited primarily because of their labile states in vivo. To address this limitation, the introduction of large amounts of growth factor has been attempted, though with only minimal success. While such concentrations might very well mitigate rapid clearance by the liver and/or the kidney, they also often lead to undesirable side effects and complications [93]. Moreover, supra-physiological concentration loads likely do not match the natural receptiveness of cells and tissues, and therefore result in natural mechanisms that attenuate cellular signaling, such as receptor down-regulation and ligand depletion [94-100]. To attend to these unresolved issues, one promising approach has been the use of novel controlled release technologies to deliver growth factors [101-105]. By protecting growth factors from whole-body clearance and tissue specific and non-specific degradation, controlled delivery can serve as a rational and beneficial approach.

Controlled-released technologies are a burgeoning field of biotechnology and research and are increasingly being capitalized upon for the delivery of therapeutic growth factors. More than ever, growth factors are delivered in a sustained-fashion to enhance their bioavailability, improve targeting, maximize dosing, and minimize systemic toxicity and costs. Indeed, a multitude of approaches have been undertaken to formulate and deliver these therapeutic agents in a novel fashion, including the use of liposomal encapsulation [106, 107], cellular therapies [108-110], biodegradable scaffolds [101], polymeric substrates, and physical immobilization and tethering [111]. Yet while there has been a concerted effort to develop new controlled-release technologies, there has been little inquiry into what constitutes optimal, physiological delivery. For instance, the notion that all growth factors will benefit from their sustained presentation is an assumption that is still relatively widely accepted, but nevertheless is without much evidence.

Previous work from the Edelman laboratory demonstrated that not all growth factors benefit from controlled delivery [112]. Whereas fibroblast growth factor (FGF-2), was found to be more potent in stimulating vascular cell proliferation when controlled-released as compared to being bolus-administered, transforming growth factor-β (TGFβ), a comparable ligand in many respects, was found to be more potent in inhibiting vascular cell proliferation when bolus administered as compared to being controlled-released [112]. Conflicting work have also suggested that the efficacy of another growth factor, vascular endothelial growth factor (VEGF) is more potent when sustained-released in one experimental situation, but not in another [113, Yu and Edelman, personal communication]. Early experiments that examined the effect of sustained delivery of insulin demonstrated that specific temporal kinetics could also govern efficacy. In many of these studies, pulsatile delivery of insulin was found to be far more potent than its sustained presentation [33, 36, 37, 54]. Similarly, growth hormone has been demonstrated to exert optimal physiological control only when presented in a pulsatile versus sustained manner [114]. These and other studies argue that the determinants of optimal delivery of therapeutic agents, growth factors in particular, remain to be understood.

As there is significant interest in the controlled delivery of growth factors for treating diseases ranging from ischemic heart disease to wound healing, and for applications in biotechnology ranging from mammalian cell culture to tissue engineering, the effects of cellular pharmacokinetics on controlled delivery efficacy was examined. Receptor-ligand trafficking was hypothesized to play an important role in determining the cellular response, since the time scale of interaction between growth factors and their receptors is typically on the order of hours to days to elicit maximal mitogenic effects [115-117]. During such time, cellular events such as receptor down-regulation, ligand depletion, and extracellular matrix sequestration can modulate the cellular response [14]. In this chapter, the mitogenic responses from the controlled release of two growth factors, epidermal growth factor (EGF) and transforming factor-α (TGFα), on an established fibroblast cell line (Swiss NR6 3T3) transfected with either the wild-type, (WT EGF-R), or internalization deficient epidermal growth factor receptor (c'973 EGF-R) were examined. These two growth factors both bind to and interact with the same cell surface receptor with similar, extracellular affinities. However, differences in their intracellular receptor binding affinity result in distinct receptor-ligand trafficking kinetics. As such, the role of cellular pharmacology on the efficacy of controlled released growth factors was specifically examined.

2.2 Materials and Methods

2.2.1 Cell culture and growth assays

Swiss 3T3-derived NR6 cells transfected with WT EGF-R or NR6 c'973 EGF-R were received as a gift from Prof. D.A. Lauffenburger and were routinely cultured in 7.5% FBS/MEMα, 1% pencillin-streptomycin, 2 mM L-glutamine, 1 mM sodium pyruvate, 0.1 mM non-essential amino acids, with cells being positively selected for receptor expression with geneticin (G418) at 350 μg/ml. These cells originally lack endogenous EGF receptors and EGF or TGFα ligands, but when transfected, express similar levels of WT-EGFR and c'973 receptors (R_{totl} ~ 100,000 #/cell) with similar affinities for EGF (K_d ~ 0.4 nM) [100]. For growth assays, cells were plated at 20,000 cells/well in Corning 6-well tissue culture plates in 7.5% FBS/MEMα and after a 24 hour serum starvation period in 1% dialyzed FBS, were presented with either a bolus administration of growth factors or polymeric control-release beads containing either EGF or TGFα placed on tissue culture inserts. Growth factors were obtained from R&D Systems, (Minneapolis, MN). Cells were incubated for various times at 37°C and 6% CO_2, and were then trypsinized and counted using a Coulter counter (Coulter Electronics Limited, Miami, FL). All cell culture reagents were obtained from GIBCO BRL (Grand Island, NY).

2.2.2 Radiolabeling of EGF and TGFα

Growth factors were radiolabeled using IODO-BEADs (Pierce, Rockford, IL) and ^{125}I (NEN Life Science Products Inc., Boston, MA) following the manufacturer's protocol and purified using G-10 gel filtration chromatography (Amersham Pharmacia Biotech, Piscataway, NJ). Specific activities of 150-200,000 cpm/ng (600 Ci/mmol) were routinely obtained as quantified using a Crystal Plus Multidetector RIA γ–counter (Packard Instruments, Downers Grove, IL).

2.2.3 Fabrication of EVAc controlled-release devices

Poly-ethylene vinyl acetate (EVAc) control release devices were prepared as published [112, 118]. Briefly, Elvax 40 (DuPont) was dissolved in dichloromethane at 10% (w/v). Bovine serum albumin (BSA) was dissolved in phosphate buffered saline as a carrier and incubated with either ^{125}I-radiolabeled or unlabeled EGF or TGFα. The mixture was lyophilized, manually

pulverized, and subsequently blended with the poly-EVAc/CH_2Cl_2 solution. Using a Pasteur pipette, the blend was dropped into a beaker of cold ethanol placed in a dry-ice ethanol bath, resulting in hard, spherical millimeter sized pellets to form immediately upon contact. After several minutes, the ethanol solution was repeatedly changed to elute the solvent, and the beads were allowed to cure overnight at –20°C in ethanol. The next day, the beads were air-dried, lyophilized, and then stored at –20°C until use.

2.2.4 Characterization of release kinetics

Three poly-EVAc controlled release beads were randomly chosen and placed into micro-centrifuge tubes. To each tube, sterile PBS was added and the beads were allowed to release radiolabeled and unlabeled growth factor at 37°C at infinite sink conditions. At various times, the supernatant was collected and the released growth factor was counted using a γ–counter after which each tube was replenished with fresh PBS. Retention of biological activity of the growth factors was confirmed in control experiments by determining the proliferative response of NR6 WT EGF-R fibroblasts to growth factor that was exposed or unexposed to dichloromethane fumes for 2 hrs.

2.2.5 Determination of receptor and ligand trafficking

Normalized receptor numbers as function of dosing and time were determined as previously published with modifications [119]. Briefly, media from cells at various time points was removed for ELISA determination, and each well was rinsed once with 2 ml/well ice cold PBS, and then incubated for 5 minutes with ice-cold acid strip (AS) (50 mM glycine-HCl, 100 mM NaCl, 1 mg/ml polyvinylpyrrolidone, pH 3.0) to remove bound, unlabeled growth factor. Cells were then washed twice with 2 ml/well ice cold PBS to remove AS, and then incubated at 4°C for more than 2.5 hrs with radiolabeled growth factor in binding buffer (1 mg/ml BSA/DMEM/Hank's, pH = 7.4) on a shaker plate to reach equilibrium binding. The concentration of radiolabeled growth factor used was greater than a minimal value determined to ensure less than 5% variation in binding due to changes in ligand concentrations. After 2.5 hrs of binding, free, unbound radiolabeled ligand was sampled, and then aspirated from each well. Cells were then rinsed 3 times with 3 ml ice-cold WHIPS (20 mM HEPES, 130 mM NaCl, 5 mM KCl, 0.5 mM $MgCl_2$, 1 mM $CaCl_2$, 1 mg/ml polyvinylpyrrolidone, pH 7.4) to further remove

unbound growth factor. Total binding was then determined by acid stripping using two 1 milliliter rinses of AS. Non-specific binding was determined by measuring the binding of radiolabeled growth factor in parallel plates of NR6 fibroblasts that lacked EGF receptors as a function of cell density. Specific binding was determined by subtracting non-specific from total binding, and surface receptor number was determined using measurements of $R_{totl}(t)$ and L(t) as a function of time, and the equation $R_{totl}(t) = C_{eq}(t) * (L(t) + K_d) / L(t)$, where $R_{totl}(t)$ is the total cell surface number, L(t) is the concentration of radiolabeled ligand, $C_{eq}(t)$ is the number of bound surface complexes, and K_d is the dissociation constant for EGF to EGF-R binding.

The concentration of EGF in the media was determined by using an ELISA kit following manufacturer's suggested protocol (R&D Systems, Minneapolis, MN). Normalized surface receptor complex numbers were determined using experimental measurements of both L(t) and $R_{totl}(t)$, and the equation, $C_{eq}(t) / R_{totl}(t=0) = R_{totl}(t) * L(t) / \{R_{totl}(t=0) * (L(t) + K_d)\}$. Published data on the binding affinity, K_d, of EGF for the EGF-receptor were taken from the literature, [119, 120].

2.2.6 Statistics

All data are reported as the mean ± standard deviation of at least three independent determinations. Student's t-tests were performed at a threshold level of $p < 0.05$ to determine statistical significance.

2.3 Results

2.3.1 Controlled-release

Controlled-release devices were fabricated by incorporating both unlabeled and ^{125}I radiolabeled EGF and TGFα into poly-ethylene vinyl acetate copolymer matrices. The kinetics of sample devices was measured in vitro over the course of several days by following the release of growth factors into PBS at 37°C under infinite sink conditions. After an initial burst of growth factor release during the first twelve hours, there was a steady, linear release of growth factor that was similar for EGF and TGFα (p = N.S., Figure 2-1). As previous reports have suggested loss of growth factor activity from dichloromethane inactivation, experiments were conducted to preclude this potential artifact. Parallel batches of growth factors were lyophilized with BSA and either exposed or not exposed to dichloromethane fumes at room temperature for

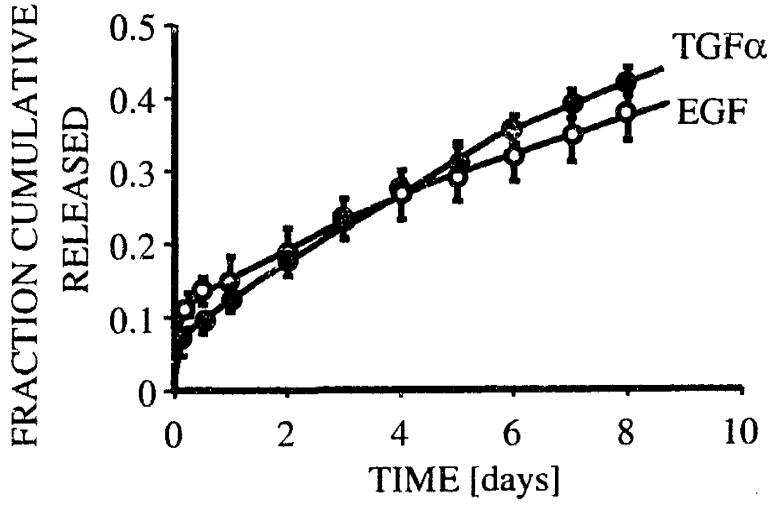

Figure 2-1: Sustained release of EGF (●) and TGFα (○) from poly-ethylene vinyl acetate controlled release devices

almost the entire two hour duration of the fabrication procedure. The mitogenic potential of these dichloromethane treated or untreated growth factors was examined by measuring cell number via Coulter counting. No loss of activity was seen for either EGF or TGFα (data not shown, p = N.S. for both). Thus, in contrast to some growth factors that lose biological activity upon exposure to dichloromethane [121], both EGF and TGFα remained completely active.

2.3.2 Cellular response

To examine the impact of cellular pharmacokinetics on controlled delivery, the proliferative responses of fibroblasts transfected with wild-type EGF-R to the sustained presentation or bolus administration of EGF or TGFα were compared. These two growth factors were chosen because previous work had demonstrated: (i) that these growth factors have very similar binding affinities for EGF-R at extracellular pH, [122, 123] (ii) that these growth factor have different binding affinities for EGF-R at pH representative of early to late sorting endosomes, [122, 123] and (iii) that these differences in intracellular binding affinity result in distinct ligand and receptor trafficking [122-125]. The use of these comparable growth factors therefore permitted the studying of the direct effects of intracellular pharmacokinetics on controlled delivery. Serum starved cells transfected with WT-EGF-R were presented with either a bolus or a sustained delivery of growth factor using controlled-release beads that were allowed to pre-release for more than one day into PBS to remove the burst phase. On day 4, cell numbers were determined via Coulter counting. In wild-type EGF-R cells, both growth factors benefited from being controlled release, as there was a left shift seen in both dose-response curves from bolus administration (Figure 2-2, Figure 2-3). However, TGFα benefited more from sustained presentation than EGF with a left shift in dose response of approximately 8 fold versus only 3-4 fold for EGF. As TGFα and EGF have similar binding affinities at the cell surface but traffic differently, these results are consistent with the hypothesis that cellular trafficking can impact controlled delivery. Indeed, this greater benefit seen for TGFα versus EGF was anticipated based on previous reports demonstrating the greater depletion of TGFα versus EGF in these cells [119, 120].

To further investigate the role of intracellular trafficking on controlled-delivery, the proliferative responses of fibroblasts transfected with internalization mutant EGF-R were examined. Cells transfected with these mutant c'973 truncated receptors have been demonstrated

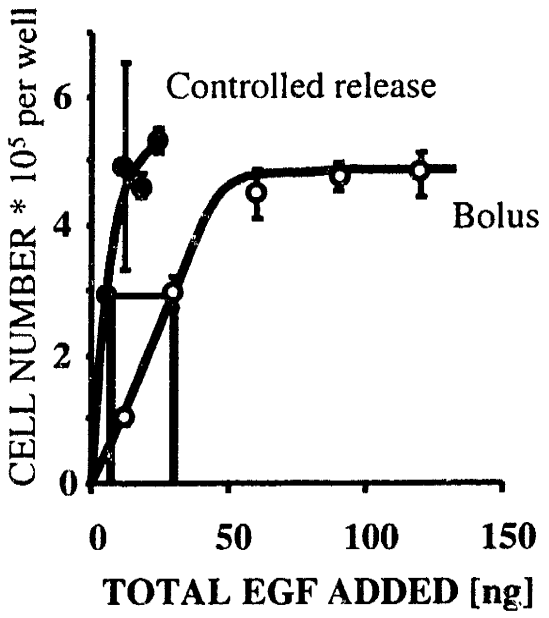

Figure 2-2: Response of NR6 cells transfected with wild-type EGF-R to controlled release (●) or bolus administration (○) of EGF.

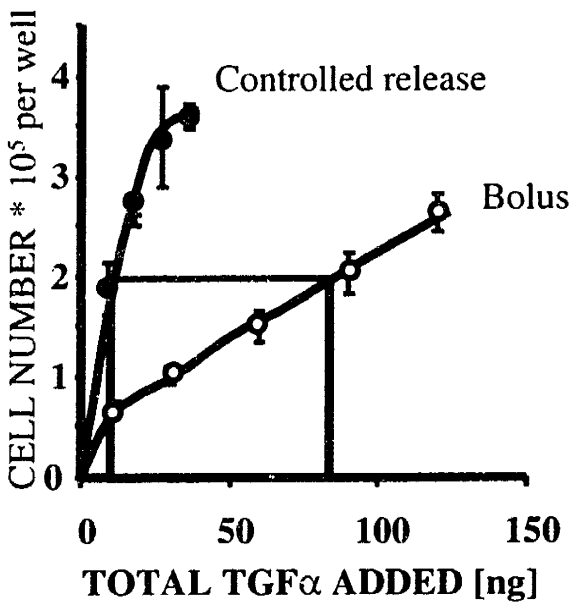

Figure 2-3: Response of NR6 cells transfected with wild-type EGF-R to controlled release (●) or bolus administration (○) of TGFα.

to exhibit a seven-fold decrease in the kinetics of ligand induced endocytosis, as assessed by the first order endocytic rate constant, k_e, [126] and to deplete significantly less ligand than their wild-type EGF-R counterparts [100], but nevertheless retain identical proliferative capacities as cells transfected with WT-EGF-R [100]. Using these cells to minimize the impact of differences in intracellular trafficking between EGF and TGFα, we compared the ensuing cellular responses to that seen in wild-type EGF-R transfected cells to the controlled delivery of both growth factors. In internalization-deficient cells, the dose-dependent proliferative responses to the controlled release of EGF and TGFα were equivalent (Figure 2-4). By contrast, wild-type EGF-R cells responded more potently to the controlled-release of EGF than TGFα most likely because intracellular trafficking differences resulted in relatively greater TGFα depletion (Figure 2-5). These data suggest that intracellular trafficking governs controlled-delivery as a decreased endocytic flux of growth factor through the internalization deficient receptor likely lessened the extent to which differences in the intracellular trafficking between EGF and TGFα were perceptible.

2.3.3 Receptor ligand trafficking

As several studies have suggested a direct correlation between the number of occupied surface receptor complexes and extent of cellular response [115, 127-129], that cellular trafficking could explain the enhanced potency of controlled delivery in comparison to bolus administration was confirmed. The number of cell surface receptor ligand complexes formed in each delivery scenario was determined. As a representative comparison, this hypothesis was examined using only one ligand, EGF, and fibroblasts transfected with the wild-type EGF-R. Cells were presented either a 120 ng/well bolus of EGF or 6-fold less amount of EGF delivered via controlled-release over 4 days, as these dosing regimens resulted in identical proliferative responses as measured on day 1 through day 4 via Coulter counting of cell numbers in separate control experiments (all p = N.S.; data not shown). To assess surface complex numbers, measurements of both surface receptor number and ligand concentration were made. Surface receptor numbers were measured using radiolabeled EGF as described in the experimental procedures. The bolus administration of EGF down-regulated surface receptor expression by greater than 80% of the initial surface expression (Figure 2-6). By comparison, the controlled-release of 6-fold less EGF minimized this down-regulation at early time points, down-regulating

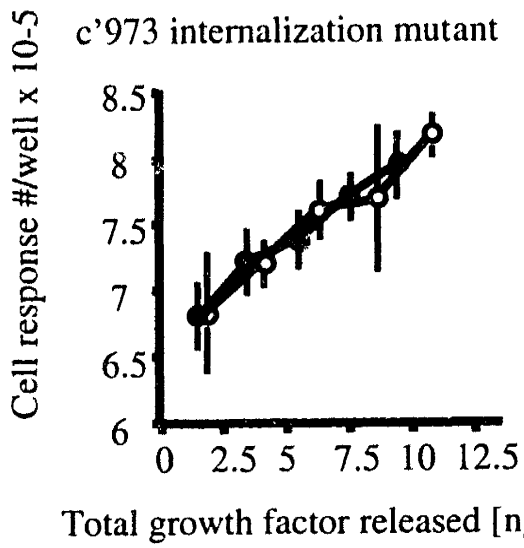

Figure 2-4: Response of mutant c'973 EGF-R internalization cells to controlled-release of both EGF (●) and TGFα (O).

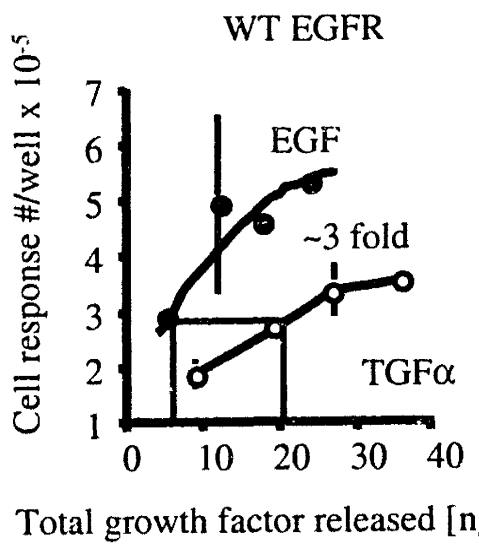

Figure 2-5: Response of wild-type EGF-R cells to controlled-release of both EGF (●) and TGFα (O).

receptors only 60%. However, at later time points, controlled-release also similarly down-regulated surface receptors (p = N.S.).

To assess ligand concentration as a function of time under these two scenarios, the cellular media was assayed for EGF concentration through the duration of the experiment using a commercially available ELISA kit. There was a rapid depletion of growth factor after the initial bolus administration on day 0. In contrast, the controlled-release of growth factor maintained a relatively steady amount of growth factor over time (Figure 2-7).

To determine the amount of occupied surface receptors predicted during the time-course of the experiment, surface receptor-ligand complex numbers were calculated using experimental measurements of receptor expression and ligand concentrations. Identical surface complex numbers were predicted throughout the time course of the experiment despite the mode of presentation or the amount of growth factor given (Figure 2-8). Our finding of equivalent surface complexes in the two delivery scenarios suggests that the biological consequences of various delivery approaches can be identical as long as receptor-ligand trafficking and cellular pharmacology are accounted for. Taken together, these data confirm that cellular pharmacokinetics govern the efficacy of controlled delivery.

2.4 Discussion

2.4.1 Local delivery

The recent, resurgence of interest in controlled delivery reflects not only a fascination with the challenges of delivering therapeutic growth factors more precisely, more biocompatibly and more stably, but an accentuated understanding of the importance of pharmacokinetics in the activity of these agents. As demonstrated in various studies, local pharmacokinetic considerations are increasingly recognized to govern therapeutic efficacy [1-5]. Accordingly, there has been renewed interest specifically in the site-specific administration of therapeutic agents, an approach known as local delivery [130]. By strategically placing polymeric devices loaded with drug near pathological sites, local delivery seeks to achieve maximal drug targeting and at the same time minimal whole-body, systemic dosing. As a result, enhanced biological effects from high local drug concentrations with reduced systemic toxicity and adverse effects are observed. In some cases, these benefits can be achieved with significantly less drug than might be administered systemically.

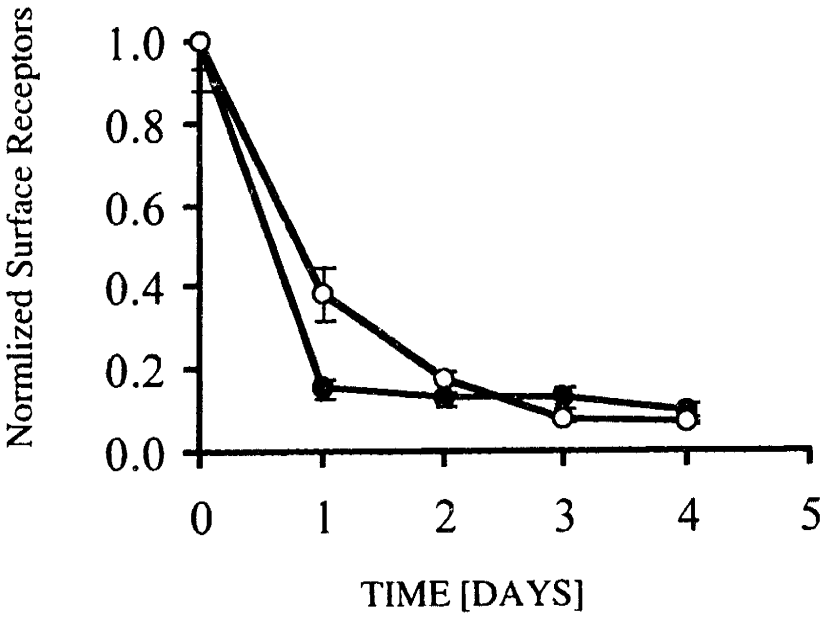

Figure 2-6: Receptor down-regulation in wild-type EGF-R cells upon bolus administration (●) or sustained release (O) of EGF

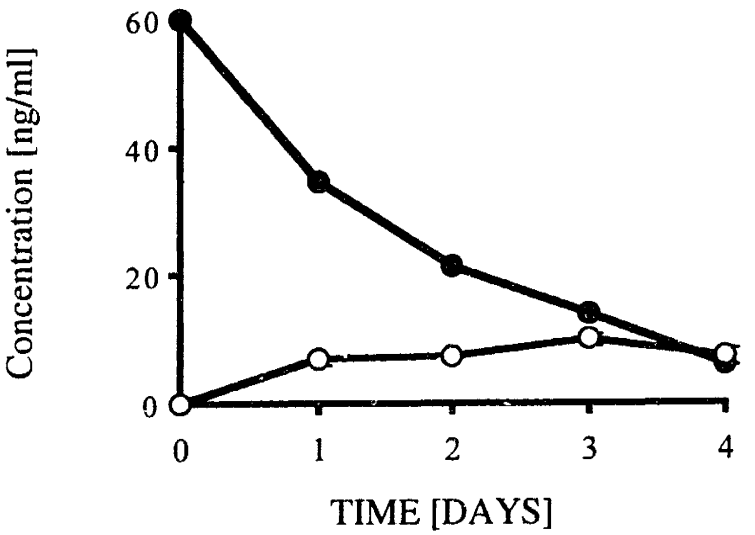

Figure 2-7: Ligand concentration profile in wild-type EGF-R cells upon bolus administration (●) or sustained release (O) of EGF.

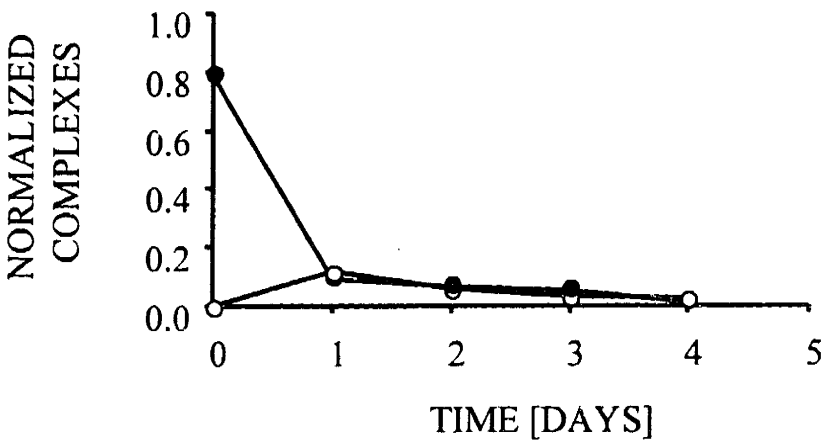

Figure 2-8: Calculated surface complexes as a function of bolus administration (●) or controlled-release (O) of EGF.

While local delivery has proven to be advantageous and successful in several experimental and pre-clinical scenarios, the lack of a framework in which to understand the mechanisms of drug delivery, drug transport, and drug-tissue interactions in these scenarios has prevented one from explaining situations in which this particular approach fails. These issues are no more as important as they are in the local delivery of growth factors for wound healing, therapeutic angiogenesis, and tissue engineering. As various growth factors and comparable therapeutic agents are locally delivered from controlled-release devices, diffusion, convection, and diverse tissue interactions including binding, metabolism, and sequestration govern their transport to the surrounding tissues [11]. Growth factors interact with extracellular proteases, enzymes, carrier proteins, and non-specific binding sites. In addition, they interact with specific cellular entities such as receptors and membrane processes that involve fluid-phase phagocytosis or transcytosis. At the cellular level, ligand depletion, receptor down-regulation and extracellular matrix sequestration are involved and intracellular endosomal sorting and endocytic regulation further complicate issues [12-14].

While classical pharmacokinetics has traditionally considered the entire organism as a limited number of homogeneous compartments between which drugs flow with definable rate constants, and from which drug is eventually cleared by way of the kidney, and/or liver [7-10]. local pharmacokinetics views the target tissue as a continuum, wherein the drug concentration varies continuously rather than in discrete steps. Classical pharmacokinetic models are sufficient to describe the time-varying concentration of drug in the compartments representing plasma, fat, solid, tissues, etc. through experimental analysis that might involve sampling a large piece of target tissue and assaying for tissue average drug content. However, such classical approaches provide only limited insight for local delivery in which physiological transport forces result in drug concentrations in one tissue region being far different from the tissue averaged concentration had the tissue been considered as a homogenous "black box". [12, 13, 50, 51, 131-133]. In local delivery, clearance, metabolism, specific and nonspecific binding, cellular internalization, and the physiological state of local tissues can all affect these gradients. Moreover, as several studies have recently demonstrated that many therapeutic agents are only minimally distributed in local delivery, local pharmacokinetics is even more important. Thus, far more information than simply dose response or clearance kinetics is required to define the response to, and therapeutic expectations of, local delivery.

The data presented in this report, therefore, have profound implications for the optimal design of controlled release systems. First, it has been demonstrated that cellular pharmacokinetics can indeed affect the efficacy of even the most ambitious of controlled delivery devices, finding that for two growth factors that bind to and interact with the same cellular receptor, but with different intracellular trafficking kinetics, optimal delivery is dependent on cellular pharmacokinetic and pharmacodynamic considerations. In cells transfected with wild-type receptors, ligands that are extensively depleted require an increased dosing regimen versus comparable ligands that are not extensively depleted. In contrast, in cells transfected with internalization deficient receptors, comparable ligands with distinct intracellular trafficking properties do not require distinct dosing regimens. Second, it has been demonstrated that despite significant disparities in loading doses, controlled delivery can achieve identical proliferative responses as bolus administration provided that receptor ligand trafficking kinetics are such that identical numbers of cellular signaling complexes are formed. By balancing ligand concentration with surface receptor levels, cells can respond to growth factors given in two different ways despite dramatic (6-fold) difference in concentration. Taken together, these data imply that rational matching of controlled release rates of growth factors with cellular pharmacokinetics is essential and that a mechanistic appreciation of cellular pharmacology can provide rational insight into appropriate delivery schemes.

2.4.2 Importance of matrix delivery and cellular pharmacokinetics

These data are consequential for controlled delivery, because it is increasingly clear that local concentrations of therapeutic agents spatially and temporally dictate subsequent pharmacodynamics and biological responses. This is readily evident not only in nature where morphogens spatially guide the discrete developmental formation of structural and functional tissues [15-25], but also in controlled delivery where local drug concentrations have now been shown to spatially correlate very specifically with the ensuing biological response [51-53]. As presented here, cellular pharmacokinetics can provide insights into the subtleties of controlled delivery and therefore potentially enable the clinical use of therapeutic agents in a manner beyond that of phenomenological trial and error.

These data are perhaps even more consequential for growth factor biology, because they provide insight into the notion as to why extracellular matrix binding interactions of some

growth factors have evolved to allow for the sustained presentation from storage depot sites [134-140]. As suggested in previous work, these matrix interactions might enable optimal cellular presentation of growth factors consistent with the intrinsic pharmacology of targeted cells [112]. Based on the findings of this study, it is suggested that through matrix interactions and delivery, growth factors have evolved the ability to overcome limitations of ligand depletion to achieve enhanced biological potency. Indeed, mathematical modeling of cellular trafficking has confirmed the possibility that formation of cellular signaling complexes can be enhanced by more than 1000-fold through matrix delivery (Chapter 3). Moreover, there appears to be specific criteria based on cellular trafficking kinetics that might guide a priori the rational delivery of growth factors (Chapter 3). In sum, a fundamental appreciation of growth factor physiology will likely enhance the rational delivery of these agents.

2.4.3 Conclusion

As growth factors are increasingly used in a variety of therapeutic processes and expected to perform optimally in complex tissue environments, there is great need for detailed pharmacokinetic understanding. Results from these studies highlight the importance of cellular trafficking in determining the potency of locally delivered growth factors. Local cellular depletion of ligand will determine adequate and optimal delivery rates. Consequently, temporal matching of growth factor presentation with intrinsic cellular pharmacokinetic responses will most likely enable optimal biological responses to be achieved.

2.5 Chapter Summary

In this chapter, the role of cellular pharmacology in determining the efficacy of sustained release growth factors was examined. It was demonstrated that for two growth factors that bind to and interact with the same receptor, differential cellular responses can result upon sustained delivery. As a consequence of differential intracellular trafficking due to differential endosomal pH sensitivities, two growth factors of the same family may benefit unequally from sustained release. To confirm the relevance of cellular trafficking in determining the response to controlled delivery, the comparative ligand receptor trafficking responses to two different loads of growth factor via bolus administration and controlled delivery was examined. It was found that cellular trafficking could reasonably explain the comparable response to growth factor administration despite dichotomous delivery approaches and growth factor loads. Taken

together, this Chapter demonstrated the importance of cellular pharmacokinetics in defining in part the efficacy and potency of local delivery.

3 COMPUTATIONAL MODELS

3.1 Background

As the findings in Chapter 2 suggest the importance of cellular pharmacokinetics in defining control-released growth factor effect, it was thought that the development of a computational model of cellular pharmaockinetics might aid in understanding a priori how cellular trafficking affects local growth factor delivery. Consequently, a theoretical model to specifically examine the role of rate-limiting cellular pharmacokinetics on local growth factor delivery was conceptualized and implemented. Computational models with mechanistic versus empirical underpinnings, such as the one described below, can provide potentially important insights into experimental results, complex situations, and allow one to also identify potential areas of future research.

In general, models for growth factor mediated cellular proliferation have been pioneered by Lauffenburger and colleagues who have attempted to formulate quantitative relationships between some measure of upstream signaling, usually ligand receptor binding, and some measure of cellular proliferation, usually growth rate [14, 141, 142]. In most, if not all of these models, correlations between cell surface complexes and cell proliferation are embodied by a cell specific growth rate for which only empirical relationships are currently available [143]. As a consequence, the relationship between cell surface receptor-ligand complexes and cell growth rate is based on experimental evidence that couples the two computational domains. This limitation is due to lack of information stemming from biology rather than computational or conceptual abilities. Because the empirical relationship between cellular trafficking and cellular response is not well defined for many growth factors, and because several studies have demonstrated receptor ligand binding can be a simple predictor of cellular response [127, 129], a computational model was developed based on using ligand receptor binding as a correlate for cellular response. With this model, the role of cellular pharmacokinetics in defining the efficacy and potency of local growth factor delivery was examined.

3.2 Methods

3.2.1 Cellular Pharmacology Model

To develop insights into the correlation between drug delivery kinetics and cellular trafficking, a model based on equations describing the law of mass action kinetics of growth factors interacting with cellular receptors was conceptualized. Included in the model were the following kinetic trafficking events: association of ligand (L) and unoccupied cell surface receptor (R_s) with a rate constant of k_a, dissociation of cell surface ligand-receptor complex (C_s) with a rate constant of k_d, ligand induced internalization of cell surface complexes with a rate constant of k_{eC}, constitutive membrane turnover for unoccupied receptors with a rate constant of k_{eR}, synthesis of new receptors with a rate constant of r_{syn}, recycling of intracellular receptors (R_i) and intracellular ligand-receptor complexes (C_i) with a rate constant of k_{rec} and fractional sorting numbers f_2 and f_1 respectively describing the fraction of sorted to recycling or degradation, lysosomal degradation of R_i and C_i with a rate constant of k_{deg}, and extracellular nonspecific proteolysis of intact ligand, L, to give degraded ligand (L_{deg}) with a rate constant of k_{prot}, (Figure 3-1). The controlled release of growth factor into the system was modeled with zeroth-order kinetics, as embodied by the rate, r_{rel}. Importantly, each of these trafficking events and rate constants are simple enough that they each can be independently, experimentally measured, thus providing for a potential connection with experimental data [14, 144]. The equations that describe the time dependence of the various cellular species and a diagram of the model are given in Figure 3-1.

To focus specifically on the dynamics of the kinetic presentation of growth factors and cellular pharmacokinetics, spatial detail was neglected to minimize confounding effects that might be due to limitations in mass transport as opposed to effects resulting exclusively from cellular trafficking events. As the relevant time scale for diffusion over a characteristic cellular length scale can be assumed to be much smaller than the time scale for relevant cellular responses, this "well-mixed" assumption of spatial homogeneity in ligand concentration is applicable.

To reduce complexity within this model, kinetic parameters were assumed to be time-averaged values with definitions of each of the parameters as given in Table 1. A base case of kinetic parameters from a literature review was selected for analyses to potentially mimic the

interactions of any growth factor with its receptor, Table 2. Because this model is readily adaptable with parameters that can be changed easily, it is reasonable that any growth factor might potentially be simulated, provided that values for each of the different kinetics processes are known and that the model is carefully adapted to fit relevant biochemical and mechanistic details.

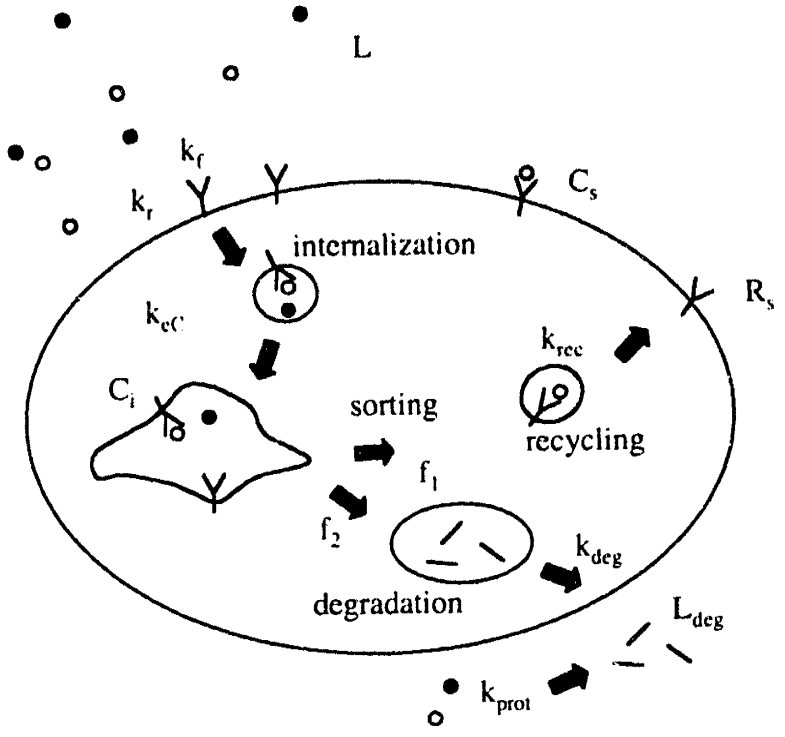

$$\frac{dL}{dt} = (-k_f L R_s + k_r C_s)\frac{n}{N_{av}} - k_{prot} L + r_{rel}$$

$$\frac{dL_{deg}}{dt} = (k_{deg} f_1 C_i)\frac{n}{N_{av}} + k_{prot} L$$

$$\frac{dR_s}{dt} = -k_f L R_s + k_r C_s + r_{syn} - k_{eR} R_s + (1 - f_2) k_{rec} C_i$$

$$\frac{dC_s}{dt} = k_f L R_s - (k_r + k_{eC}) C_s + (1 - f_1) k_{rec} C_i$$

$$\frac{dC_i}{dt} = k_{eC} C_s - [(1 - f_1) k_{rec} + f_1 k_{deg}] C_i$$

$$\frac{dR_i}{dt} = k_{eR} R_s - [(1 - f_2) k_{rec} + f_2 k_{deg}] R_i$$

Figure 3-1: Cellular pharmacology model and diagram of rate-limiting trafficking events, and mass action equations used in model.

Table 1: Definition of parameters and rate constants for cellular pharmacology model.

Species	**Definition**
R_s	Free surface receptors [#/cell]
R_i	Free internal receptors [#/cell]
C_s	Surface receptor-ligand complex [#/cell]
C_i	Internal receptor-ligand complex [#/cell]
L_i	Intact ligand [M]
L_{deg}	Degraded ligand [M]
ECM	Extracellular matrix binding site [#/cell]
Parameters	
k_f	Association rate constant of receptor [M^{-1} sec^{-1}]
k_r	Dissociation rate constant of receptor [sec^{-1}]
k_{rec}	Recycling rate constant [sec^{-1}]
k_{eC}	Induced endocytosis rate constant [sec^{-1}]
k_{eR}	Constituitive endocytosis rate constant [sec^{-1}]
k_{deg}	Specific cellular degradation rate constant [sec^{-1}]
k_{prot}	Extracellular proteolysis rate constant [sec^{-1}]
r_{rel}	Release rate from polymeric source [M sec^{-1}]
k_{f2}	Association rate constant to ECM site [M^{-1} sec^{-1}]
k_{r2}	Dissociation rate constant from ECM site [sec^{-1}]
r_{syn}	Receptor synthesis rate [#/cell/sec]
f_1	Fraction of receptors sorted to recycling
f_2	Fraction of complexes sorted to recycling

Table 2: Parameter Estimates for cellular pharmacology model.

Species	Base case at t=0	Reference
R_s	20,000	-
R_i	0	-
C_s	0	-
C_i	0	-
L_i	$1x10^{-9}$	-
L_{deg}	0	-
ECM sites	variable	-
Parameters		
k_f	$1x10^{6}$	[14]
k_r	$1x10^{-4}$	-
k_{rec}	$1.54x10^{-3}$	[12]
k_{eC}	0.005	[145]
k_{eR}	0.0005	[145]
k_{deg}	$1x10^{-3}$	[12]
k_{prot}	$6.7x10^{-4}$	[12]
r_{rel}	variable	-
k_{f2}	$1.67x10^{6}$	[146]
k_{r2}	0.001	[146]
r_{syn}	0.33	[12]
f_1	0.5	[13, 14]
f_2	0.05	[13, 14]

3.2.1.1 Simulation of the Delivery of Growth Factors

For simplicity, the temporal ligand profile in the sustained release case was modeled as a linear increase in concentration, while the bolus administration was modeled as a step increase in ligand concentration at t= 0 (Figure 3-2). The total amount of ligand presented in either case was conserved based on the total area under the curve, A.U.C., plot of ligand versus time in the situation with no extracellular proteolysis and cellular interactions. An alternative comparison conserving the total amount of ligand presented based on mass balance was examined as well. Results from either comparison method were similar. In the data presented here, conservation of A.U.C. was chosen, because it is a widely used parameter for comparing the potency and efficacy of alternative delivery approaches.

3.2.1.2 Numerical Method

The six first-order, non-linear, coupled ordinary differential equations were non-dimensionalized and solved using a stiff, variable order method based on numerical differentiation formulas using MATLAB 5.2.0 (The MathWorks, Natick, MA) with standard relative error tolerances. Simulations were run for a total time of 5 days. Separate simulations demonstrated that variations in this endpoint resulted in minimal quantitative changes in results. The MATLAB m-files for these simulations are included in the Section 7.

3.2.1.3 Defining Cellular Signaling Activity

To compare the efficacy of sustained release and bolus administration in generating a cellular response, a parameter defined as the time-integrated surface receptor-ligand complexes, $\int C_s dt$ (Integral C_s), was chosen to assess whether one delivery mode was superior in generating cell surface complexes versus another. As previous studies have suggested linear relationships between receptor occupancy and cellular responses such as DNA synthesis [127, 129], Integral C_s is a reasonable and relevant parameter that should correlate well with subsequent biological responses. In this scenario, growth factor bound to receptors at the cell surface contribute to this measure of cellular signaling, while free, unbound ligand and receptors or internalized receptor ligand complexes do not. A temporally averaged value was chosen as a relevant measure of biological signaling, because cellular responses occur on a time scale that is long compared to

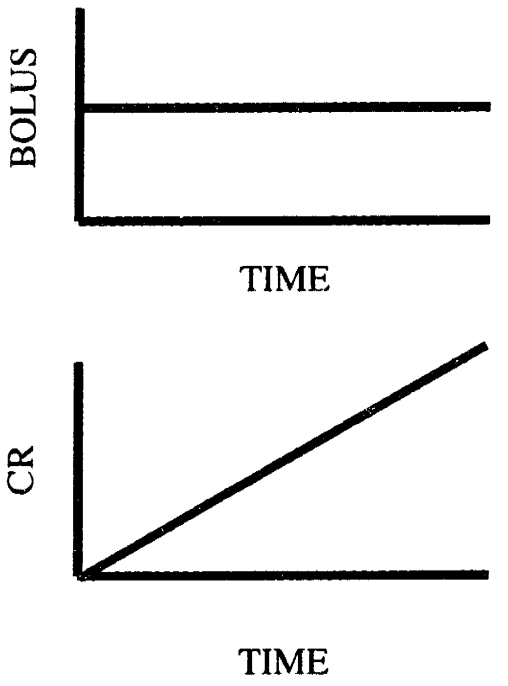

Figure 3-2: Two delivery approaches for cellular pharmacology mode, bolus administration (top) and controlled-release (CR, bottom).

cellular trafficking, so that temporal signal averaging by the cell appears to occur. Moreover, this time integral form can adequately account for both the time and magnitude of the ligand-receptor interactions. Through the use of this parameter, the role of cellular trafficking in local delivery could be defined.

3.2.1.4 Sensitivity Analysis

To determine the sensitivity of cellular signaling activity to perturbations in trafficking constants, a dimensionless sensitivity coefficient, $S_{PERTURBED/BASE}$, was mathematically defined as the ratio of the amount of cellular signaling units, Integral $C_{s\ PERTURBED}$, obtained for the case in which a trafficking parameter was perturbed from its base value, to the amount of cellular signaling units, Integral $C_{s\ BASE}$, obtained for the base case. By varying individually each of the base kinetic parameters over several orders of magnitude, the sensitivity coefficient was computed and allowed for the categorization of two groups of trafficking events: those that positively correlated with changes in cellular signaling activity versus those that negatively correlated with changes in cellular signaling activity. Comprehensive computational simulations were then conducted to examine all possible combinations for the pairing of these two categories, and the results of the simulations were plotted in a $\log_{10}$ scale contour plot format of the ratio of Integral C_s as described below.

3.2.1.5 Analysis of Optimal Delivery Kinetics

As the principal goal of this model was to determine a priori when the sustained presentation versus the bolus administration of growth factor might elicit quantitatively greater cellular signaling, a dimensionless parameter, $E_{CR/Bolus}$, was defined to describe the enhancement in signaling due to the controlled-delivery versus bolus administration of growth factors. $E_{CR/Bolus}$ is defined as the ratio of the time-integrated number of surface complexes, Integral C_s, generated via controlled-release versus bolus administration of growth factor, and is given mathematically as $E_{CR/Bolus} = [\int C_s dt / T]_{Controlled\text{-}release} / [\int C_s dt / T]_{Bolus\ administration}$. For $E_{CR/Bolus} > 1$, this parameter suggests that sustained-release results in a greater generation of cellular signaling activity than bolus administration. In contrast, for $E_{CR/Bolus} < 1$, this parameter suggests that bolus administration results in a greater generation of cellular signaling activity than sustained release. For $E_{CR/Bolus} = 1$, there is no appreciable difference in delivery modality, as equal units of cellular signaling are generated in both delivery methods. One caveat to the definition of this

variable is that it reflects only a comparison between two delivery modes, and not an absolute determination of cellular signal generation. As a consequence, for instance, if both presentation schemes under a set of parameters lead to large cellular signaling activities, $E_{CR/Bolus}$ might be approximately 1. Similarly, if both delivery approaches under an alternative set of parameters lead to small cellular signaling activities, $E_{CR/Bolus}$ might also be approximately 1. Thus, as defined, $E_{CR/Bolus}$ represents only the relative enhancement achieved in cell signal generation by controlled-release versus bolus administration, and not an absolute enhancement in cellular signal activity.

3.2.1.6 Modeling of Growth Factor Extracellular Matrix Interactions

Interactions of growth factors with extracellular matrix binding sites were modeled through inclusion of either 0- 10-, 100-, or 1000- fold molar ratios of matrix binding sites to specific receptor sites. Rate constants for the association and dissociation of the growth factor and matrix were taken from the literature [146]. Growth factor was allowed to bind reversibly to matrix sites, and when bound was assumed to be protected from extracellular proteolysis. Thus, this reservoir of matrix sites served as a natural controlled-release device from which growth factor could be presented.

3.2.1.7 Experimental Connection: An Interleukin-2 model

As a result of a limited quantitative and mechanistic information describing trafficking and the response to controlled delivery, the results proposed from the computational simulations were difficult to correlate experimentally. While this is acknowledged to be a limitation of this model, the facts that the model is: (i) fundamentally based on well-described rate-limiting trafficking events that are experimentally accessible, and (ii) based on a measure of cellular responsive that is likewise simple and experimentally accessible, should make it meaningful in providing at the least a zeroth order level of insight into the role of cellular pharmacology on local growth factor delivery. Nevertheless, future experimental work is necessary to validate the conclusions from this model.

Because of the difficulty in directly validating this model, an indirect approach was made. Using an experimentally validated system describing interleukin-2 receptor ligand trafficking kinetics and resulting control of T-cell proliferation, [143], predictions were made about the comparative approaches of growth factor delivery, either bolus administration or

sustained release. This system was chosen primarily, because it has been demonstrated to be able to correlate experimental data on ligand depletion and cellular proliferation with computational predictions based on independent measurements of trafficking parameters [143]. Moreover, this system was chosen as its form and assumptions are very similar to those proposed in the cellular pharmacology model described in Section 3.2.1. As such, the results and insights derived form this analysis should be a natural extension of the conclusions derived from the previous section.

3.2.2 Tissue Pharmacology Model

To address one of many interesting questions in the field of local delivery of how local tissue concentrations correlate with subsequent biological responses, a computational model was developed that simultaneously incorporated diffusive transport, cellular trafficking, and tissue response. The computational approach for modeling diffusive transport in this section was a direct application of the Crank Nicholson method that has been more than adequately described in the literature [147]. The approach for modeling tissue response was accomplished through incorporating the theoretical model proposed by Fallon et al., described above in Section 3.2.1.7. As described in Section 3.2.1.7, this interleukin-2 model was chosen instead of the theoretical model posed in Section 3.2.1, because it has been experimentally validated, and because it is very similar in form as the one posed in Section 3.2.1. Together, the coupling of Crank Nicholson method and the IL-2 model by Fallon (2000) allowed for the simultaneous simulation of diffusion, cellular trafficking, and tissue response. As a result, the correlation between spatial concentrations of growth factor with tissue response could be determined.

Schematically, the tissue was conceptualized as a series of T-cells lined sequentially next to each other (Figure 3-3). Though this scenario is obviously non-physical, its importance and relevance lies in the conceptual formulation of the problem and approach, wherein the effects of cellular trafficking can now be specifically examined in the context of spatial concentration gradients. It is easily imaginable that a model of similar form might be adapted for another set of cells or growth factor when the appropriate mechanistic details become available. For the moment, this idealized, conceptual approach serves well. Accordingly, each T-cell served as a computational node in an alternating direction algorithm, so that spatial variations in proliferative responses could be determined as a function of transport rates. Computationally,

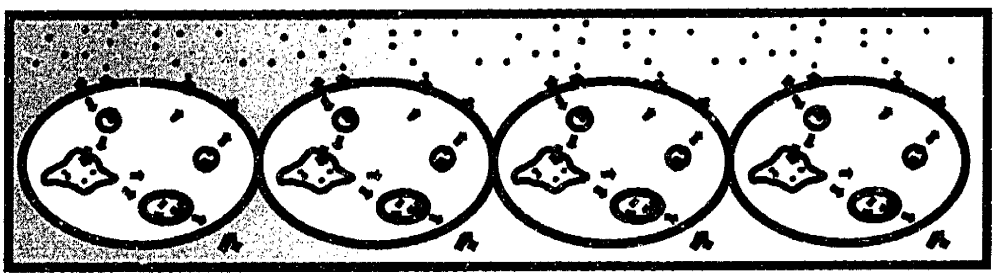

Figure 3-3: Schematic diagram of the tissue pharmacology model. Note gradient in ligand concentration imposed by boundary conditions. Diffusion was modeled using *Crank-Nicholson* algorithm. Cellular trafficking and proliferation was modeled using system published by Fallon *et. al. (2000)* on interleukin-2. Transport was offset from trafficking by one-half time-step to simplify the computation as described by Rippley and Stokes (1995).

the simulation was simplified by offsetting the time step for diffusion from that for cellular trafficking and proliferation by one half time step. Boundary conditions were defined such that at one edge of the hypothetical tissue, for $t \geq 0$, $x = 0$, the defined drug concentration was constant at a dimensionless concentration of one, being maintained by a polymeric controlled release device. At the other edge of the hypothetical tissue, for $t \geq 0$, $x = 1$, the full length of the dimensionless space, the tissue concentration was arbitrarily set to 0, mimicking distal washout. Initial conditions were set such that there was no drug throughout the theoretical tissue (at $t=0$, $0 \leq x \leq L$, $C=0$), and that all cellular receptors were unbound and distributed as a function of rates of receptor synthesis, recycling, and constitutive internalization for the IL-2 receptor system [143]. Simulations were allowed to run for five days, and the time course of drug diffusion into the tissue, cellular response as embodied by the spatial profile of surface receptor ligand receptor complexes, and the tissue response as embodied by the proliferative response, or the fold-increase in cell density, were plotted. Variations in a hypothetical effective diffusivity D_{eff}, were examined by varying the diffusivity by ten-fold and monitoring the effects on the three parameters described above (ligand concentration, ligand receptor profile, and cell response profile).

3.3 Results

To begin to develop an understanding for the optimal delivery of growth factors, computational models based on cellular trafficking were conceptualized and implemented. With these models, the effects of cellular pharmacology, ie. the role of ligand receptor trafficking, and the effects of tissue pharmacology, ie. the role of transport and tissue gradients, on control-released growth factor efficacy were examined.

3.3.1 Cellular Pharmacology

As data from the experiments in Chapter 2 have shown, receptor ligand trafficking can be important in defining the efficacy of control released growth factors. As such, a quantitative model was conceptualized based on simple, experimentally accessible trafficking parameters and was implemented to examine the role of various trafficking parameters on local growth factor delivery as described above in Section 3.2.1.

3.3.1.1 Sensitivity analysis

To first define the role of each trafficking step on the model, each of the rate constants or rates was independently varied to assess the sensitivity of the model to their variation. Ligand receptor complexes were numerically integrated as a function of the trafficking parameter and then compared as a ratio between the result obtained with the perturbed rate constants versus the result obtained with the base model case. An example of this sensitivity analysis is shown in Figure 3-4 for variations in receptor synthesis rates, r_{syn}. By increasing the rate of receptor synthesis from the base values described in Section 3.2.1.1, the generation of Integrai C_s progressively increased. In contrast, decreasing the rate of receptor synthesis from base values led to a progressive decrease in Integral C_s. These data suggest that receptor synthesis rates, as embodied by the parameter, r_{syn}, is positively correlated with cellular signaling activity.

Variations in all other trafficking rate constants were conducted and the responses as embodied by the sensitivity coefficient, $S_{PERTURBED/BASE}$, were categorized according to their effects on the generation of signaling complexes as shown in Table 3. These results suggest that certain trafficking parameters, when perturbed, lead to more cellular signaling, whereas other trafficking parameters, when perturbed, lead to less cellular signaling.

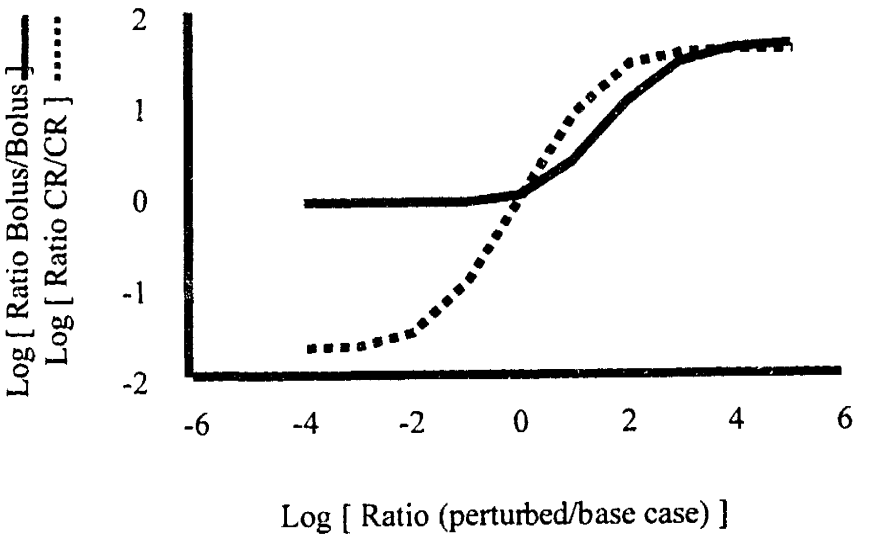

Figure 3-4: Sample data demonstrating sensitivity analysis for cellular pharmacology model. Shown here are variations in the ratio of the receptor synthesis rate, r_{syn} for both bolus administration and controlled-release and effect on the generation of cellular signaling activity.

Table 3: Sensitivity analysis. Variations in each of the parameter were conducted and the response on cellular signaling was determined.

Positive correlation	**Negative correlation**
Recycling	Extracellular proteolysis
Receptor synthesis	Cell mediated degradation
Ligand dose	Ligand induced endocytosis
Initial receptor number	Constituitive endocytosis

3.3.1.2 Effects of cellular trafficking parameters

To determine the role of cellular pharmacokinetics on controlled-release growth factors, computational simulations were conducted based on the cellular trafficking model described in Section 3.2.1.1. Growth factor was presented to the cell suspension system either as a bolus or as a sustained formulation, so that the total mass or area under the curve was conserved between the two scenarios. Under both delivery approaches, either bolus administration or sustained release, ligand receptor complexes were numerically averaged over the time course of the simulation and then compared as a dimensionless ratio to determine which approach resulted in more signaling complexes. These data were then plotted as a function of variations in the trafficking constants. For example, data are shown in Figure 3-5 that describe the dependency of the dimensionless ratio, $E_{CR/Bolus}$, as a function of variations in the proteolytic rate constant, k_{prot}. Here, $E_{CR/Bolus}$ is plotted versus the proteolytic rate constant, k_{prot}. These results predict that for small extracellular proteolytic rate constants, there is little enhancement ($E_{CR/Bolus} \sim 1$), achieved with controlled-delivery of growth factor over bolus administration. In this case, growth factor remains around adequately in both delivery approaches to sustain equivalent biological responses. Similarly, for large extracellular proteolytic rate constants, there is little enhancement ($E_{CR/bolus} \sim 1$) seen upon controlled-delivery of growth factor over bolus administration. In this case, growth factor is so rapidly degraded that regardless of the delivery approach, few signaling complexes are sustained. Thus, there is no inherent benefit to either delivery method, as both would be equally poor. For intermediate proteolytic rates, such as those experimentally observed, there is a significant 3-4 fold enhancement in ($E_{CR/bolus} > 1$) upon the controlled-delivery of a hypothetical growth factor versus its bolus administration [12, 73, 148]. In this example, the results obtained from the model appear to suggest an intuitively acceptable regime in which control-release may potentially enhance the biological response to growth factor administration.

To extend these results to other potential growth factor concentrations, comparable simulations were run using different concentrations, and the data obtained were plotted in contour plot format. On the z-axis, is plotted the logarithm ($\log_{10}$) of the dimensionless ratio, $E_{CR/bolus}$ as a function of the proteolytic rate constant on the y-axis and the initial ligand

concentration on the x-axis (Figure 3-6). As shown in this plot, regions in which controlled-release of growth factor generated 100-fold more signaling units than bolus administration were shaded black ($Log_{10}(100) = 2$). In contrast, regions in which the bolus administration of growth factor generated 100-fold more signaling units than controlled-release were unshaded white ($Log_{10}(0.01) = -2$). As the results show, the use of the contour plot allowed the delineation of theoretical regions where the sustained delivery of growth factor might result in greater biological responses than bolus administration. Notably, at higher ligand concentrations, the range of proteolytic rate constants over which sustained release generates a greater number of signaling complex increases.

Based on the categorization of all trafficking parameters into two broad categories, those that positively correlated with cellular response versus those that negatively correlated with cellular response, simulations were conducted to further define other regions where sustained delivery might result in a greater quantitative response than bolus administration. From these simulations, several intriguing domains in the multidimensional space of trafficking parameters were identified (Figure 3-7). In each of these, the dimensionless ratio, $Log_{10}(E_{CR/Bolus})$ is again plotted on the z-axis versus other trafficking parameters plot on the x- and y-axes. As shown in these data, there appear to be theoretical regions where the sustained presentation of growth factor resulted in the generation of more than 100 fold signaling complexes versus the bolus administration and conversely, the reverse. For example, in the plot of extracellular proteolysis rate constant, $k_{proteolysis}$ versus Initial Total Receptor Number, at high proteolytic rates, sustained release leads to almost 10,000-fold more signaling complexes at low receptor number, but 10-fold less signaling complexes at high receptor numbers than bolus administration. In contrast, at low proteolytic rates, the generation of signaling complexes between sustained release and bolus administration is more comparable. As another example, in the plot of intracellular recycling rate constant, $k_{recycle}$, versus Initial Total Receptor Number, at high recycling rates, sustained release leads to more than 100-fold generation of signaling complexes versus bolus administration at low receptor numbers. In contrast, at high receptor numbers, bolus administration leads to 10-fold more signaling complexes than sustained release. Along with other data shown in the above figure, and those not included, these data are consistent with the conclusion that cellular trafficking can be important in defining optimal approaches for growth factor delivery. The results of the model can be summarized as follows: the kinetics of receptor

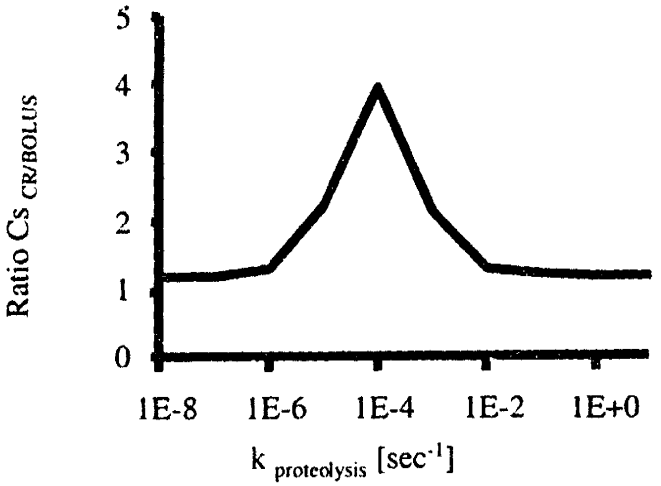

Figure 3-5: Plot of dimensionless ratio of Integral Cs $_{\text{Controlled-Release/Bolus}}$ as a function of changes in the extracellular proteolysis rate constant, k $_{\text{proteolysis}}$.

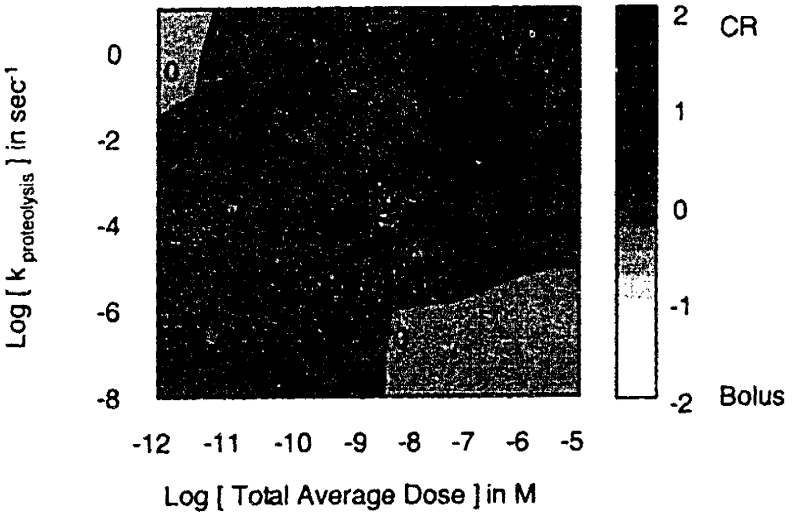

Figure 3-6: Contour plot of $\log_{10}$ of the Ratio $_{\text{CR/Bolus}}$ for variations in extracellular proteolysis rates and Total Averaged Dose. Shaded areas indicate theoretical differences in generation of signaling between controlled-release and bolus administration.

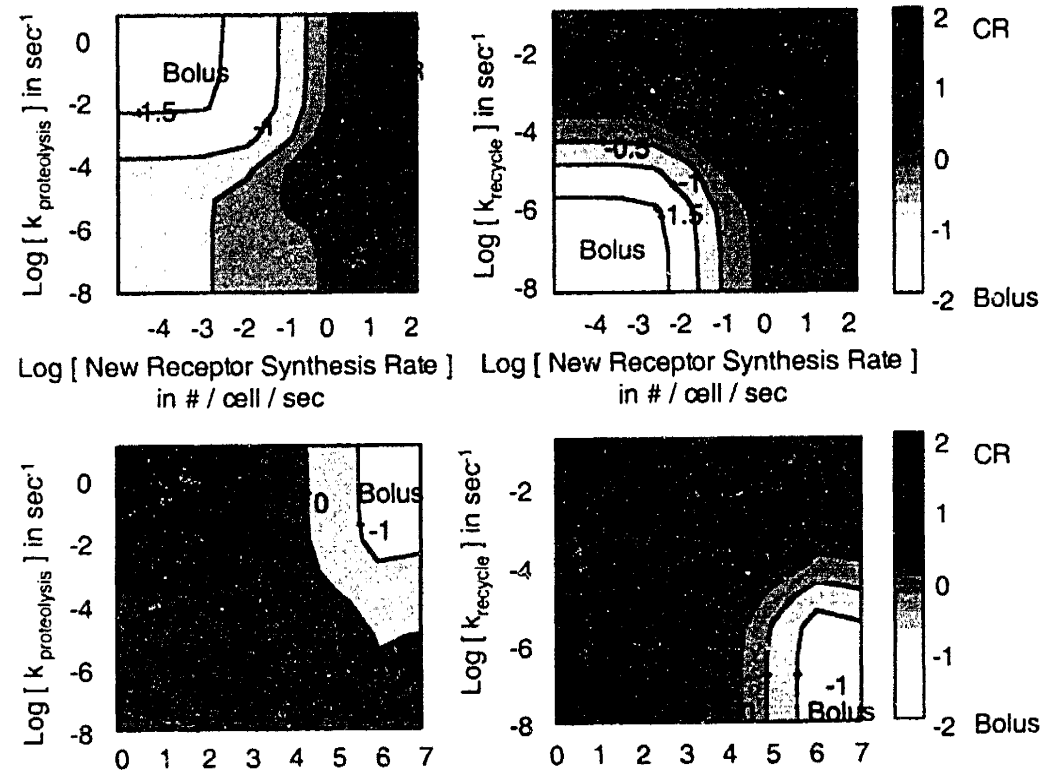

Figure 3-7: Theoretical plots of $\log_{10}$ of Ratio $_{CR/Bolus}$ for other trafficking parameters. Note distinct regions where controlled-release results in greater and lesser amounts of signaling complexes versus bolus administration.

recycling and ligand proteolysis appear to be important determinants of whether a growth factor might benefit from being control released; cells with receptors that rapidly recycle or ligands that are physiocochemically unstable would benefit from sustained delivery; in contrast, slow receptor synthesis rates, high receptor number, and fast constitutive receptor turnover appear to be important determinants of whether a growth factor might instead benefit from bolus administration. The theoretical insights proposed by these mathematical analyses may be potentially relevant for optimizing delivery approaches. In addition, these data suggest key trafficking parameters that might theoretically guide the rational reverse engineering of growth factors for a given delivery approach.

3.3.1.3 Effects of extracellular matrix

As many reports have postulated that growth factor and extracellular matrix interactions might serve as a kinetic storage depot from which growth factor can be sustained released in a natural fashion [137, 139, 140, 149], the extent to which these binding sites might enhance cellular signaling was examined. The model for cellular pharmacology was adapted to include the presence of low affinity binding sites for hypothetical growth factor interactions with extracellular matrix. Rate constants were defined from the literature [146] and the delivery of growth factor in a bolus fashion was compared for the case in which low affinity binding sites were included versus excluded. To evaluate the potential gain in cellular signaling arising from the ECM interactions, an analogous dimensionless ratio, $E_{ECM/Bolus}$, was used to describe the enhancement in cellular signaling due to the presence of extracellular matrix interactions versus its absence. As shown in Figure 3-8, the presence of ECM interactions shown in molar ratios of total receptor number (from 0 to 1000) can significantly enhance cellular signaling by nearly 1,000 to 10,000-fold, (Log $[E_{ECM/Bolus}] \sim 0$-4) depending on extracellular proteolytic rates. These results suggest an explanation for the importance of matrix binding properties of many physically unstable growth factors. Growth factors may have naturally evolved matrix-binding properties to circumvent susceptibility to extensive tissue degradation and to enhance cellular signaling.

3.3.1.4 Experimental Connection: An Interleukin-2 model

Because little experimental data are available in the literature to validate the model, the results obtained in Sections 3.3.1.1, 3.3.1.2, and 3.3.1.3 are acknowledged to be in part

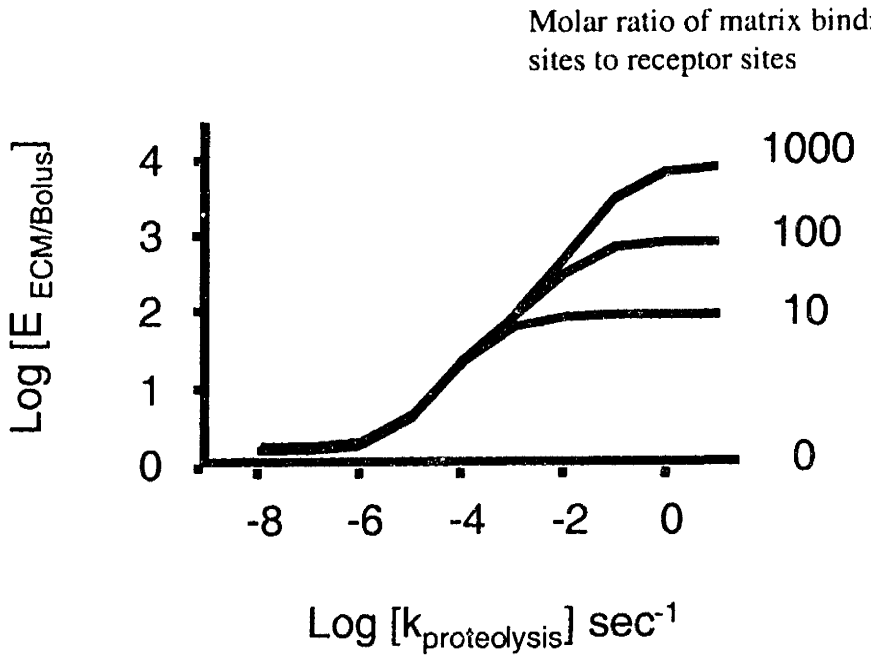

Figure 3-8: Role of extracellular matrix binding sites in enhancing theoretical growth factor receptor signaling.

speculative. Unfortunately, this is simply due to the lack of information describing all permutations of the various rate constants and rates considered. As an attempt to tie this model with experimental reality, a published computational model describing IL-2 trafficking and T-cell proliferation was incorporated as described in Section 3.2.1.7 [143]. This published model describes in much the same format, the rate-limiting trafficking events that define the interactions between the interleukin-2 ligand and receptor. Because of the inherent similarity in this published model and the model proposed in Figure 3-1, the insights obtained from the incorporation of this system should be useful for optimizing IL-2 delivery. Using this system, the proliferative responses of T-lymphocytes to either the sustained presentation of growth factor or the bolus administration were determined. As shown in Figure 3-9, when there is minimal extracellular proteolysis, the dose responses of T-cells to IL-2 delivered via sustained release and bolus administration are predicted to be generally similar. In contrast, as the rates of proteolysis increase sustained release progressively becomes a more effective delivery approach, resulting in higher cell densities after 5 days than bolus administration, Figure 3-10 and Figure 3-11. When the ligand concentration is followed over the increase of proteolysis rates, it is clear that sustained release protects the decay of growth factor far better than bolus administration, and therefore results in a higher proliferative response by the T-lymphocytes to growth factor, Figure 3-12. Taken together, these results suggest that theoretically IL-2 would benefit greatly from being sustained release. Comparison of this prediction with results in a published paper describing the whole-body clearance of IL-2 in animal models confirms that this conclusion is reasonable [150]. Upon intraveneous bolus administration of IL-2 to pigs, interleukin-2 is rapidly cleared with a half life, $t_{1/2}$ of less than one hour [150]. Sustained presentation of IL-2 would therefore intuitively enhance its bioavailability and its therapeutic potential. In summary, through the incorporation of a published model of interleukin-2 trafficking and proliferation into the computational model proposed in Section 3.2.1, insight into the optimal clinical use of IL-2 has been obtained. This finding discursively verifies the validity of the model and approach.

3.3.2 Tissue Pharmacology

The role of local tissue concentrations in defining the tissue response has not been defined clearly, especially from a computational perspective. The importance of this knowledge is underscored by the fact that the in vivo success of any therapeutic is equally dependent on

Figure 3-9: Cell response versus IL-2 dose. Sustained release (dotted line), bolus administration (solid line) with $k_{proteolysis} = 1x10^{-4}$.

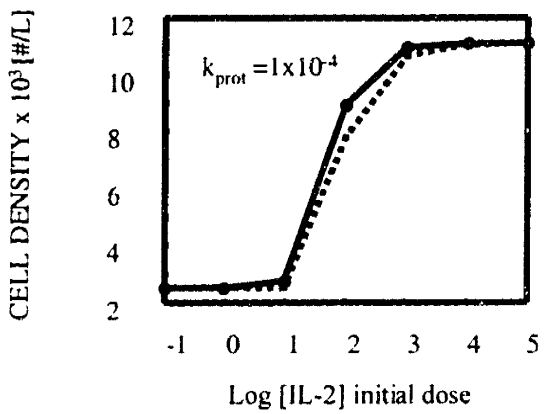

Figure 3-10: Cell response versus IL-2 dose. Sustained release (dotted line), bolus administration (solid line) with $k_{proteolysis} = 1x10^{-3}$.

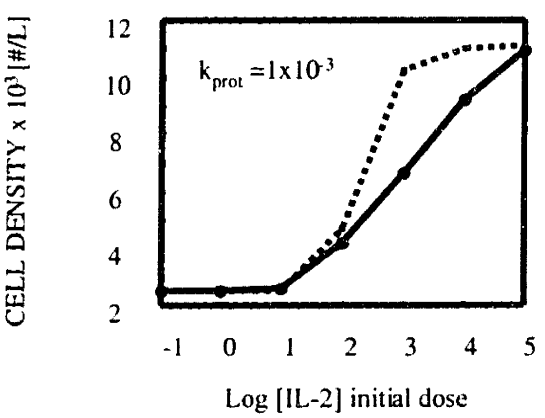

Figure 3-11: Cell response versus IL-2 dose. Sustained release (dotted line), bolus administration (solid line) with $k_{proteolysis} = 1x10^{-2}$.

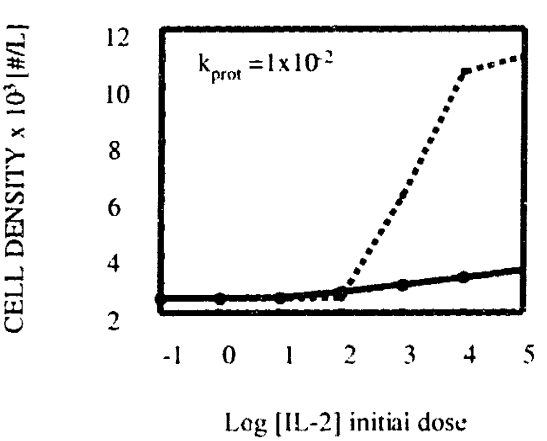

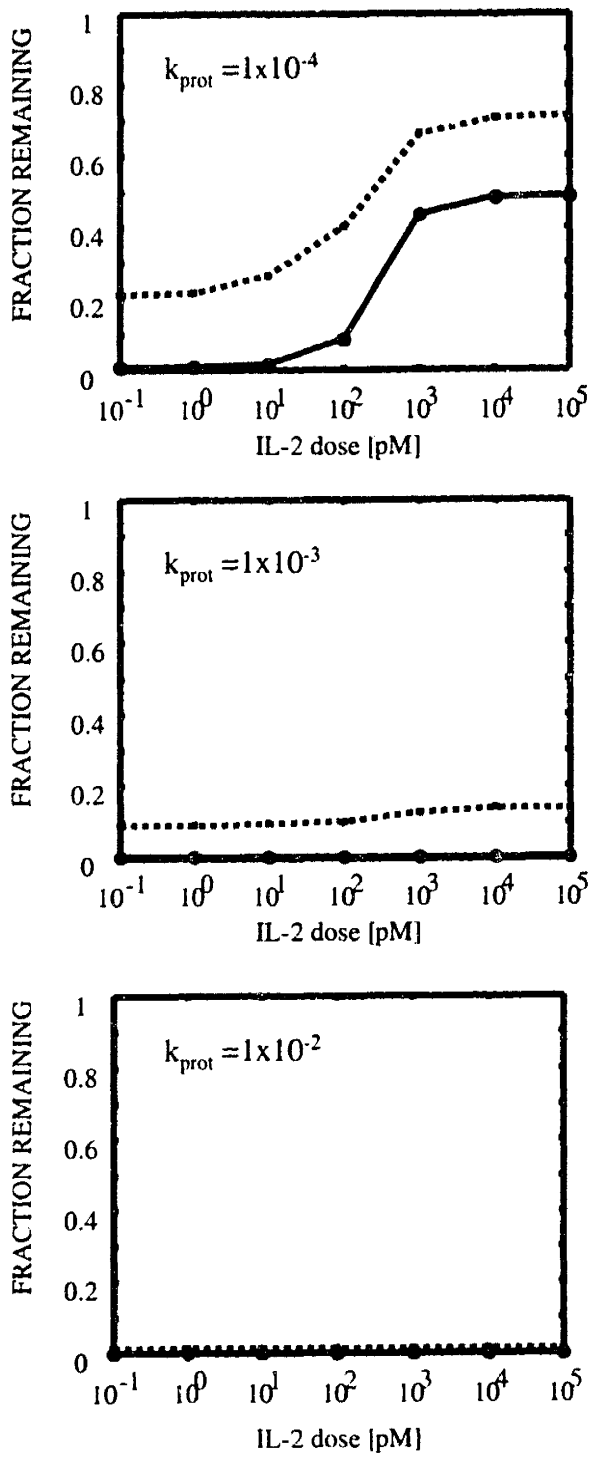

Figure 3-12: Extent of IL-2 ligand depletion as a function of proteolytic rate constant and delivery approach, either controlled-release (dotted line) or bolus administration (solid line).

maintaining sufficient tissue concentrations as on the intrinsic biochemistry by which the agent acts. Using the approach described in Section 3.2.2, spatial concentration profiles of interleukin-2 were defined by arbitrarily assigning an effective diffusion coefficient of 1 x 10^{-9} cm^2/sec, and by computationally determining the spatial profile of cellular signaling complexes as well as the ensuing tissue level proliferative response. For comparison, identical simulations were run using an effective diffusion coefficient of 1 x 10^{-8} cm^2/sec to assess the role of transport in defining tissue responses. As shown in Figure 3-13 and as expected, the penetration of growth factor was far greater when the diffusion coefficient was an order of magnitude greater. When the spatial profile of cellular response was determined by computationally measuring the number of cellular signaling complexes, there was a spatial mapping of complex number with the functional penetration of growth factors into the tissue, Figure 3-14. Moreover, when the cell density was computationally plotted, there was again spatial mapping between growth factor tissue concentration with tissue proliferation, suggesting a theoretical correlation between tissue concentration and response, Figure 3-15. Notably however, this relationship between tissue concentration and tissue response was found to be highly non-linear, Figure 3-16.

3.4 Discussion

3.4.1 Cellular pharmacology

As shown in data obtained in Section 3.3.1, ligand receptor trafficking was found in computational simulations to theoretically play an important role in determining the response to sustained delivery and bolus administration. Not surprisingly, individual trafficking parameters defined theoretical regions where sustained-release enhanced cellular signaling as compared to bolus administration. Parameters such as the rates of extracellular proteolysis, receptor recycling, receptor synthesis, and initial receptor number were found to be important determinants of theoretical delivery outcomes. Contour plots demonstrated dramatic variations in the relative number of complexes that were formed via sustained release versus bolus administration. Notably, changes in individual rate constants were found to lead to either large or small changes in receptor-ligand complex generation. Lastly, computational modeling of growth factor interaction with matrix binding suggests that functionally matrix binding sites mimic sustained delivery, as reported in the literature, and lead to enhanced signaling.

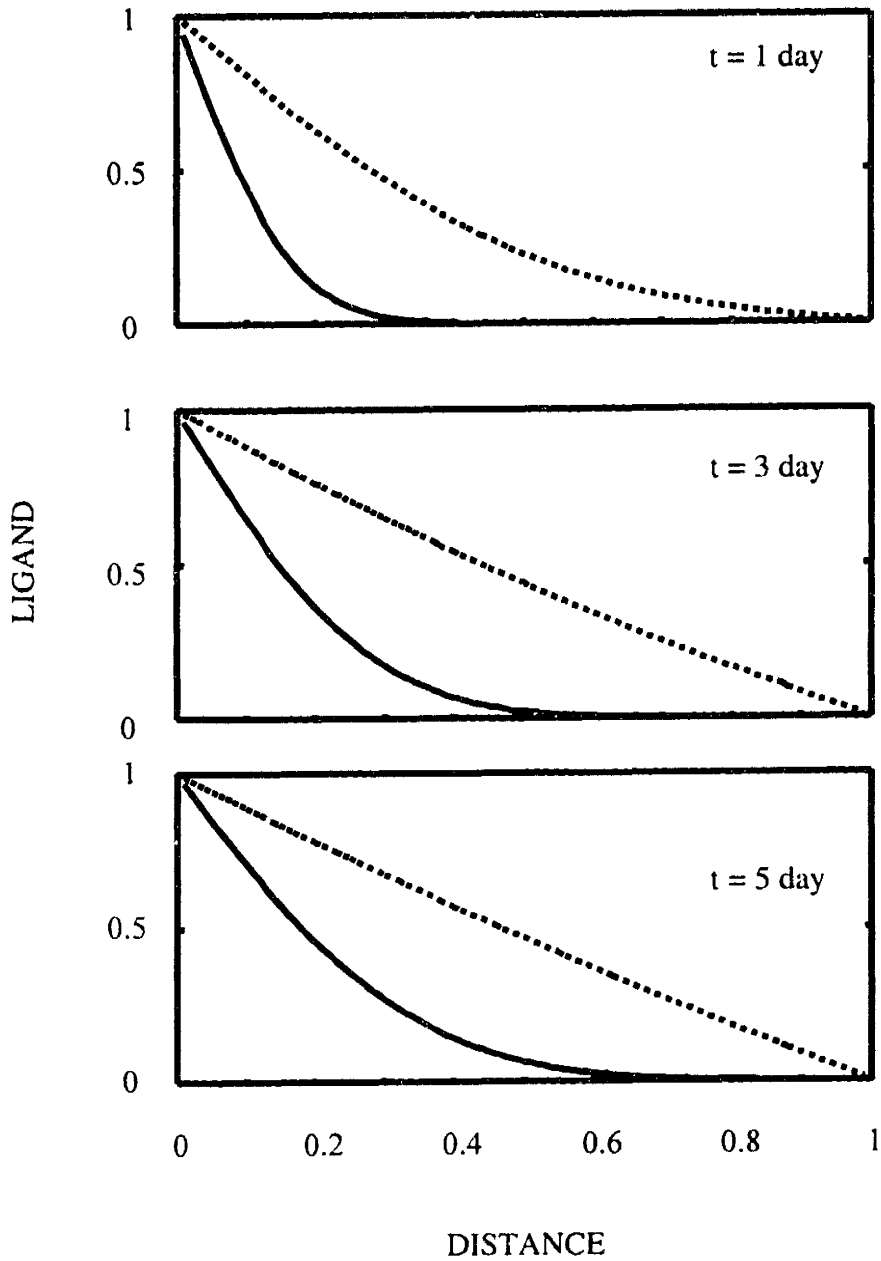

Figure 3-13: Scaled ligand profiles as a function of time for tissue pharmacology model. IL-2 with hypothetical 10-fold increase in diffusivity is plotted as the dotted data versus solid data control.

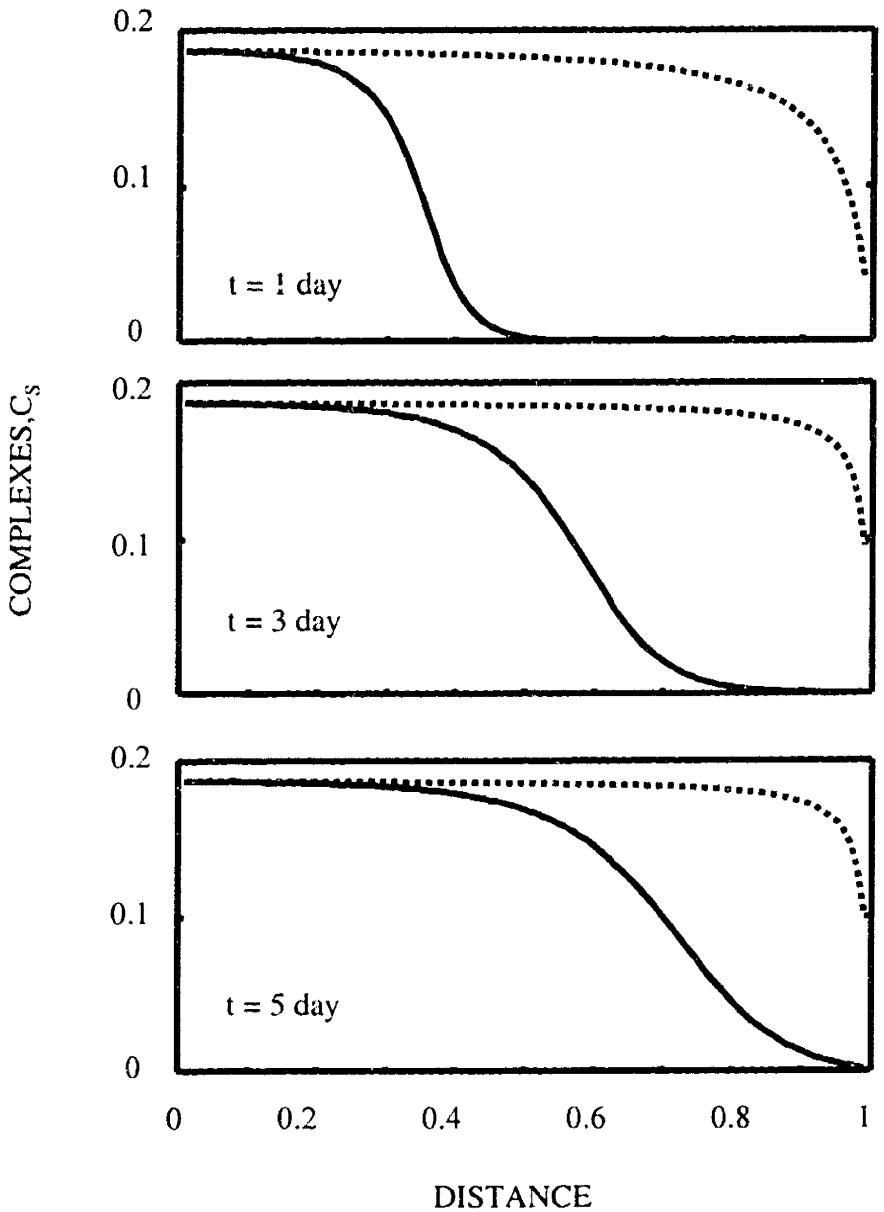

Figure 3-14: Scaled complex profiles as a function of time for tissue pharmacology model. IL-2 with hypothetical 10-fold increase in diffusivity is plotted as the dotted data versus solid data control.

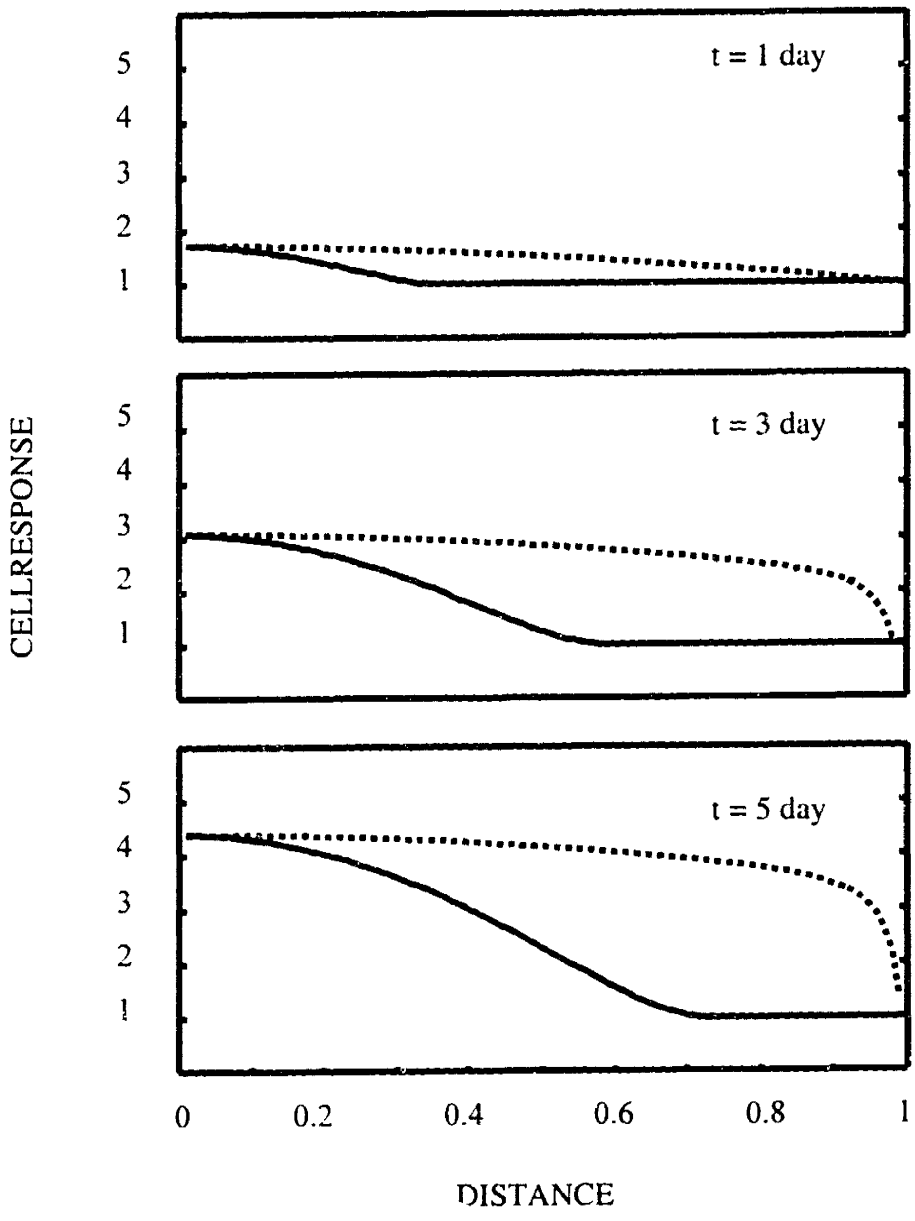

Figure 3-15: Scaled cell density as a function of time. IL-2 with hypothetical 10-fold increase in diffusivity is plotted as the dotted data versus solid data control.

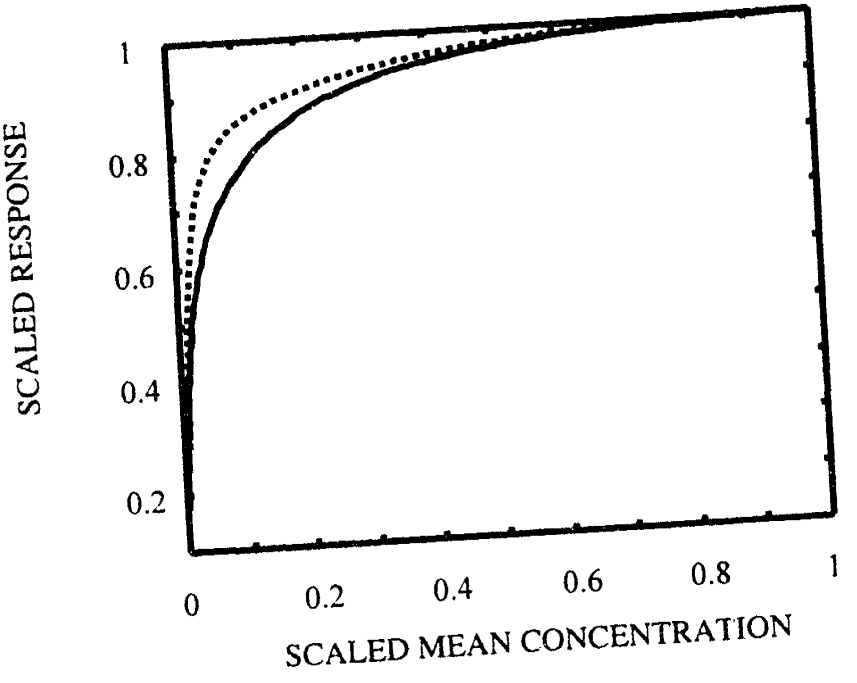

Figure 3-16: Correlation of theoretical mean tissue concentrations with tissue response. IL-2 with hypothetical 10-fold increase in diffusivity is plotted as the dotted data versus solid data control.

The importance of these data and this computational model is that together they allow one to determine a priori optimal delivery approaches based simply on knowledge of trafficking kinetics. Moreover, these data theoretically allow one to predict the functional response to the sustained delivery of a growth factor, as was demonstrated with the interleukin-2 system. As a result, potentially rational approaches can be devised for the optimal delivery of these agents.

3.4.2 Tissue pharmacology

Correlation between local concentrations and tissue responses is likely to become increasingly important in defining the therapeutic potential of locally delivered agents. Computational models such as that proposed in this Chapter may provide unique insights into theoretical approaches for optimizing tissue distribution and consequently biological effect for novel drugs. As shown in the model in Section 3.3.2, the effective transport of the drug into the tissue can spatially define local tissue concentrations, so that the subsequent biological response can be highly spatially non-linear. The importance of this sort of modeling is that it again allows one to determine a priori optimal delivery approaches based simply on knowledge of trafficking kinetics and transport parameters. As a result, potentially rational approaches can be devised for the optimal delivery of these agents.

3.5 Chapter Summary

To attempt to computationally model and predict the role of cellular and tissue pharmacokinetics on local growth factor delivery, two conceptual models based on cellular receptor-ligand trafficking events were implemented. In the cellular pharmacology model, variations in rate-limiting, experimentally accessible trafficking steps were conducted to determine optimal cellular responses as defined by a dimensionless ratio of cellular signaling achieved via sustained delivery versus bolus administration. Results from these studies identified theoretical domains where sustained delivery may engender significant enhancement in cell signaling versus bolus administration. Using an adaptation of this model, the role of matrix tissue interactions was assessed. Results from this study suggested a functional role of matrix interactions in enhancing cellular responses in face of tissue proteolysis. In the tissue pharmacology model, the relationship between tissue growth factor distribution and biological response was examined. It was found that this correlation was dependent on both transport

properties and cellular pharmacokinetics, and that spatial concentrations correlated non-linearly with tissue response.

4 TISSUE PHARMACOLOGY

Having defined experimentally the importance of cellular pharmacokinetics and also potential theoretical considerations for optimizing growth factor delivery, the roles of physiological transport forces and proteolytic limitations were examined next. The importance of these two potential barriers has not yet been considered for local growth factor delivery.

4.1 Background

The distribution of growth factors, or any therapeutic agent for that matter, can be limited by convection, molecular diffusion, and specific or nonspecific cell and tissue interactions. Impermeable barriers, such as the endothelium, may block the transport of growth factors across the blood vessels. Proteolytic fibroblasts or other cell types may degrade these molecules. Extracellular matrix binding sites may sequester growth factors and prevent their deep penetration. These mechanisms may serve together in part to limit the targeted delivery of growth factors. Conversely, growth factors may be specifically targeted to various sites as a result of high affinity binding to cellular receptors and tissue binding sites. Enhancement of growth factor transport may occur due to sequestration from extracellular proteolysis and vesicle mediated transcytosis [12]. Consequently, diffusion, convection, and diverse tissue interactions such as binding, metabolism, and sequestration complicate growth factor transport into target tissues [11]. The ability to define the mechanisms of transport of these proteins and definitively localize them in tissues may potentially be of quite great utility in enhancing the efficacy of their clinical use.

Several clinical examples exist where optimal targeted delivery of growth factors is of great importance. Foremost is the delivery of growth factors to enhance wound healing responses, tissue regeneration, and/or angiogenesis [6, 151-157]. In these applications, the delivery of intact, functional growth factor to a targeted site at an optimal concentration for a sufficient period is thought to be prerequisite for achieving the desired biological effect. Another important example is the delivery of molecular conjugates of growth factors. Through molecular cross-linking of bacterial toxins or specific genes with growth factors, molecular conjugates have been engineered to specifically target a certain population of cells based on selective receptor targeting. In these studies, receptor-mediated approaches for toxin and gene delivery, have resulted in increased specificity of targeting [158, 159].

As an extension of considerations at the cellular level, the effects of tissue pharmacokinetics on the efficacy of locally delivered growth factors was examined. An appreciation of the transport limitations and the degradative potential of tissues to which therapeutic growth factors are targeted in vivo, will potentially aid in the rational design and implementation of clinically useful delivery regimens. Moreover, this information may provide insight into the natural mechanisms that limit the spatial efficacy of paracrine growth factors. Therefore, this thesis considered first the role of physiological transport forces in governing the movement of drug from a model local delivery device, and second, the effect of proteolytic constraints in defining the functional penetration of therapeutic angiogenic molecules, specifically FGF-2 in the arterial wall. Insight into these two areas may be potentially useful for optimizing growth factor delivery.

4.1.1 Physiological transport forces

4.1.1.1 Pharmacokinetics of Heparin and Paclitaxel as model Growth Factors

To examine the role of physiological transport forces on growth factor delivery, an abundance of tissue specific pharmacokinetic data, such as effective diffusivities, convective velocities, and tissue partitioning constants, are necessary to be able to conceptualize a meaningful computational model. However, since there is only limited data of this type available in the literature, and since this laboratory has generated an abundance of pharmacokinetic data on two molecules, heparin and paclitaxel that span the potential range of binding and partitioning interactions that growth factors might have with tissues, these molecules were used as idealized substitutes for growth factors. In doing so, the role of physiological transport forces in local delivery was experimentally and computationally examined. The justification for this approach is grounded in the fact that the mathematical formulation for drug partitioning for heparin and paclitaxel is identical to that for growth factor tissue binding, as only equilibrium partitioning information is required to capture adequate detail for large Damkohler numbers [50, 160, 161]. Heparin, being a hydrophilic molecule and thus partitioning only sparingly into tissues, is representative of growth factors with minimal tissue binding such as TGFα and EGF. In contrast, paclitaxel, being a hydrophobic molecule and thus partitioning extensively into tissues, is representative of growth factors with significant tissue binding, such

as the heparin binding family of growth factors. With heparin and paclitaxel as conceptualized "growth factors," the role of physiological transport forces on local delivery was examined.

4.1.1.2 Stent-based Delivery

Stent-based drug delivery provides an intriguing paradox wherein the biological motivation for drug use does not necessarily predict efficacy. Drugs like heparin and dexamethasone inhibit smooth muscle cell proliferation in culture and intimal hyperplasia in animal models. However, clinically they have only mixed success in limiting thrombosis [162-164], and often, little effect in controlling intimal hyperplasia [165, 166]. The most recent compounds considered for stent release, paclitaxel for example, are of a far different sort than many of the compounds tested thus far, being hydrophobic in nature. Their effects in reducing intimal hyperplasia seem far more profound, and they have refueled enthusiasm for stent-based therapies [167]. The question, then, is whether drugs that have an effect when stent-released do so because of fundamentally different biological effects or because of different physicochemical properties and targeting.

Effective therapeutic delivery and targeting have profound importance above and beyond the treatment of proliferative vascular diseases. As blood vessels pose an excellent model in which to study how local delivery and transport determine and correlate with observed biological effect, the limitations imposed by local pharmacokinetics on the efficacy of stent-based drug delivery was examined. Both hydrophilic compounds with little partitioning into tissues, like heparin, and hydrophobic compounds with significant partitioning into tissues, like paclitaxel, as delivered from coated endovascular stents were considered. It was found that stent-based delivery leads to large Péclet number dependent concentration variability. While hydrophobic drugs exhibited more heterogeneous local tissue concentrations across the vessel wall than hydrophilic drugs, they achieved higher mean tissue concentrations and remained closer to the intima. The importance of acknowledging this difference between local and mean tissue concentrations becomes increasingly relevant as stent designs evolve to more complex geometries with inherent inhomogeneity in the circumferential and longitudinal distribution of stent struts. Since local drug concentrations and concentration gradients are inextricably linked to a drug's biological effect, these results provide a potential explanation for the variable success of stent-based delivery.

4.1.2 Proteolytic constraints on targeted growth factor delivery

While the localization of therapeutic compounds in tissues can provide an understanding of important rate-limiting steps and barriers to the targeted distribution of drugs, many conventional approaches for following drug transport and distribution are in fact limited in the information they can accurately provide. This is because with many of these approaches, one can only be certain of where the label distributes and not of where the drug distributes. Moreover, current methods cannot provide any information about the molecular integrity of the drug within the tissue environment. In general, it is assumed that the distribution of the label correlates identically with the distribution of the drug, and that no dissociation of label and drug or metabolism of the drug-label complex occurs. Due to this fundamental limitation, a novel method to ascertain molecular integrity for local delivery was developed, characterized, and tested in an ex vivo explanted bovine carotid artery model. This method was based generally on the phenomenon of fluorescence resonance energy transfer (FRET) and specifically on the phenomenon of intramolecular fluorescence quenching (IFQ).

Fluorescence resonance energy transfer (FRET) is the non-radiative energy transfer between appropriately oriented dipoles of two fluorophores located within 10-100 angstroms of each other [168-170]. Upon excitation of the donor group by a photon of appropriate wavelength, energy is non-radiatively transferred from the donor group to the acceptor group by resonance via transiently induced dipoles of the two dyes. Effectively, the conjugate pair fluoresces at the acceptor's emission wavelength rather than at the donor's emission wavelength (Figure 4-1). When this resonance energy transfer is physically disrupted due to physical separation of the dye pair, the acceptor dye no longer fluoresces, and the donor begins to fluoresce at its characteristic emission wavelength (Figure 4-2). The use of this phenomenon can thus provide detail about the molecular integrity of the double labeled conjugate [171-174].

A comparable method, known as intramolecular fluorescence quenching (IFQ) is based upon the same mechanism in which fluorescence is quenched due to resonance energy transfer between one fluorescent donor group and this time a non-fluorescent acceptor group [175, 176]. As a result of resonance energy transfer, fluorescence from the donor dye is quenched when the dye pair is physically localized together, Figure 4-3. When the dyes are separated, quenching is relieved and the molecular conjugate fluoresces at the donor emission's wavelength. Thus, like

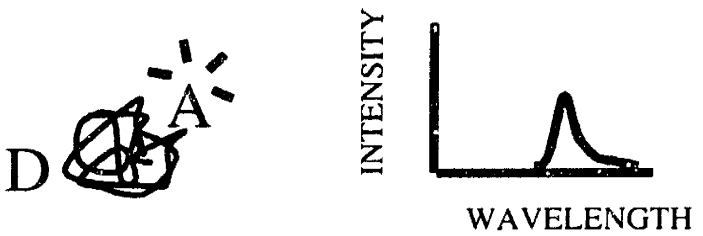

Figure 4-1: Fluorescence resonance energy transfer demonstrating quenching of donor dye, and fluorescence of acceptor dye.

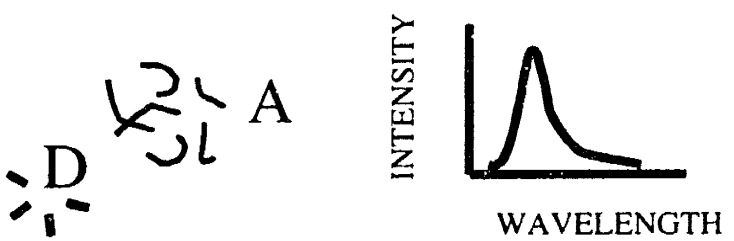

Figure 4-2: Fluorescence resonance energy transfer demonstrating relief of quenching and fluorescence of donor dye.

FRET, IFQ can provide information about the molecular integrity of a double-labeled substrate, Figure 4-4.

In studies performed in this thesis, a molecular conjugate capable of IFQ was synthesized, characterized, and tested in an experimental tissue model to determine the effects of tissue level proteolysis on local delivery. Using both cysteine and lysine chemistry with QSY-7 maleimide as a non-fluorescent acceptor and tetramethylrhodamine succinimidyl ester as a fluorescent donor respectively, (Molecular Probes, Eugene, OR), an IFQ conjugate was constructed using basic fibroblast growth factor (FGF-2). The conjugate was assayed for fluorescence activity when subjected to degradation by the proteolytic enzymes trypsin, plasmin, and thrombin. Moreover, its heparin binding activity was probed with fast liquid protein chemistry and biological activity with cellular proliferation studies. Ex vivo studies using an explanted bovine carotid artery model demonstrated lack of proteolytic activity on FGF-2 in the arterial media. Quantitative fluorescence microscopy demonstrated that there was no increase in fluorescence intensity as compared to identical conditions incubated either protease inhibitors or heparin. In contrast, pre-digested conjugate via trypsin proteolysis fluoresced intensely in the arterial media. To generalize these findings, the general proteolytic potential of this tissue model was examined through the use of several commercially available intramolecularly quenched substrates. These studies revealed a high level of thrombin or thrombin-like activity found in the arterial wall. These data together provide a novel approach for assessing the molecular integrity of growth factors in local delivery and demonstrate that in face of high proteolytic activity within the arterial wall, FGF-2 is not substantially degraded.

4.2 Materials and Methods

4.2.1 Physiological transport forces

4.2.1.1 Stent Delivery Devices

Palmaz-Schatz Crown stents (Cordis, Johnson & Johnson, NJ, 15 x 4 mm) were spray coated with 33% wt/wt fluorescein sodium/ethylene vinyl acetate copolymer (Elvax 40P, Dupont Chemical Co., DE) dissolved in dichloromethane. Bovine carotid arteries were obtained from a slaughterhouse, and cylindrical segments, 2-4 cm long, were cleaned, inspected for leaks, and cannulated. Drug coated stents were balloon expanded into cannulated artery segments at 12

Figure 4-3: Intramolecular fluorescence quenching demonstrating quenching of donor dye when dye pair are within Förster distance.

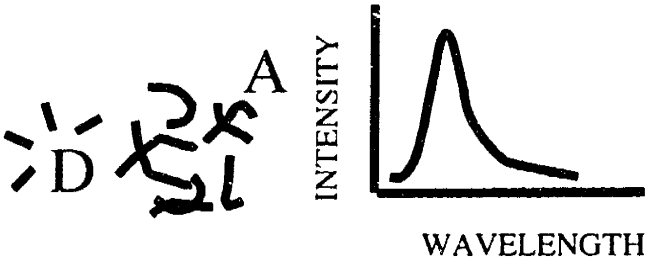

Figure 4-4: Intramolecular fluorscence quenching demonstrating relief of quenching due to physical separation of dye pair.

ATM. Stented arteries were positioned in an ex vivo perfusion apparatus [86] and immersed in a perivascular bath of PBS^{++} (Sigma-Aldrich, MO). PBS^{++} was circulated in an open loop at 0.6 ~ 0.7 mL/sec and 100 mm Hg pressure to simulate flows in coronary arteries. After a 3-hour perfusion, arteries were transversely cut in half for bulk elution and imaging. Arteries were cryosectioned into 20-μm thick en face slices (Cryotome SME, Shandon). The length and width of each slice were measured to compute the slice volume (V_{Slice}). Sections for bulk elution were transferred in groups of three into a 5 mL PBS^{++} bath (V_{Bath}), and stored at 4°C for 48 hours. The bath fluorescein concentration (c_{Bath}) was measured with a spectrofluorimeter (Fluorolog 1681, SPEX), and the tissue concentration was determined. Images of drug distribution were obtained immediately after sectioning using a fluorescence microscope (Optiphot-2, Nikon) with a 465-495 nm excitation filter, a 505 nm dichroic filter, and a 515-555 nm barrier filter. The average fluorescence intensities, and thus concentrations of regions corresponding to unit stent cells, were compared to bulk elution measurements. To convert fluorescence intensities to tissue concentrations, separate arteries were incubated in serial dilutions of fluorescein for 48 hours and imaged with the identical setup. The average intensity of a 40,000-square-pixel region was correlated with bulk phase incubation fluorescein concentration [177]. This was then converted to tissue concentration by multiplying the former by the fractional free space available to fluorescein in the media, measured in separate equilibrium incubation experiments.

4.2.1.2 Computational Model

In contrast to the computational approach used in Chapter 3 which was especially theoretical, the model implemented here was conceptualized so that it depended entirely upon experimental data previously obtained from the Edelman laboratory. As such, not only is the model approach here inherently more robust and better suited to provide insight into experimental data, it is much more interesting and relevant for local delivery. In addition, this model investigates the roles of convection, diffusion, and partitioning, whereas the model in Chapter 3 investigated only diffusion and cellular trafficking.

Transport in the arterial media is described by the convection-diffusion equation:

$$\frac{\partial C}{\partial t} + V_r \frac{\partial C}{\partial r} + \frac{V_\theta}{r}\frac{\partial C}{\partial \theta} + V_z \frac{\partial C}{\partial z} = D_r\left(\frac{1}{r}\frac{\partial}{\partial r}\left(r\frac{\partial C}{\partial r}\right)\right) + D_\theta\left(\frac{1}{r^2}\frac{\partial^2 C}{\partial \theta^2}\right) + D_z\left(\frac{\partial^2 C}{\partial z^2}\right),$$ where C denotes local tissue drug concentration. Both diffusion (D_r, D_θ, D_z) and convection (v_r, v_θ, v_z) are

directionally dependent. However, the only significant pressure drop occurs across the arterial wall, and therefore convection in all but the radial direction can be neglected. Hydrophobic drugs are modeled with a partition coefficient κ, defined as the tissue to bulk phase concentration ratio, which is dramatically different for hydrophilic and hydrophobic drugs and can be spatially dependent [178]. The intima flux is $J_{in} = R_{end}^{-1}(C_{ev}-C_{im}\kappa_{im})-V_r C_{ev}$, , where C_{ev} is the endovascular drug concentration, and C_{im} and κ_{im} are the tissue drug concentration and partition coefficient in the media adjacent to the intima. The adventitial flux has a similar form.

Assuming a media thickness, L, and defining dimensionless variables $K = C/C_{sd}$, $\eta = r/L$, $\zeta = z/L$, $\tau = D_r t/L^2$, the model can be reduced to a finite difference form as:

$$\frac{\Delta K_{m,n,q}}{\Delta \tau} = \frac{\Delta K_{m-1,n,q} - 2K_{m,n,q} + K_{m+1,n,q}}{\Delta \eta^2} + \frac{1}{\eta_{m,n,q}} \frac{K_{m-1,n,q} - K_{m+1,n,q} + K_{m+1,n,q}}{2\Delta \eta}$$

$$+ \frac{D_\theta}{D_r} \frac{1}{\eta_{m,n,q}^2} \frac{K_{m,n-1,q} - 2K_{m,n,q} + K_{m+1,n,q}}{(\Delta \theta)^2} + \frac{D_z}{D_r} \frac{1}{\eta_{m,n,q}^2} \left(\frac{K_{m,n,q-1} - 2K_{m,n,q} + K_{m,n,q+1}}{(\Delta \zeta)^2} \right)$$

$$- Pe \left(\frac{K_{m-1,n,q} - K_{m,n,q}}{\Delta \eta} \right)$$

where the only relevant transport parameters are now the dimensionless diffusivity ratios D_θ/D_r and D_z/D_r, and the transmural Péclet number, Pé = $V_r L/D_r$, the ratio of convection to diffusion. Experimental measurements and order of magnitude analysis suggest an anisotropic media diffusivity, $D_\theta \sim 10\ D_r$ (data not shown). This result was implemented without loss of generality since the solution for other degrees of anisotropy can be obtained by scaling the θ and z coordinates by appropriate factors.

4.2.1.3 Simulation Parameters

Stents were modeled as comprising variably-spaced drug-eluting struts with steady zero-order release. The dimensionless strut concentration C_{sd} was defined as the maximal exposed tissue dose. Transmural Péclet numbers were from 0 to 100, spanning beyond the physiological range of drugs as determined from experiments previously performed with heparin [86] and paclitaxel [178]. Drug entering the lumen was presumed to be washed out, resulting in the luminal condition $C_{ev} = 0$. Endothelial denudation with stenting was assumed to reduce luminal resistance to 0 sec/μm [69]. The perivascular condition was defined by an adventitial resistance, R_{adv}, of 5 sec/μm [69]. Hydrophobic compounds have spatially dependent partition coefficients,

and in this study, data accumulated with paclitaxel were employed [178]. To examine how inhomogeneous strut placement affects drug distribution, Monte Carlo simulations (n = 90) were conducted by randomly placing struts in non-overlapping positions. The concentration variability was then assessed using the Coefficient of Variation, defined as the standard deviation of local concentrations referenced to the overall mean concentration. All simulations were run to steady-state, defined as a change in overall drug concentration of less than 0.0005 dimensionless drug units/sec.

4.2.2 Proteolytic constraints on local delivery

Because the local concentrations of soluble growth factors are presumably important for defining the subsequent tissue response, it has been unclear to what extent poor targeting versus proteolysis and degradation of growth factor is limiting. In a parallel inquiry to the role of transport forces, the role of proteolysis is examined as a potential barrier for local growth factor delivery.

4.2.2.1 Synthesis of Intramolecular Quenched FGF-2

Generally, basic fibroblast growth factor, FGF-2, a gift from Dr. A. Protter, was loaded onto a 1 ml HiTrap Heparin column (Amersham Pharmacia-Biotechonlogy) at 10 μg/μl in PBS^{++}, preloaded with 1 mg/ml ovalbumin in PBS, pH 7.0 to minimize non-specific binding. Growth factor was allowed to bind for at least one hour on ice with or without ^{125}I-Bolton-Hunter-Reagent-FGF-2 in some cases to enable tracking of the fluorescent conjugate. 20-fold molar excess relative to FGF-2 of QSY-7 maleimide dye (Molecular Probes, Eugene, Oregon) was then added to the column via syringe in 1 ml of 1 mg/ml ovalbumin in PBS, pH 7.0. The reaction was allowed to proceed for at least 7 hours on ice. Next, using fast protein liquid affinity chromatography (FPLC) (Amersham Pharmacia Biotechonlogy, Piscataway, NJ), the unconjugated QSY-7 dye was removed with at least 200 column volumes of 0.15 M NaCl in PBS, pH 7.4. The elution was monitored by γ-counting and measuring absorbance at 280 nm. In addition, the eluent was visually assessed for the presence of the non-fluorescent dye. The pH was then rapidly changed to pH 8.5 through the introduction of 5 ml of sodium bicarbonate, pH 8.5, and confirmed by testing with pH paper. 20 fold-molar excess of TAMRA-TMR succinimidyl ester (Molecular Probes, Eugene, OR) relative to FGF-2 was diluted into 1 ml of sodium bicarbonate buffer, pH 8.4, centrifuged to remove precipitates, and loaded onto the

HiTrap column. The reaction was allowed to proceed for a minimum of 12 hours on ice. The HiTrap column was then again placed in-line on the FPLC and the unconjugated TAMRA-TMR-SE dye was eluted with approximately 200 column volumes of 0.15 M NaCl in PBS, pH 7.4. Elution was monitored by γ-counting, measuring absorbance at 280 nm, and fluorescence using Fluoroskan II, excitation 544 and emission 590 nm (Lab Systems Oy, Helsinki, Finland). The FGF-2 dual labeled conjugate was subsequently eluted off using a step gradient from 0.15 M NaCl to 2 M NaCl in 10 mM phosphate buffer, pH 7.4. Fractions were collected and subjected to ultracentrifugation to desalt and remove unbound, unconjugated dye using a nominal molecular weight cutoff of 10,000 g/mol (Millipore, Bedford, MA). Dye labeling ratios were calculated as described in product literature and protein concentrations were determined by absorbance at 280 nm or by ELISA (R&D Products, Minneapolis, MN).

4.2.2.2 Proteolytic assays

To define the functional response of the Quenched FGF-2 conjugate to protease digestion, conjugate was mixed either with PBS^{++}, chondroitin sulfate A (final concentration 100 μg/ml) or heparin (final concentration 100 μg/ml) and allowed to pre-equilibrate for at least 10 minutes on ice. Next, either trypsin (50 mg/ml), plasmin (1 Unit/ml) or thrombin (50 units/ml) were mixed into 100 ml of PBS++. The proteolytic solutions mixed with the quenched conjugate were subsequently added to 96-well plates and assayed for fluorescence activity as a function of time at room temperature using a 96-well plate fluorescent reader, Fluoroskan II, (Lab Systems Oy, Helsinki, Finland). Results were normalized to the initial fluorescence at time zero, t=0, and plotted as the mean ± standard deviation of at least 3 independent replicates.

4.2.2.3 Ex vivo tissue model and assessment of proteolytic activity

To assess the proteolytic activity of quenched FGF-2 in the arterial wall, bovine carotid arteries were harvested as described in Section 4.2.1.1. Next, the arteries were sectioned into 5 mm cylindrical segments and incubated in 2% penicillin-streptomycin in PBS^{++} at 4°C to minimize bacterial contamination. The tissues were then cultured routinely in Dulbecco's Modified Eagle's Medium and 10% fetal bovine serum under 10% CO_2 at 37°C. To assess the health of the tissue during ex vivo culturing, the LIVE/DEAD Assay by Molecular Probes (Eugene, OR) was used at various times from one to eight days.

Quenched substrates were incubated in DMEM/10% FBS at either 500 nM concentrations for commercially available substrates (R-6501, R-6502, R-6507, R-6516 from Molecular Probes, Eugene OR) or 50 to 100 μg/ml for quenched FGF-2. The solutions were then added to the explanted carotid segments alone, in the presence of heparin (final concentration 100 μg/ml, Pharmacia & Upjohn, Peapack, N.J.), or in the presence of protease inhibitors (Mini Complete, Roche Molecular Biochemicals, Indianapolis, IN). After the experiments, the cylindrical carotid segments were cryosectioned into 20-μm thick slices (Cryotome SME, Shandon) and imaged immediately using a fluorescence microscope (Optiphot-2, Nikon) with a 546/10 nm excitation filter, a 575 nm dichroic filter, and a 580 nm longpass filter. Specific regions of interest within the arterial media were highlighted and quantified for mean intensity using approximately 15,000 to 20,000 pixels after conversion of the color images to intensity plots using software from IP Lab Spectrum. Equilibrium experiments comparable to those described in Section 4.2.1.1 were used to define the functional response of the fluorescent microscope to varying concentrations of free tetramethylrhodamine incorporated into carotid arteries as done in Section 4.2.1.1.

4.3 Results

4.3.1 Physiological transport forces

As one obvious limitation of growth factor efficacy in vivo is adequate targeting, the role of physiological forces such as diffusion, convection and partitioning was examined. These studies are described in the following sections.

4.3.1.1 Concentration Variability

The initial impact of local drug delivery on the arterial wall and drug redistribution thereafter was examined. Initial attempts using bulk elution to determine uniformity of drug targeting following stent-based delivery revealed a flat radial drug concentration profile in the media that was indicative of convective transport with an average tissue concentration of 0.24 ± 0.02 mg/mL, (Figure 4-5). However, upon more detailed studies using quantitative fluorescence microscopy, dramatic spatial heterogeneity in tissue concentrations was observed, (Figure 4-6). Microscopic imaging of the arteries revealed zones of high and low fluorescein concentrations throughout the media that identically followed stent geometry. These zones corresponded to

tissue concentrations ranging from 0.06 to 0.97+ mg/mL, (Figure 4-7). Average media concentrations determined by microscopy were 0.22±0.03 mg/mL, matching bulk elution. Together, these results suggest that compartmental pharmacokinetics does not document the heterogeneous drug distribution as accurately as continuum pharmacokinetics.

4.3.1.2 Models of Transport

Theoretical models of stent-based drug delivery were developed to account for the experimental observations of dramatic concentration variations. These models demonstrated that for both hydrophobic and hydrophilic compounds, considerable variation of drug concentration in the arterial wall is present following stent-based delivery Figure 4-8. Large areas of high and low drug levels, relative to mean concentration, exist simultaneously at steady-state and are very close to one another. Such variations are present in both the circumferential and longitudinal directions. For hydrophilic drugs, some regions of the superficial layers of the media are nearly devoid of drug, while deeper layers have levels of drug several times the mean concentration. High drug regions increase in area with depth into the tissue. While hydrophobic compounds manifest similar variation patterns, they nevertheless distribute better, as regions with nearly no drug relative to mean concentration are in some cases 60% smaller than those of hydrophilic agents, depending on strut configuration. Both circumferential and radial concentration gradients are greatest near the struts and decay rapidly away before increasing again near the perivascular space. For hydrophilic drugs, peak circumferential gradients approach a concentration change of 20% C_{sd} per cell length and are independent of strut number in diffusion-dominated systems.

4.3.1.3 Transport Forces

Drug distribution is mediated first, by the use of struts as sources and second, by the balance between convective and diffusive forces on the specific compound. Strut-adherent release dictates sharp circumferential concentration gradients near the superficial layer where high drug zones are juxtaposed to stent struts with low drug zones in the interstrut spaces. The superficial drug distribution variation and mean concentration, which were lowest and highest respectively at low Pé, change minimally until Pé ~ 10, while overall tissue concentrations actually increase. Beyond this value, convection dominates, the variation increases, and both superficial and overall concentrations significantly drop (Figure 4-9). At very large Pé, where

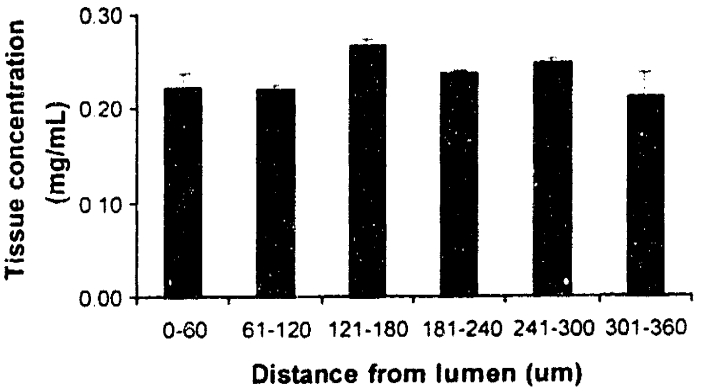

Figure 4-5: Elution studies suggest uniform concentration of fluorescein in arterial media

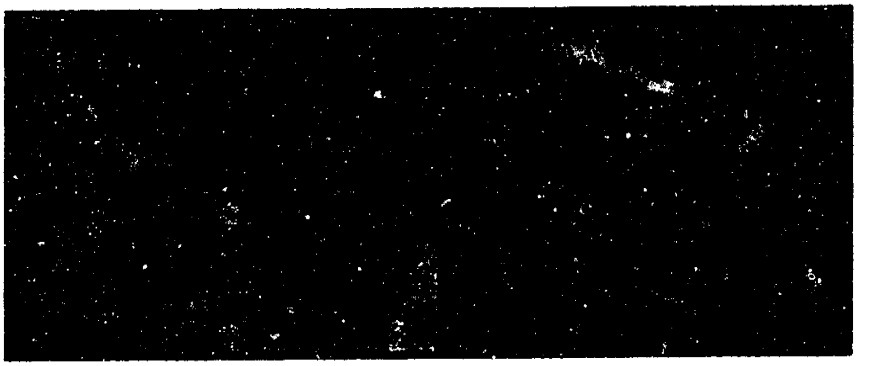

Figure 4-6: *En face* fluorescent microscopy image obtained at steady-state for stent-based drug delivery. Section taken at 200 μm depth into artery.

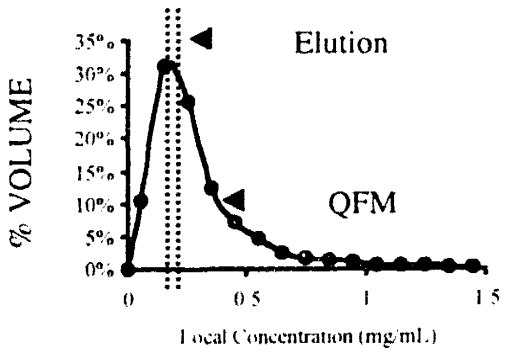

Figure 4-7: Comparison of drug distribution as assessed by bulk elution versus quantitative fluorescence imaging.

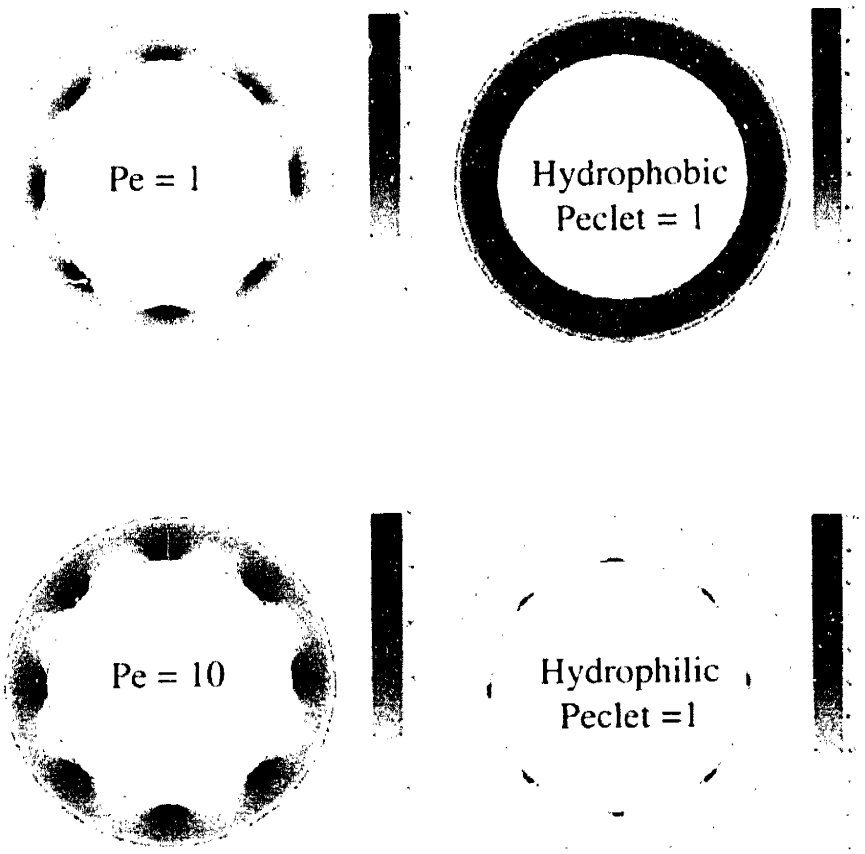

Figure 4-8: Computational simulations of stent-based delivery. Examples of various Peclet driven flows (left) and effect of drug partitioning (right).

drugs move exclusively by convection, superficial and overall mean tissue concentrations converge as alternating bands of transarterial high and low drug zones form. While hydrophobic drugs exhibit a higher overall variability than hydrophilic drugs, they preferentially remain significantly closer to the intima than hydrophilic drugs at all Pé (Figure 4-10).

4.3.1.4 Stent Geometry

As stent designs evolve toward more complex and more inhomogeneous strut configurations, the role of strut placement in determining drug distribution was examined. Monte Carlo simulations were conducted by randomly assigning strut positions without overlap (Figure 4-11). Mean arterial wall concentrations were independent of strut arrangement, but increased with strut number (n = 90) (Figure 4-12). Hydrophobic drugs distributed significantly more into the arterial wall than hydrophilic drugs. Uniformity of drug distribution also increased with strut number, but in contrast, was significantly dependent on strut arrangement. For hydrophilic drugs, the average difference in uniformity between homogeneous and inhomogeneous stent strut placement increased from 11% for a 4-strut stent to 33% for a 12-strut stent. In contrast, the distribution of hydrophobic compounds was slightly less dependent on strut arrangement, with the difference in uniformity increasing from 8% for a 4-strut stent to 21% for a 12-strut stent before decreasing for higher strut numbers.

4.3.2 Proteolytic constraints on growth factor delivery

To examine the role of tissue pharmacology on local growth factor delivery, the use of intramolecular fluorescence quenching was proposed as a method for assaying molecular integrity. In the following section, the set of experiments describe the experimental data that suggest that quenched FGF-2 is not significantly degraded upon local delivery to an explant bovine carotid artery model.

4.3.2.1 Synthesis and Characterization of Quenched FGF-2

To double label FGF-2 with an intramolecular quenched pair, two dyes, QSY-7 maleimide and TMR-TAMRA succinimidyl ester were chosen on the basis of their absorption and emission properties and reactivity for lysine and cysteine groups (Figure 4-13). As shown in this figure, the emission of TMR, the fluorescent donor in this dye pair, overlaps identically the absorption spectrum of the QSY-7 dye, the non-fluorescent acceptor. Coupling of these two

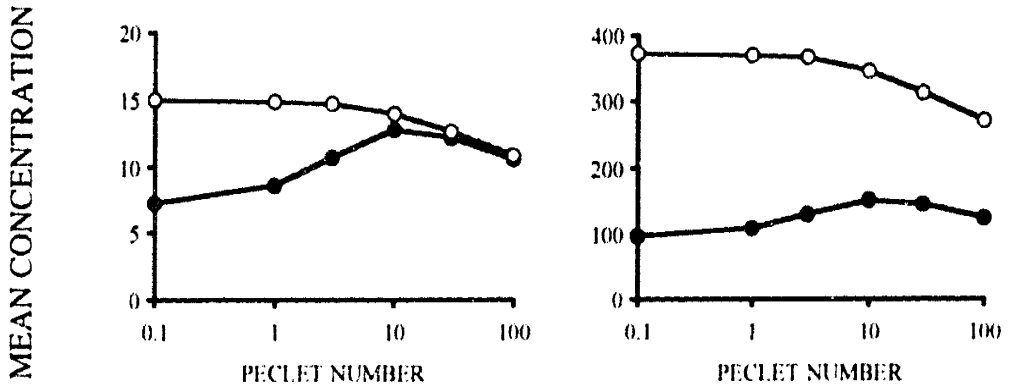

Figure 4-9: Comparison of hydrophilic (left) versus hydrophobic (right) superficial and overall tissue concentrations. Plotted are data averaged over the whole tissue (●) and data from the superficial lumenal layers only (○).

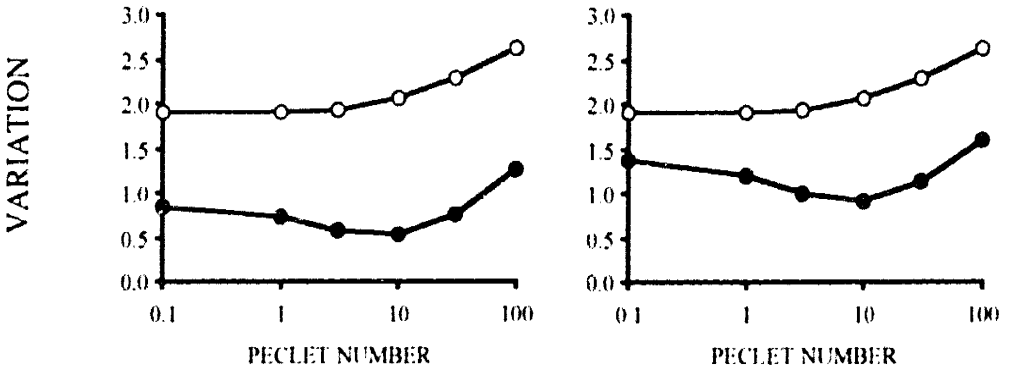

Figure 4-10: Comparison of hydrophilic (left) versus hydrophobic (right) superficial and overall variation in drug distribution. Plotted are data averaged over the whole tissue (●) and data from the superficial lumenal layers only (○).

Figure 4-11: Monte Carlo simulations examining the role of strut placement on subsequent drug distribution. The top result is for even strut distribution. The bottom two results are two representative Monte Carlo examples.

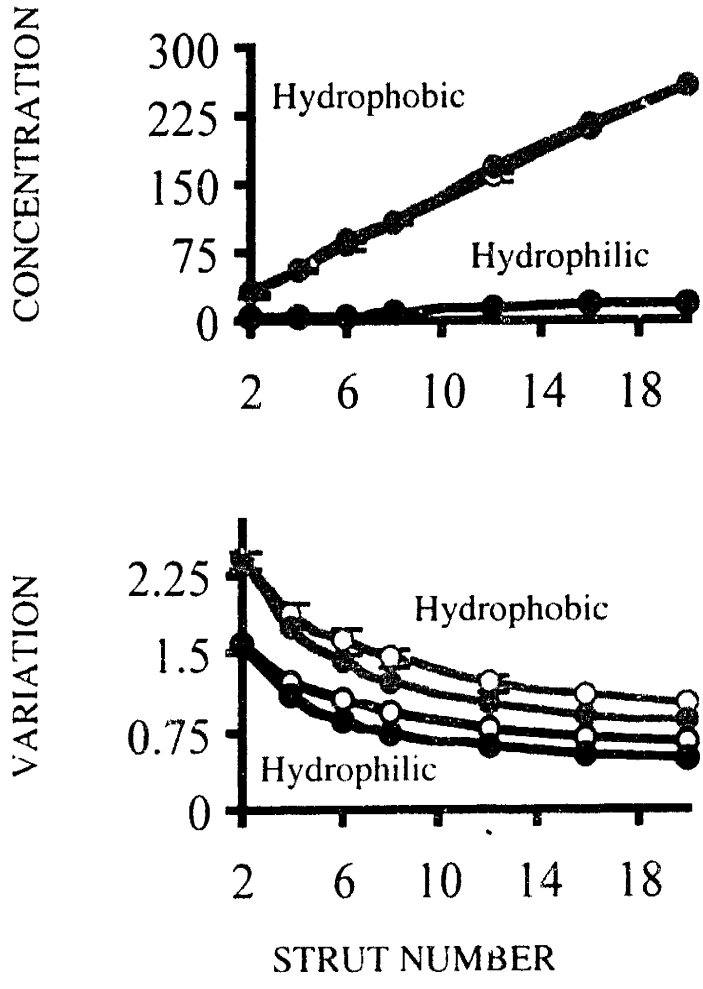

Figure 4-12: Comparison of Even versus Uneven (random) strut placement on Mean Concentration (top) and Variation (bottom) in drug distribution for hydrophilic (black) and hydrophobic (grey) compounds. Plotted are data for Monte Carlo simulations (O) versus data for even stent expansion (●).

dyes by resonance energy transfer therefore allows for efficient intramolecular quenching of TMR when the dyes are effectively within their Forster distances. FGF-2 was labeled using a method based on protecting key residues on the molecule through heparin binding as described in the experimental methods [179]. Published x-ray crystallography data from the Protein Data Bank allowed the identification of two potential solvent accessible cysteine groups for sulfhydryl-chemistry and a plethora of lysine residues for amino-chemistry. In some labeling experiments, ^{125}I-Bolton-Hunter radiolabeled FGF-2 was used to aid in the isolation and assessment of heparin binding activity. After pre-blocking the column with ovalbumin, reactions with QSY-7 maleimide and TMR-TAMRA were allowed to proceed sequentially as described in the Section 4.2.2.1. The molecular conjugate was then eluted with a step change in salt concentration from 0.15 M to 2 M NaCl, and subsequently de-salted by centrifugation against a 10,000 nominal molecular weight cutoff membrane (Millipore, Bedford, MA). To characterize the dual conjugation of this molecule, absorbance measurements were made using a Perkin-Elmer Spectrophotometer. As shown in Figure 4-14, the presence of both dyes in the de-salted 2 M NaCl eluent was confirmed with maximal peaks centered about 534 nm and 562 nm. In contrast, absorbance scans of PBS^{++} and the ultrafiltrate obtained from centrifugation through the 10,000 MWCO nominal cut-off demonstrated no peaks in the range of interest. Together, these data suggest that two dyes that constitute a pair for intramoleculer fluorescence quenching were successfully labeled onto a heparin binding protein of nominal molecular weight greater than 10,000, namely FGF-2.

To determine whether fluorescent labeling of FGF-2 negatively impacted on its heparin binding activity, a well-recognized property of FGF-2, the conjugate was re-loaded onto a 1 ml HiTrap heparin column and probed for binding specificity using a salt gradient from 0.15 M NaCl to 2 M NaCl. After an initial pre-wash of the column with approximately 45 mls of 0.15 M NaCl, a steep gradient of increased salt was run. As shown in Figure 4-15, increased salt concentration resulted in disruption of the ionic interaction between quenched FGF-2 and the heparin column, leading to elution off of the column with the main peak centered around 1.5-1.6 M NaCl. Comparison of the elution profile of the quenched conjugate with that obtained using radiolabeled FGF-2 that was not fluorescently labeled demonstrated that quenched FGF-2 maintained very similar heparin binding activity. This and other studies suggest that quenched

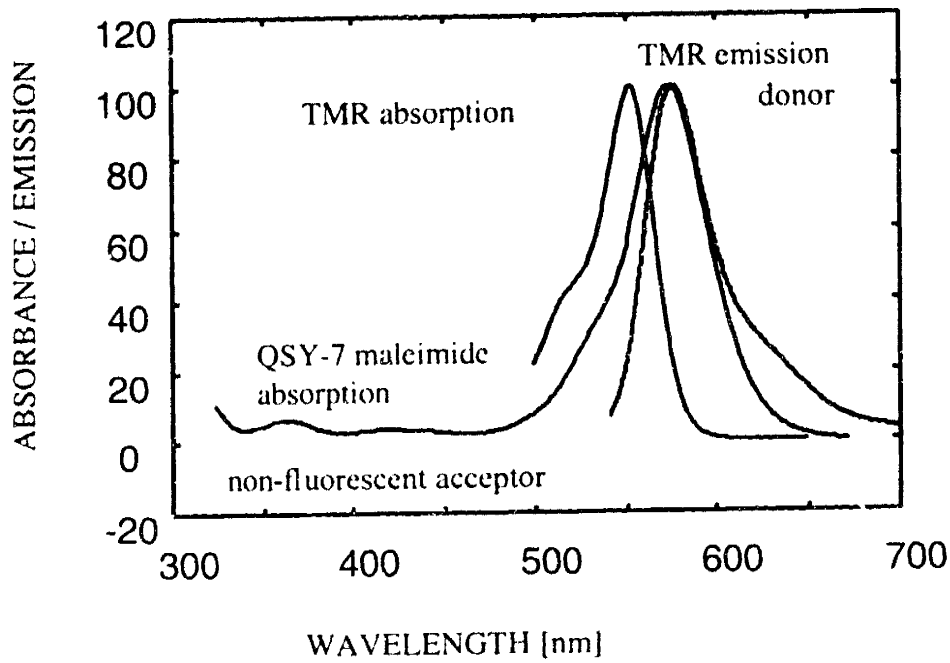

Figure 4-13: Absorption and emission scans of commercially available dyes chosen for intramolecular fluorescence quenching studies on FGF-2.

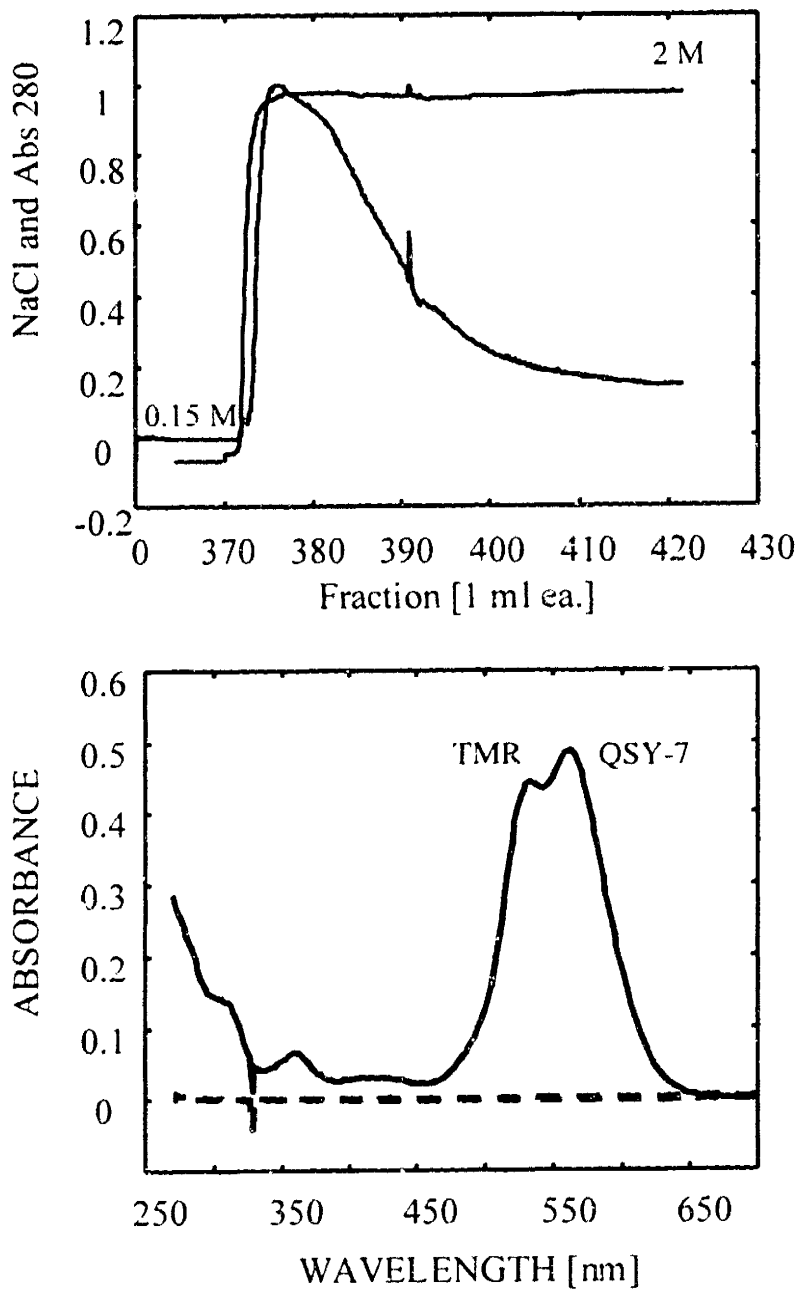

Figure 4-14: Top figure is 2 M NaCl elution of conjugate from Heparin column. Bottom figure is absorbance of de-salted conjugate (solid line) versus PBS^{++} and ultrafiltrate through 10,000 MWCO (dotted lines). Unlabeled FGF-2 has a similar absorbance profile as the PBS^{++} and ultrafiltrate curves in the range from 400 to 700 nm (data not shown).

FGF-2 retained its ability bind to heparin, and that the binding of this quenched conjugate to heparin is identical to that of unlabeled FGF-2.

To determine the biological activity of this quenched conjugate, NR6 3T3 fibroblasts were plated out at 5,000 cells per well, serum starved for 24 hours, and then treated with either quenched conjugate or unlabeled FGF-2. Cell number was determined on Day 3 by Coulter counting. As shown in Figure 4-16, cells responded equally to two doses of quenched FGF-2 and unlabeled FGF-2. These data are consistent with the fact that double labeling of the quenched conjugate on a heparin column effectively protects its biological activity.

To quantify the fluorescence response of quenched FGF-2, and thus determine whether enzymatic proteolysis would in fact relieve intramolecular quenching as hypothesized, PBS^{++}, heparin or chondroitin sulfate A at final concentrations of 100 μg/ml (Sigma Aldrich, St. Louis, MO), and either trypsin (50 μg/ml) or plasmin (1 unit/ml) was added to quenched FGF-2 in PBS^{++} in a total volume of 200 μl per well in a 96-well plate. Samples were then allowed to digest at room temperature over the time course of several hours to two days, and the level of fluorescence was measured using a fluorescent 96-well plate reader. As shown in Figure 4-17, chondroitin sulfate A did not protect the conjugate from proteolysis by trypsin. Thus, relief of intramolecular quenching by QSY-7 via tryspin digestion resulted in a relative increase in fluorescence. In contrast, heparin did protect the conjugate from proteolysis by trypsin, and hence no increase in fluorescence was observed. To confirm that this effect was specifically due to heparin binding to quenched FGF-2, conjugates (approximately 5 to 10 μg/ml) were first incubated with heparin at a final concentration of 100 μg/ml. After 10 minutes to allow for initial binding of quenched FGF-2 to heparin, trypsin was added to the system. Next, either enough salt to achieve a 2 M NaCl concentration or an equivalent amount of PBS^{++} was introduced. As shown in Figure 4-18, the introduction of high salt disrupted the protection of quenched FGF-2 by heparin binding and allowed the tryptic digestion of the conjugate, thus relieving intramolecular quenching. As a result, a relative increase in fluorescence was measured. In contrast, the addition of PBS^{++} did not result in a relative increase in fluorescence. To define the greatest potential change in relative fluorescence upon proteolysis, the conjugate was incubated for 24 hours and the resulting fluorescence was assessed. As shown in Figure 4-19, there was an approximately 12-fold increase in fluorescence after incubation for 24 hours at 37°C in the absence of heparin at 100 μg/ml and in the presence of trypsin (approximately 10

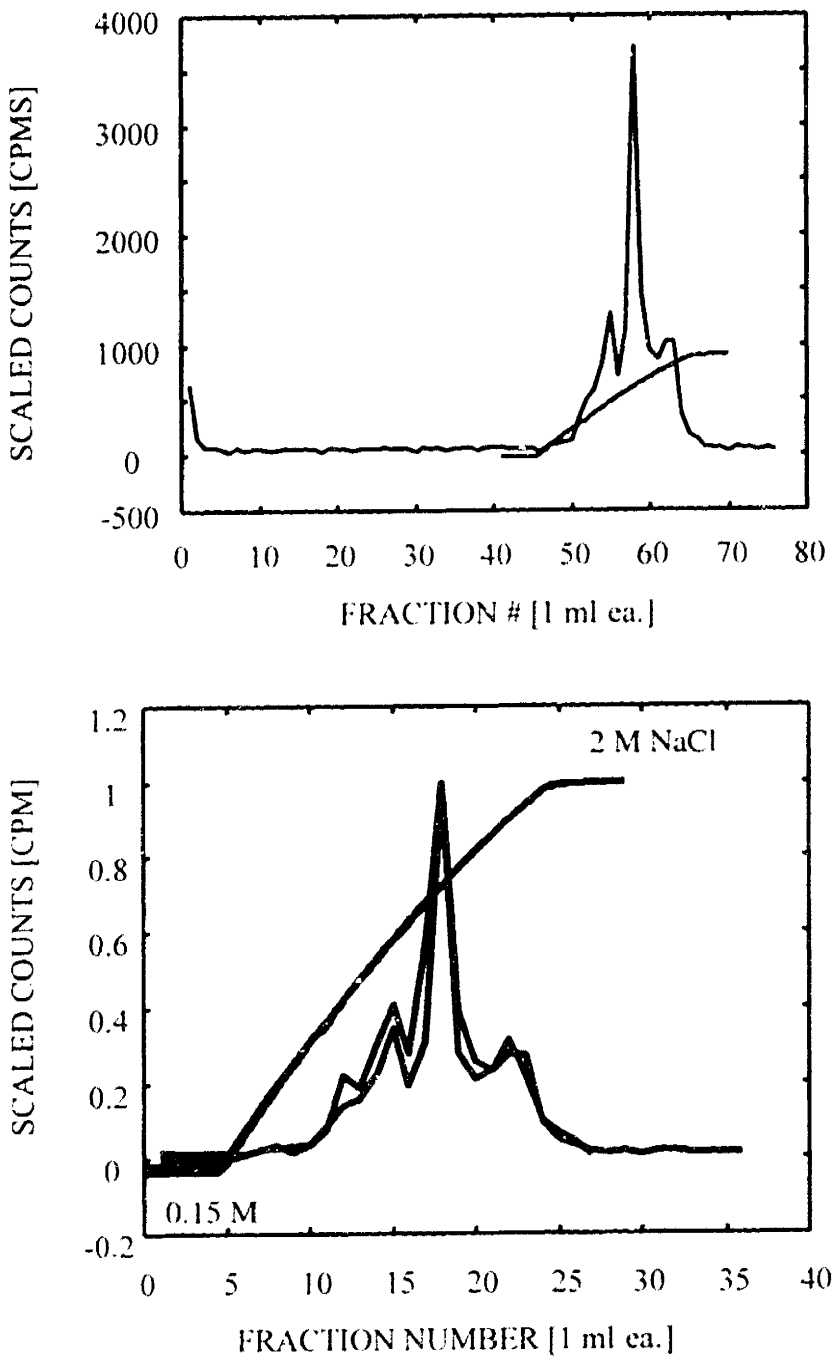

Figure 4-15: Elution of conjugate with salt gradient from heparin column to determine binding activity. Top is elution of conjugate alone. Bottom is elution of conjugate versus non-fluorescently labeled species.

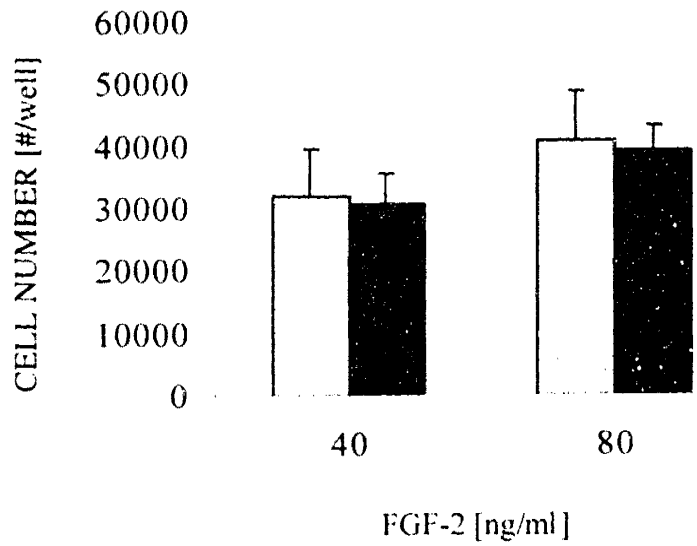

Figure 4-16: Determination of the biological activity of quenched FGF-2 (grey) versus unlabeled FGF-2 (black) in NR6 3T3 fibroblasts, Day 3 by Coulter counting.

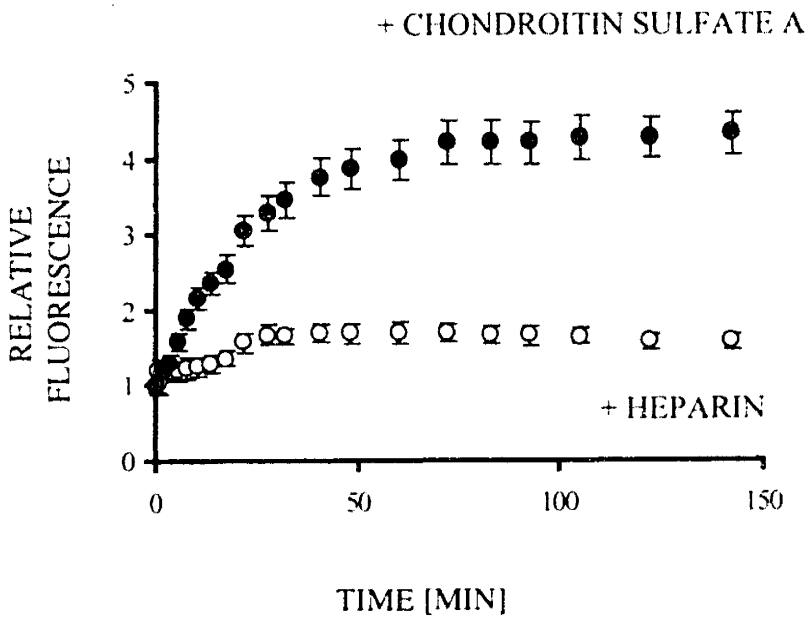

Figure 4-17: Effect of chondroitin sulfate A (●) or heparin (O) both at final concentrations of 100 µg/ml on protection of quenched conjugate from digestion by trypsin.

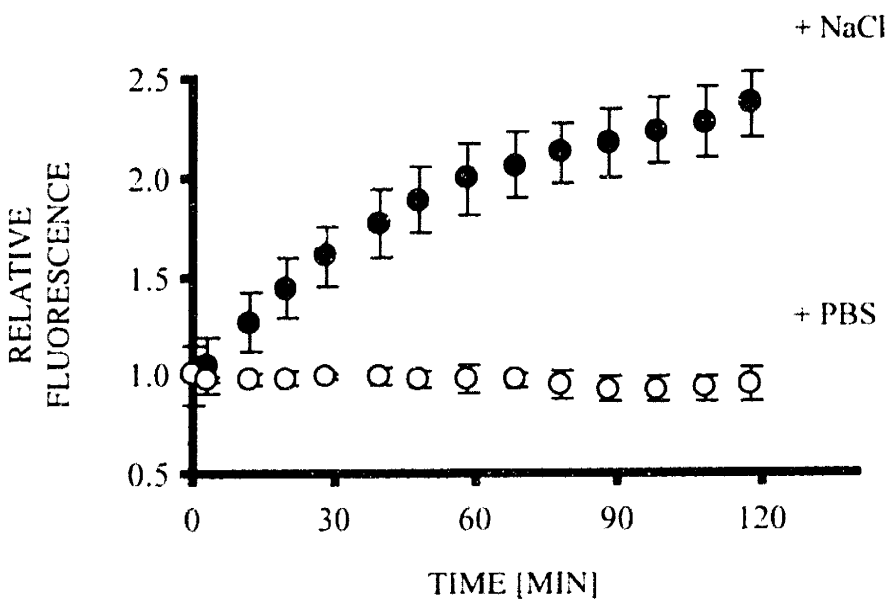

Figure 4-18: Effect of 2 M NaCl (●) or PBS (○) on disruption of protection by heparin of quenched conjugate from trypsin digestion.

μg/ml). In contrast, in the presence of heparin, there was only a minimal increase in relative fluorescence. Taken together, these results confirm that heparin can protect the integrity of the quenched growth factor from trypsin digestion, and that the interaction between quenched FGF-2 and heparin is specifically able to be disrupted by high salt concentrations and not PBS^{++}. Thus, FGF-2 has been successfully labeled with a dye pair that exhibits resonance energy transfer.

To further define the proteolytic sensitivity of the quenched conjugate, either plasmin (Sigma-Aldrich, St. Louis, MO) or PBS^{++} was added at a final concentration of 1 unit/ml to the quenched growth factor, and the time course of fluorescence was monitored versus the addition of PBS^{++}. As shown in Figure 4-20, there was a substantial increase in relative fluorescence upon the addition of plasmin that was similar to the increased fluorescence observed upon trypsin digestion. In contrast, no relative increase in fluorescence was detected upon the addition of PBS^{++}. These data suggest that the molecular conjugate is also sensitive to plasmin, confirming previous proteolytic studies on FGF-2 [180, 181].

4.3.2.2 Ex vivo Tissue models

To test the susceptibility of the quenched FGF-2 molecular conjugate to tissue pharmacokinetics, several attempts were first made to establish a rat myocardial model as this would have been most relevant and interesting with regard to clinical approaches for therapeutic angiogenesis. However, because of multiple difficulties, this approach was abandoned, and instead, an explanted bovine carotid artery model was used. This carotid artery model tissue is comparable to a porcine aortic tissue model that has been used extensively in the literature that has been demonstrated to remain functionally intact over the course of four weeks [182-184]. In these studies, rapid intimal hyperplasia can be induced under certain experimental conditions and mimic to an extent the in vivo pathophysiological process [182-184]. To confirm the reliability of this system, tissue viability was assessed using a pair of commercially available dyes that distiguish functionally live cells as defined by intracellular esterase activity versus functionally dead cells as defined by disrupted membrane integrity. Carotid artery explants were obtained as described in Section 4.2.1.1 and the adventitia was carefully teased off. Cylindrical segments approximately 5 mm in length were then distinguished using a sterile scalpel and incubated for 10 minutes in PBS^{++} with 2% penicillin-streptomycin to minimize bacterial contamination. Next, after culturing as described in the Section 4.2.2.3 and at various end points, Molecular

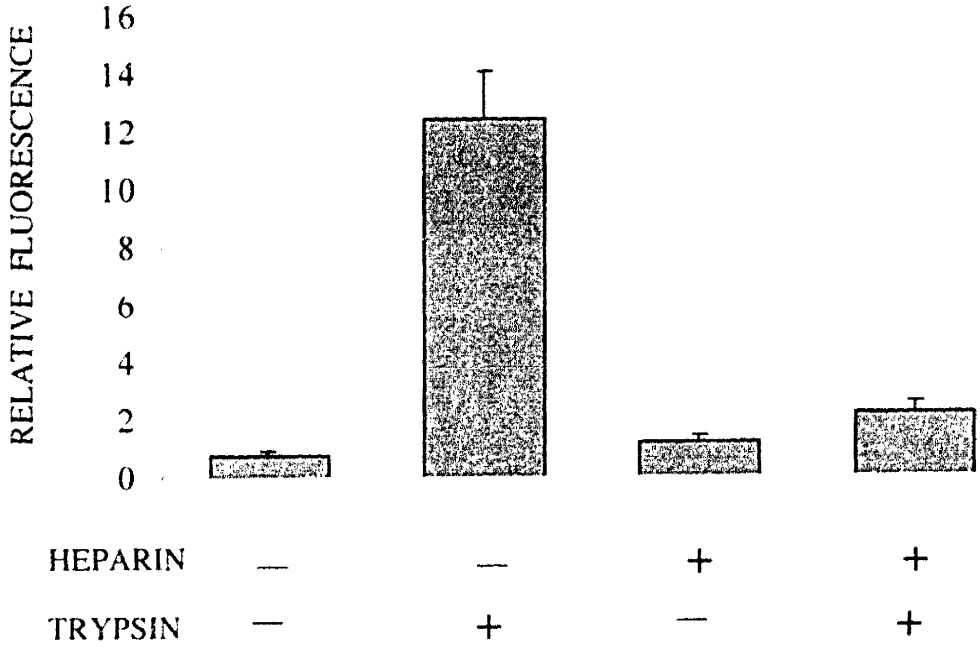

Figure 4-19: Exhaustive digestion of quenched conjugate in the presence or absence of heparin (100 µg/ml) and/or trypsin (10 µg/ml) at 24 hours at 37° C.

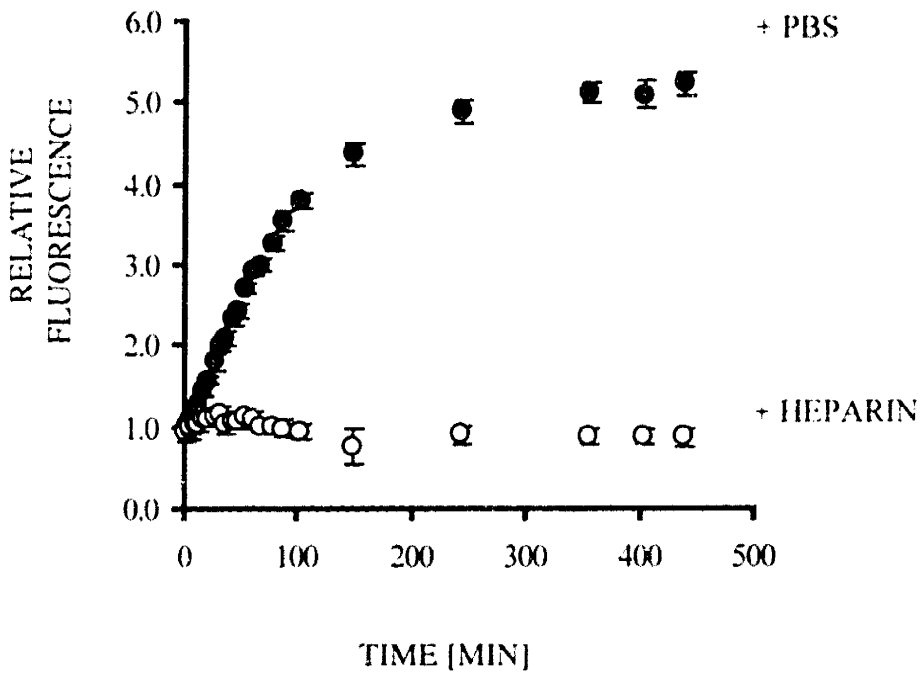

Figure 4-20: Effect of PBS (●) or heparin (○) on protecting quenched conjugate from digestion by plasmin as described in Methods.

Probes' LIVE/DEAD assay was used to functionally assess the health of the tissue. As shown in Figure 4-21, a high density of green punctate staining was visualized using en face fluorescent microscopy, suggesting the presence of functional cells on both Day 1 and Day 8. In contrast, in identical field of views, only minimal punctate red staining was observed, suggesting the presence of only few cells with disrupted membranes. These images were representative of at least six different sections and six different arterial explants at each time point. In this bovine carotid tissue model then, there is functionally intact intracellular esterase activity over the time course of 8 days and more importantly little, if any change at all, over this time period.

4.3.2.3 Tissue Response

Quenched FGF-2 was added with cylindrical segments of explanted bovine carotid arteries and incubated in the presence of protease inhibitors and heparin (100 μg/ml final concentration) in 10% FBS/DMEM. As a positive control, quenched FGF-2 was pre-treated with trypsin for four hours at 37°C before addition into the system. Based on an order-of-magnitude analysis for the minimum time required for effective diffusion into the carotid tissue, it was estimated that incubation of the carotid explants with quenched FGF-2 would need at the minimum two days to effectively penetrate the arterial wall [160]. Accordingly, explants were assessed for fluorescence activity within the arterial wall at an end time point of two days.

Using quantitative fluorescent microscopy, arterial segments were assayed for fluorescence in the arterial media after sectioning into 20 μm thick cylindrical segments. As shown in Figure 4-22, there was minimal fluorescence activity observed in carotid segments treated with approximately 80 μg/ml quenched FGF-2 alone, with quenched FGF-2 and protease inhibitors, and with quenched FGF-2 and heparin (n = 4 arterial samples, randomly sampled at 10 locations throughout the length of the explant.) In contrast, in carotid segments incubated with pre-digested FGF-2, there was bright fluorescence observed in the arterial media. Through the use of digital imaging software from IP Lab Spectrum, these images were quantified for intensity and the data are plotted in Figure 4-23. As shown similarly in the previous figure, only the carotid samples that were incubated with pre-digested quenched FGF-2 demonstrated significant fluorescence. These data suggest that in this bovine explant model, there is little proteolysis of quenched FGF-2.

To confirm this result and probe the conditioned media for the molecular integrity of

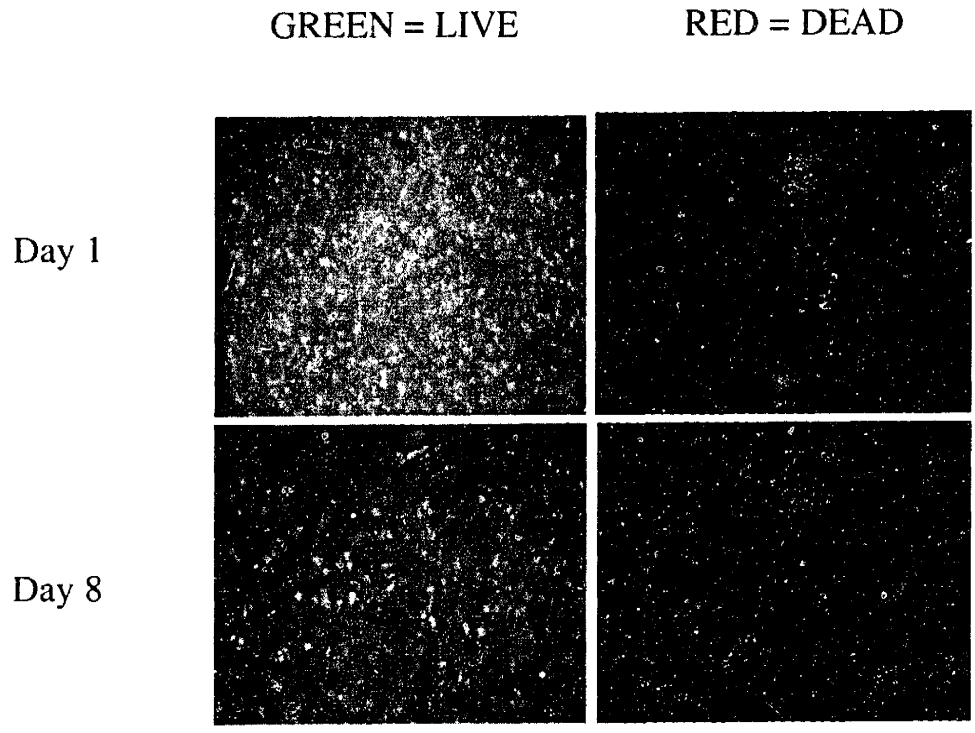

Figure 4-21: LIVE/DEAD Molecular Probes Assay used to probe integrity and health of explanted bovine carotid arteries on Day 1 and Day 8. Different specimens were imaged on each day. Representative images are shown.

growth factor, samples were taken of the conditioned media and were quantified for fluorescence using a 96-well plate reader. As shown in Figure 4-24, there was little fluorescence detected in the conditioned media of carotid explants incubated with quenched FGF-2 alone, with quenched FGF-2 and protease inhibitors, and with quenched FGF-2 and heparin. In contrast, there was a significant amount of fluorescence measured in the conditioned media obtained from carotid samples that were incubated with pre-digested quenched FGF-2. To confirm that quenched FGF-2 within the samples that demonstrated no fluorescence was not inactivated as an artifact, trypsin digestion was conducted on the media obtained from samples incubated with quenched conjugate alone and from samples incubated with conjugate and heparin, Figure 4-25. As shown in these data, conditioned media obtained from samples of conjugate alone fluoresced significantly upon the addition of trypsin, but not PBS^{++}. In contrast, conditioned media obtained from samples of conjugate and heparin did not fluoresce upon the addition of trypsin. This latter result was presumably due to protection of the quenched conjugate by heparin. Taken together, these results suggest the presence of intact quenched FGF-2 in all of the conditioned media of all samples considered except the one pre-treated with trypsin.

As the data obtained thus far provided only insight into the proteolytic susceptibility of one growth factor, FGF-2, within this model, the general proteolytic potential of the explant carotid model was defined. Using four commercially available intramolecularly quenched substrates, fluorescence activity in both the arterial wall and conditioned media was assayed as previously described. First, using the substrate R-6501 with susceptibility to plasmin and cathepsins, no enzymatic activity of this sort was found as shown in Figure 4-26. Second, using substrate R-6507, with susceptibility to trypsin and thrombin, a significant increase in fluorescence was measured in the arterial wall in the absence of protease inhibitors versus in their presence. This data suggest that there is high thrombin- or trypsin-like enzymatic activity in the wall. Lastly, using substrates R-6502 and R-6516 with respective susceptibilities to trypsin and thrombin like enzymes, the proteolytic activity observed with substrate R-6507 was determined to be the result of high thrombin or thrombin-like enzymatic activity and not trypsin or trypsin-like activity. Taken together, these data define the general proteolytic potential of the explanted bovine carotid artery model and extend the paradigm of using intramolecularly quenched substrates for defining the role of tissue pharmacokinetics in the arterial wall.

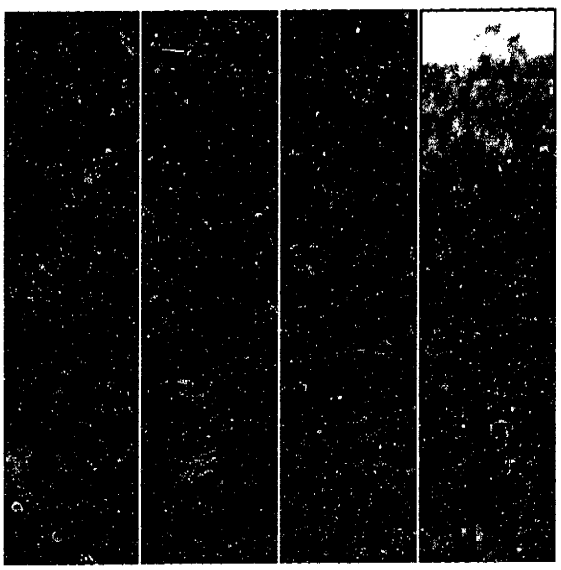

Figure 4-22: Fluorescence detected in explanted carotid tissue upon incubation with quenched FGF-2 alone, with protease inhibitors, heparin or trypsin pre-treatment, as described in Methods. Images were taken 48 hours after initial incubation of quenched FGF-2 to ensure adequate growth factor penetration, based on order of magnitude estimates. Representative images are shown.

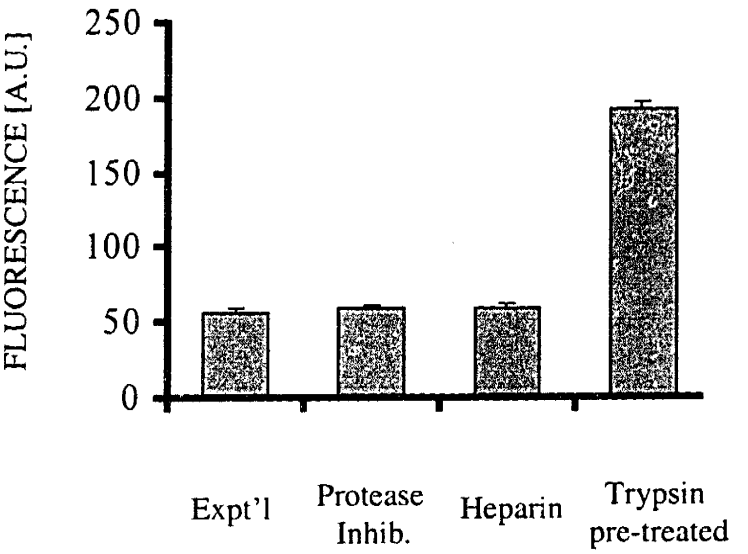

Figure 4-23: Quantitative determination of fluorescence intensity within the arterial media as described in Methods. Sample images are shown in previous figure.

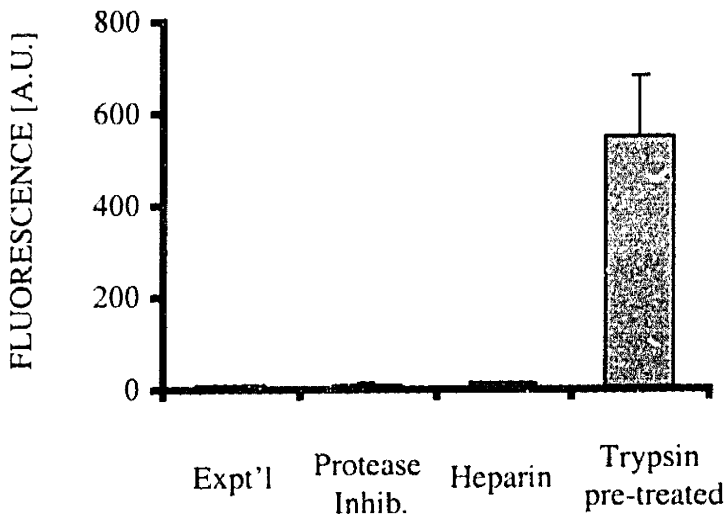

Figure 4-24: Fluorescence of conditioned media for each of the four groups of samples tested, as described in the Methods.

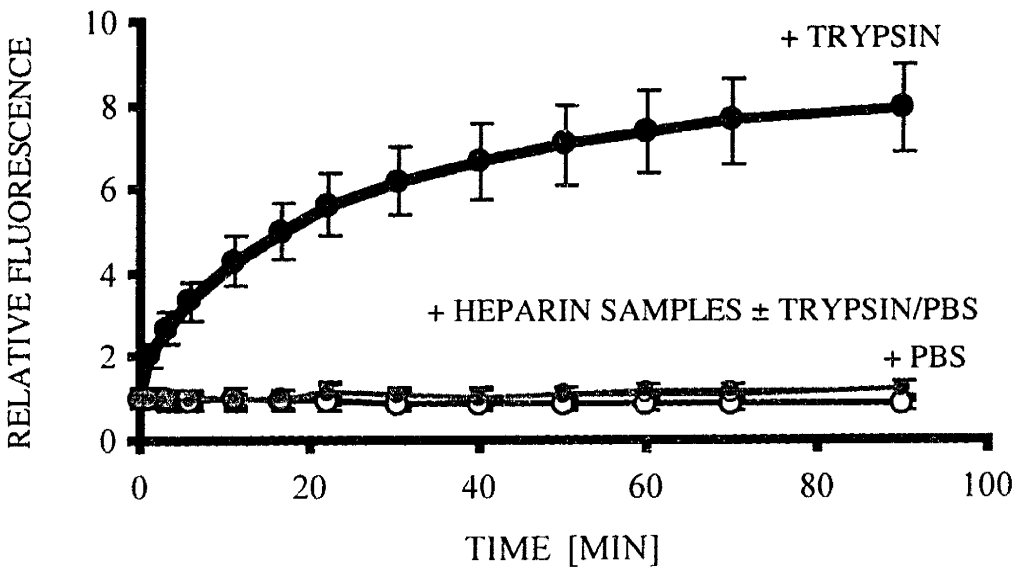

Figure 4-25: Trypsin digestion of conditioned media obtained from wells incubated with quenched FGF-2 alone (black) or quenched FGF-2 and heparin (grey). Trypsin (●) or PBS^{++} (O) was added and the fluorescence measured as a function of time.

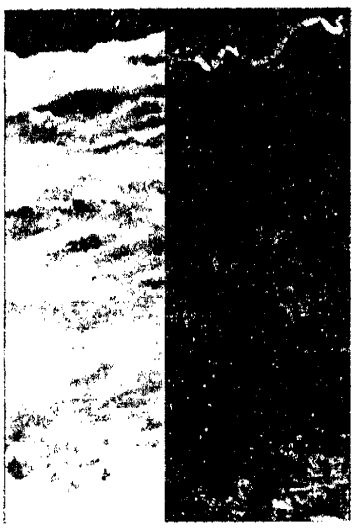

— +

PROTEASE INHIBITORS

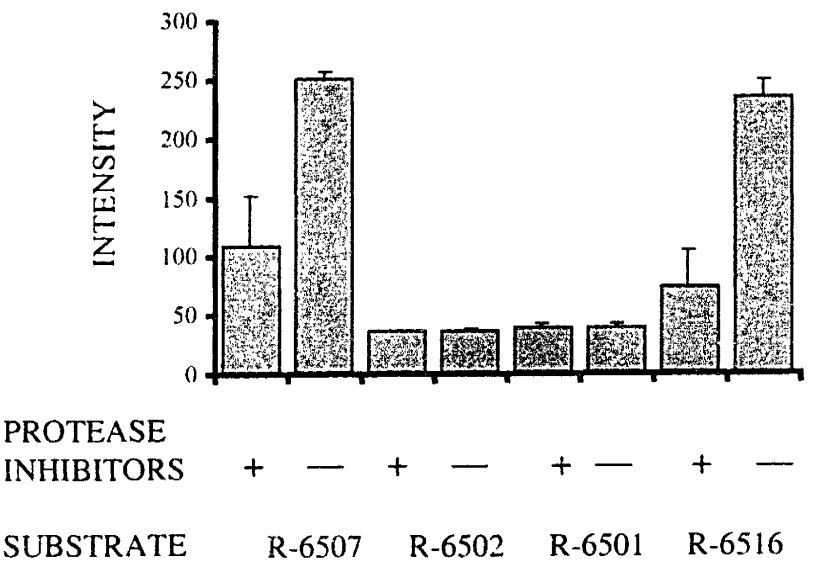

Figure 4-26: Defining the general proteolytic potential of explanted bovine carotid arteries. Commercially available quenched substrates were used to define proteolytic activity in samples. Top is sample image of incubation with R-6507. Bottom is quantitative comparison of the results of four specific substrates. Intensities were measured in arterial media.

As the sum of these experiments and data suggest the lack of proteolysis of quenched FGF-2 in the explant model in face of high thrombin or thrombin-like enzymatic activity, the fact that FGF-2 was not susceptible to thrombin digestion was confirmed in a separate experiment. Quenched FGF-2 was first incubated with PBS^{++} or heparin (final concentration of 100 μg/ml) for 10 minutes. Next, thrombin (10 units/ml final concentration) was added to the solution and the fluorescence was monitored. As shown in Figure 4-27, there was no increase in fluorescence of the quenched conjugate detected over the time course of one hour in samples not protected by heparin. Similarly, there was no increase in fluorescence in the heparin treated samples over one hour and over one day (data not shown). Together, these data are consistent with the fact that quenched FGF-2 is unsusceptible to thrombin digestion. Indeed, this conclusion is confirmed by Western blot studies by Lobb that demonstrate that FGF-2 is not susceptible to thrombin digestion, whereas FGF-1, a comparable growth factor in many respects, is [185]. Thus, with the results of this experiment and data from the published literature [185], it is reasonable to conclude that in the face of high thrombin or thrombin-like activity within the arterial wall, no significant degradation of FGF-2 occurs. In fact then, these studies are not confounded by an artifact of labeling, Figure 4-28.

4.4 Discussion

4.4.1 Physiological transport forces

4.4.1.1 Continuum Pharmacokinetics

The lackluster performance of stent-based delivery systems for hydrophilic drugs may arise in part from the inability to effectively distribute drug at the target site at therapeutic concentrations for a sufficient period of time [11, 186]. To appreciate pharmacokinetic limitations of drug efficacy, detailed information about drug tissue interactions and drug transport mechanisms is required. Several studies have applied traditional pharmacokinetics to examine the distribution of stent-delivered drugs at a gross level by assaying for tissue average drug content [133, 187-189]. Yet, it appears that stent-based delivery can produce high tissue averaged concentrations relative to plasma, but simultaneously less than optimal therapeutic effects [187]. In contrast, other studies with far less mobile compounds, such as paclitaxel, have shown more promising data in reducing intimal hyperplasia [167]. These confounding results

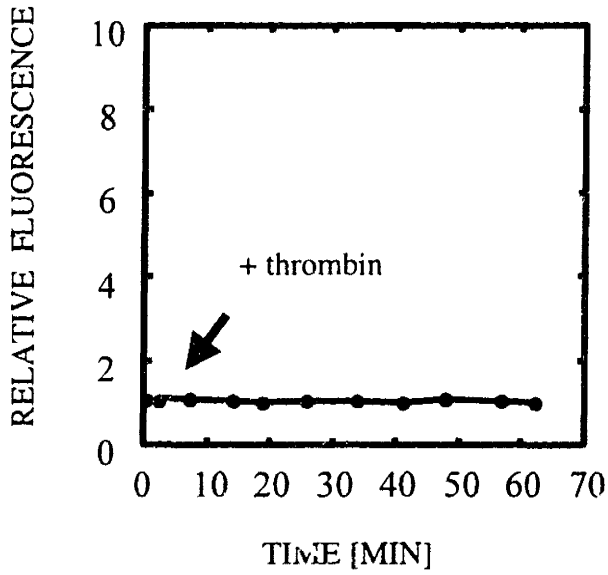

Figure 4-27: Effect of thrombin incubation with quenched FGF-2, as described in the Methods.

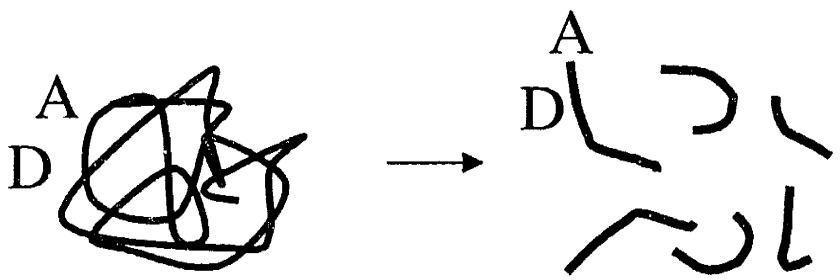

Figure 4-28: Potential labeling artifact that would invalidate intramolecular fluorescence quenching approach. Donor and acceptor dyes could be potentially labeled on the same peptide chain so that after proteolysis, they remain within Förster distances, with no relief of quenching.

might be explained first, by the relatively enhanced targeting of hydrophobic compared to hydrophilic agents, and second, by the large spatial concentration variations observed for both drug types in the arterial wall. The results from this study suggest that control release devices establish concentrations that can vary from nearly nil to several times the tissue average concentration over very short distances, resulting in local concentrations that may be both toxic and inadequate. As such, compartmental pharmacokinetics needs to be augmented by a continuum pharmacokinetic evaluation for optimizing local delivery.

The need for a microscopic appreciation of the forces of drug distribution and transport is substantiated by recent studies that directly correlate local concentrations of therapeutic agents with ensuing biologic response [50, 51]. While it is clear that absolute concentrations can determine biologic effect, gradients in concentrations may also affect biological behavior. For instance, morphogens direct tissue formation in embryos by specifying cell fates along a concentration profile [24, 25] while the graded distribution of cytokines lead to the directed recruitment of inflammatory cells to sites of injury, minimizing their activities elsewhere [28, 32]. Similarly, the brain tissue concentration gradient of locally delivered nerve growth factor (NGF) correlated identically with the biologic response gradient of NGF-induced enhancement in choline acetyltransferase immunoreactivity [51]. As both local drug concentrations and their gradients on microscopic length scales are critical in determining biological effect, these same relationships are likely to be relevant for the design of effective drug delivery modalities.

4.4.1.2 Concentration gradients depend on drug physicochemical properties

Physicochemical properties remain important determinants of drug distribution even in local delivery. Charge, molecular weight, and drug partitioning determine the relative impact of convective versus diffusive forces on drug transport [190]. Compounds that partition significantly into tissues will have smaller low drug regions, as these drugs would be less prone to both diffusive backwash into the endovascular space and convective washout into the perivascular space. Paclitaxel, rapamycin, and other drugs currently being considered for stent-based release partition extremely well into arterial tissues as a result of hydrophobic and vascular wall protein interactions [178, 191]. These drugs are consequently retained more effectively than heparin.

Computational simulations indicate there is an intimate dependence of the variability of drug distribution on the Péclet number, a dimensionless ratio of convective and diffusive forces. If spatially uniform drug distribution remains a clinical goal of local delivery for restenosis, designer drugs might be chemically modified or genetically engineered to capitalize on the intrinsic balance of transport mechanisms. For example, these studies suggest that when a hydrophilic drug is subject to almost equivalent forces of convective versus diffusive transport characterized by a Pé between 1 and 10, there is decreased overall concentration variability without adverse effects on superficial concentration variability. Moreover, while hydrophobic drugs achieve significantly higher tissue levels in the arterial wall than hydrophilic drugs, they tend to do so with relatively larger concentration variability, and remain in regions closer to the intima. Given their lower concentration variability, the hydrophilic nature of a drug may be advantageous when that drug possesses a small therapeutic window, while the hydrophobic nature of a drug may be advantageous to maintain high therapeutic doses close to the intima.

4.4.1.3 Concentration gradients depend on expanded stent configuration

In addition to physicochemical properties of the drug, geometric characteristics of the delivery device must be considered. Simple proximity of the target tissue to the coated stent does not ensure adequate distribution, as the theoretical results show unequivocally that distribution is most non-uniform in the layers of the artery closest to the stent. The potential difference between local drug distribution and mean tissue concentration actually becomes increasingly important as stent designs evolve to progressively more complex forms. While the mean tissue concentration of a stent-released drug is independent of stent strut position, local concentrations, which ultimately govern biologic effect, are highly spacing-dependent. Newer stent designs will inherently produce inhomogeneous arrays of stent struts in the circumferential and longitudinal directions. This variance in distance between stent struts will amplify the vicissitudes in concentrations and the areas of overlap toxicity where struts are close together, and sub-therapeutic areas in between widely spaced struts. Taken together, inhomogeneous stent strut placement can lead to sub-optimal drug delivery. Disparity in drug distribution between stents with homogeneous and inhomogeneous strut designs increases with strut numbers, and is more apparent for hydrophilic drugs than for hydrophobic drugs. Optimization of drug

distribution therefore requires symmetric expansion of stents with homogeneous distributions of struts.

4.4.2 Proteolytic constraints on growth factor delivery

In recent years, a plethora of approaches involving growth factors have been attempted clinically for the treatment of a variety of diseases from wound healing to therapeutic angiogenesis. Because the local concentrations of soluble growth factors are presumably important for defining the subsequent tissue response, it has been unclear to what extent proteolysis and degradation of growth factor is limiting, versus poor targeting. In Section 4.3.1, the role of physiological transport forces was examined as a rate-limiting step in efficacy of a growth factor. Here, using a novel approach involving intramolecular fluorscence quenching, the role of local tissue pharmacokinetics, specifically tissue proteolysis, in defining the efficacy of control-release growth factors has been defined.

The data from these study demonstrate first that the use of intramolecular fluorescence quenching can be a feasible method by which to discern the molecular integrity of growth factors upon local delivery and second, that quenched FGF-2 is not significantly degraded upon delivery to a bovine carotid artery explant model. That extensive proteolytic degradation is a concern for local delivery was initially posed by Saltzman and Radomsky when they noted that spatially averaged concentrations approach maximal concentrations, a virtual steady-state condition, when degradation is less dominant than diffusion [68]. They found in contrast, when diffusion is overshadowed by degradation, significant concentration gradients exist. Such gradients mean that tissues closest to the source receive high, perhaps toxic, doses of drug, whereas tissues furthest from the source receive little or none. For peptides and proteins, Saltzman and Radomsky estimated the ratio of degradation to diffusion to be approximately between ~1 to 100, so that within this critical range, the influence of chemical reactions such as degradation/metabolism is comparable or greater than that of diffusion. As a result, significant deviations in local concentrations from uncomplicated, steady-state Fickian diffusion profiles are likely to be observed. In published work, several other groups have both computational and experimentally confirmed the potential for significant proteolysis. Rippley and Stokes computationally demonstrated the role of cellular pharmacokinetics in limiting transferrin distribution, whereas Chu and Lauffenburger described the limitations of EGF transport through

cells suspended in agarose gels. [12, 13, 73]. Mahoney and Saltzman experimentally measured steep concentration gradients of NGF upon local delivery in the brain [51]. Together, these studies suggest the role of active tissue pharmacokinetics in partially limiting the establishment of effective tissue concentrations of growth factors.

In data presented in Section 4.3.2, no significant proteolysis of quenched FGF-2 was observed, despite the findings of high thrombin or thrombin-like activity in the arterial wall. This result was confirmed in several ways. First, control studies and published literature confirmed that quenched FGF-2 is not susceptible to thrombin digestion [185]. Second, that pre-digested quenched FGF-2 was able to be fluorescently detected within the arterial wall and conditioned media confirmed that there was sufficient sensitivity to assay for a functional response if there were one. Third, the addition of heparin and protease inhibitors did not result in decreased fluorescence; a result that would have been expected if quenched FGF-2 was at all degraded by the arterial wall. Fourth, conditioned media from carotid explants incubated with quenched FGF-2 retained their trypsin sensitivity, fluorescing rapidly, and therefore suggested the presence of intact, quenched growth factor in the media. Together. these data are consistent with the conclusion that in the face of high thrombin, or thrombin-like protelytic activity within the explant model, local FGF-2 delivery was not substantially constrained by degradation.

The result that quenched FGF-2 remained intact could be in part due to the low presence of enzymes within the arterial wall that are capable of degrading FGF-2, such as trypsin- or plasmin- like enzymes as shown in Section 4.3.2.3. In addition, quenched FGF-2 could have remained intact due to the high concentrations of heparan sulfate found within extracellular matrix and on cellular surfaces [160]. Indeed, several reports have demonstrated the role of heparan sulfate proteoglycans in protecting growth factor as a kinetic storage depot for later presentation [53, 136, 139, 181]. Moreover, matrix elements have been shown in Chapter 3 to protect growth factor from proteolysis as a method for theoretically enhancing cellular signaling. Alternatively, the quenched conjugate could have been partially degraded, yet because of a poor signal to noise ratio, the fluorescence was undetectable. While this might be a possibility, it is nevertheless irrelevant for local growth factor delivery where concentrations that far exceed the equilibrium binding constants for growth receptor binding are employed. Since there was no significant increase in fluorescence at all, it is reasonable to conclude that within this experimental model system, tissue proteolysis imposes minimal constraints on FGF-2 delivery.

4.5 Chapter Summary

In this chapter, the role of physiological transport forces and proteolytic constraints on local delivery were examined using ex vivo explanted bovine carotid arteries as a relevant tissue model. Computational simulations were conducted to determine the role of convection, diffusion, and partitioning in determining drug distribution was obtained through the local delivery of a fluorescent hydrophilic compound. Results from these studies argue that physiological transport forces can dictate drug distribution significantly and that close juxtaposition of delivery devices next to focal lesions does not necessarily guarantee adequate delivery.

Experimental studies using intramolecular fluorescence quenching demonstrated the feasibility of using this phenomenon as a tool for probing the proteolytic constraints imposed by tissue pharamcokinetics on local growth factor delivery. FGF-2 was successfully labeled with a dye pair that responded to enzymatic digestion by trypsin, plasmin, and not thrombin. Using this approach, the arterial wall was shown to not impose a proteolytic constraint on FGF-2 delivery. With the use of commercially available substrates, the general proteolytic potential of the arterial wall was defined to encompass a high thrombin, or thrombin-like enzymatic activity.

5 NEXT STEPS

There has been a great deal of research not only from the Edelman lab, but from throughout the field that has actively characterized and defined constraints for local growth factor delivery. However, there are many important areas that remain to be explored:

1. What defines the functional cell response in vivo to growth factors? By probing the intracellular signal transduction cascade in a more quantitative fashion, it is expected that models of cellular proliferation that rely on mechanistic detail versus empirical detail will become available. Models such as these should provide great insight into the delivery of exogenous growth factors and should open approaches to define what rational delivery might mean.

2. How does a cell in vitro differ from when it is in vivo? One assumption that is made throughout this thesis is that if sufficient concentrations of growth factors are adequately targeted to a particular tissue for an adequate amount of time, and that both transport limitations and proteolytic constraints are non-existent, the tissue response will be as robust as it is in cell culture systems. However, what happens if this is not the case? It is entirely possible that the cell within tissues behaves quite differently from the cell in tissue culture, so that growth factors may not be as potent as they have been in vitro. To explore this question, it will be important to define what it means to be a tissue. For example, what is the role of gap junctions and matrix interactions in defining cellular responses in vivo?

As first steps, insights into these broad areas should enable a better understanding of how to optimally deliver growth factors.

6 CONCLUDING REMARKS

In this thesis, an attempt was made to experimentally and computationally define pharmacokinetic issues, such as cellular ligand and receptor trafficking, tissue physiological transport forces, and tissue proteolytic constraints, that might potentially determine the efficacy and potency of locally delivered growth factors.

Studies at the cellular level revealed the importance of ligand and receptor trafficking to determine potency of control-released growth factors, and highlighted the relevance of intracellular pharmacokinetics by demonstrating that two growth factors that bind identically to the same receptor can nevertheless benefit to varying degrees depending on appropriate delivery. Moreover, these studies demonstrated the roles of ligand depletion and receptor trafficking in quantitatively determining the potency of controlled-release growth factors.

Computational studies next provided a framework founded on simple mass-action kinetic trafficking events that enabled theoretical insight into optimal delivery approaches. Through this analysis, distinct theoretical approaches for growth factor delivery were identified depending on specific trafficking parameters. In parallel simulations, the relationship between spatial tissue concentrations of growth factor and tissue responses was examined and found to be highly non-linear. These computational studies and methodologies together offer the potential to provide theoretical insight into appropriate delivery approaches.

Lastly, studies at the tissue level examined the roles physiological transport forces and proteolytic constraints. These studies highlighted pharmacokinetic tissue forces, such as convection and diffusion, partition and proteolysis as potential barriers for effective growth factor delivery and targeting. In addition, a novel approach for assessing the molecular state of locally delivered growth factors was developed and tested on an ex vivo carotid explant model.

Taking these three approaches together, this thesis has attempted to develop novel concepts and approaches for thinking about the effective local delivery of therapeutic growth factors. It is hoped that the insights and results from this work will be potentially clinically relevant, and at the very least, thought provoking for clinicians and scientists alike.

7 APPENDICES

The following sections contain MATLAB script for the computational simulations of cellular and tissue pharmacokinetics.

7.1 MATLAB files for cellular pharmacology simulations

7.1.1 Traffickinga.m

```
% This m-file controls 'runsima.m' and allows one to do loops of varying
% parameters.  It calls 'runsima.m' which then calls 'traffickinga.m' and can
% be called from the command line.

clear global, clear all global
clear, clear all

global samedose tday kdeg kprot kec f1 krec Ro keR kf kr Rsyn Leo f2
global ratioLi ratioLd ratioRs ratioRi ratioCs ratioCi ratioCell
global deplete Nav leftover CsCi
tday=5;              % turn off %tday in 'runsima.m' (line 20) when using this m-file

%kf=1e2;
%kdeg=1e-12;%8;
kprot=1e-8;
%kec=1e-8;
%f1=0.0;
%f2=0.0;
%krec=1e-6;
%Ro=1;
%keR=1e-8;
%kr=1e-9;
%Rsyn=1e-6;
%Leo=1e-10;

for j=1:10,j
        tday=j*0.5;
        runsima;

        ratioLihold(j)=ratioLi;
        ratioLdhold(j)=ratioLd;
        ratioRshold(j)=ratioRs;
        ratioRihold(j)=ratioRi;
        ratioCshold(j)=ratioCs;
        ratioCihold(j)=ratioCi;
        %ratioCellhold(j)=ratioCell;

        samedosehold(j)=samedose;
        ratioarrayhold(:,j)=ratioarray';
        depletehold(j)=deplete;
        leftoverhold(j)=leftover;
        CsCihold(j)=CsCi;
```

```
        %tdayhold(j)=tday;
        %kdeghold(j)=kdeg;
        kprothold(j)=kprot;
        %kechold(j)=kec;
        %f1hold(j)=f1;
        %f2hold(j)=f2;
        %krechold(j)=krec;
        %Rohold(j)=Ro;
        %keRhold(j)=keR;
        %kfhold(j)=kf;
        %krhold(j)=kr;
        %Rsynhold(j)=Rsyn;
        %Leohold(j)=Leo;

        %kdeg=kdeg*10
        kprot=kprot*10;
        %kec=kec*10;
        %f1=f1+0.1;
        %f2=f2+0.1;
        %krec=krec*2;
        %Ro=Ro*10;
        %keR=keR*10;
        %kf=kf*10;
        %kr=kr*10;
        %Rsyn=Rsyn*10;
        %Leo=Leo*2;

% new added section

        bolusAveCshold(j)=bolusAveCs;
        CRAveCshold(j)=CRAveCs;

        clear global ratioLi ratioLd ratioRs ratioRi ratioCs ratioCi
        clear global samedose ratioCell ratioarray deplete leftover CsCi
end

clear global ratioLi ratioLd ratioRs ratioRi ratioCs ratioCi samedose ratioarray
clear global f1 f2 Leo Ro Rsyn kf kr kdeg krec k1 kr1 kcl kec keR n Nav rrel kprot
clear bottm bottom bottmCR last i j ff last
clear bolusAveLi bolusAveLd bolusAveRs bolusAveRi bolusAveCs bolusAveCi
clear CRAveCi CRAveCs CRAveLd CRAveLi CRAveRi CRAveRs
clear CRIntCidt CRIntCsdt CRIntLddt CRIntLidt CRIntRsdt CRIntRidt
clear bolusIntCsdt bolusIntCidt bolusIntRsdt bolusIntRidt bolusIntLddt bolusIntLidt
clear ttmin t y y0 total totalCR ttempBolus ttempCR final
clear global tday tCR tbolus yCR ybolus T
clear averageBolus averageCR thr ytempBolus ytempCR

-------------------------------------------------------------------------------------
% This m-file is similar to runsim.m except that there is no spatial
% dependence for variables.  Here, this m-file compares the results of
% bolus versus controlled-release by normalizing total amount delivered,
% assuming constant volume and clearance (k1,kr1,kcl) kinetics.

%clear global, clear all global
%clear, clear all
```

```
global T tday
global kf kr kdeg krec f1 f2 kec keR Leo Rsyn Ro n kprot
global k1 kr1 kcl
global rrel
global tbolus ybolus tCR yCR

global samedose tday n Nav
global ratioLi ratioLd ratioRs ratioRi ratioCs ratioCi ratioCell ratioarray

ff=2;           % ff=1 for conserved mass/moles added; ff=2 for conserved A.U.C.
                % 'ff' is a fudge-factor that varies the rate at which drug is released.
                % For comparisons between bolus and CR, one can use either equivalent
                % doses of growth factor, (ff=1), or equivalent time-averaged doses, (ff=2).
                % Since most people seem to compare total AUC, ff=2 is done in most cases.

tday=5;  % turn this off when using 'control.m' if the time-effect
         % is desired.  tday is the length in days for the simulation.
thr=tday*24;
ttmin=thr*60;           % Time length of simulation in hours
T=ttmin*60;             % converted to seconds.

kftemp=kf;              % Temporary ariables to hold values while changes are made
kprottemp=kprot; % Temporary ariables to hold values while changes are made

% Determines the in vivo profile without cellular pharmacology to get AUC
                y0=[1 0 1 0 0 0 0];
                rrel=0;kprot=0;kf=0;
                [ttempBolus,ytempBolus]=ode15s('traffickinga', [0 T], y0);

                total=cumtrapz(ttempBolus,ytempBolus(:,1));
                bottm=size(total);
                averageBolus=total(bottm(1,1))/T;

% Using AUC, determines rrel, and runs CR simulation
                y0=[0 0 1 0 0 0 0];rrel=Leo/T*ff;kprot=0;kf=0;
                [ttempCR,ytempCR]=ode15s('traffickinga', [0 T], y0);

                totalCR=cumtrapz(ttempCR,ytempCR(:,1));
                bottmCR=size(totalCR);
                averageCR=totalCR(bottmCR(1,1))/T;

%plot(ttempBolus/(24*3600),ytempBolus(:,1),ttempCR/(24*3600),ytempCR(:,1)), pause, pause
%xlabel('Time [days]'), ylabel('L/Leo'),title('Ligand Concentration = f(dosing)')
%will need to also set kprot, kdeg = 0 for ligand profile = f(t)

samedose=averageBolus/averageCR;  % Tests to see if the integrated doses are the same

kprot=kprottemp; clear kprottemp
kf=kftemp; clear kftemp

%*****************************************************************
%       Initial conditions
%                               base case       revisited       enhanced
%                               --------        ---------       --------
%               y(6)= Ri        2.00E+00        3.45E+00        3.30E-01
```

```
%                y(3)= Rs          5.80E-01          1.00E+00          1.00E+00
%
%*****************************************************************s

for i=1:2
        if i==1
                % Runs bolus simulation
                y0=[1 0 1 0 0 0.33 0];
                rrel=0;
                [tbolus,ybolus]=ode15s('traffickinga', [0 T], y0);

                % Calculates integrated values = f(time)
                bolusIntLidt=cumtrapz(tbolus,ybolus(:,1));
                bolusIntLddt=cumtrapz(tbolus,ybolus(:,2));
                bolusIntRsdt=cumtrapz(tbolus,ybolus(:,3));
                bolusIntCsdt=cumtrapz(tbolus,ybolus(:,4));
                bolusIntCidt=cumtrapz(tbolus,ybolus(:,5));
                bolusIntRidt=cumtrapz(tbolus,ybolus(:,6));
                last=size(tbolus);

                % Calculates average values
                bolusAveLi=bolusIntLidt(last(1,1))/T;       % gives ave Li = [M]
                bolusAveLd=bolusIntLddt(last(1,1))/T;       % gives ave Ld = [M]
                bolusAveRs=bolusIntRsdt(last(1,1))/T;       % gives ave Rs = [#/cell]
                bolusAveCs=bolusIntCsdt(last(1,1))/T;       % gives ave Cs = [#/cell]
                bolusAveCi=bolusIntCidt(last(1,1))/T;       % gives ave Ci = [#/cell]
                bolusAveRi=bolusIntRidt(last(1,1))/T;       % gives ave Ri = [#/cell]

        else

                % Runs controlled-release simulation
                y0=[0 0 1 0 0 0.33 0];
                rrel=Leo/T*ff;
                [tCR,yCR]=ode15s('traffickinga', [0 T], y0);

                % Calculates integrated values = f(time)

                CRIntLidt=cumtrapz(tCR,yCR(:,1));
                CRIntLddt=cumtrapz(tCR,yCR(:,2));
                CRIntRsdt=cumtrapz(tCR,yCR(:,3));
                CRIntCsdt=cumtrapz(tCR,yCR(:,4));
                CRIntCidt=cumtrapz(tCR,yCR(:,5));
                CRIntRidt=cumtrapz(tCR,yCR(:,6));
                bottom=size(tCR);

                % Calculates average values
                CRAveLi=CRIntLidt(bottom(1,1))/T;       % gives ave Li = [M]
                CRAveLd=CRIntLddt(bottom(1,1))/T;       % gives ave Ld = [M]
                CRAveRs=CRIntRsdt(bottom(1,1))/T;       % gives ave Rs = [#/cell]
                CRAveCs=CRIntCsdt(bottom(1,1))/T;       % gives ave Cs = [#/cell]
                CRAveCi=CRIntCidt(bottom(1,1))/T;       % gives ave Ci = [#/cell]
                CRAveRi=CRIntRidt(bottom(1,1))/T;       % gives ave Ri = [#/cell]
        end
end

% Calculates ratio of CR:Bolus for efficacy determination
```

```
ratioLi=CRAveLi/bolusAveLi;ratioLd=CRAveLd/bolusAveLd;
ratioRs=CRAveRs/bolusAveRs;ratioRi=CRAveRi/bolusAveRi;
ratioCs=CRAveCs/bolusAveCs;ratioCi=CRAveCi/bolusAveCi;

%ratioCell=yCR(bottom(1,1),8)/ybolus(last(1,1),8);
ratioarray(1)=ratioLi;ratioarray(2)=ratioLd;ratioarray(3)=ratioRs;
ratioarray(4)=ratioCs;ratioarray(5)=ratioCi;ratioarray(6)=ratioRi;
%plotcompare


global deplete                          % This variable holds the amount of degraded ligand
                                        % present at the end of the simulation and includes
                                        % contributions from cellular metabolism and lumped
                                        % extracellular proteolysis. (It appears to be only
                                        % the amount for the bolus scenario, written much later
                                        % than this variable was defined).

final=size(tbolus);deplete=ybolus(final(1,1),2);

global leftover                         % leftover is the free intact ligand

leftover=ybolus(final(1,1),1);          % This gives the leftover amount of intact ligand

global CsCi
CsCi=ybolus(final(1,1),4)+ybolus(final(1,1),5)*n/6.023e23;
-------------------------------------------------------------------------------------------
function yp=traffickinga(t,y)

% This m-file is based on the model of Chu and Lauffenburger from Tissue Eng.
% Its purpose is to compare the bolus versus controlled-release response of
% growth factor on averaged Cs or averaged Ci over time. It is not spatially
% varying as there is no "tissue" invovled. It is simply a model of cells
% in suspension and the goal is to determine if the saturation of receptors is
% potentially a limiting factor for the delivery of growth factors and the uptake
% of such.
%
% It incorporates both "in vivo" clearance kinetics with constants k1, kr1, kcl
% and also a potential to release drug at rate constant rrel = molar/time
%
% It is called out of the command line with no other m-files within.
% The initial condition vector y0 needs to be included each time. Sample command is:
%
% clear all, clear all global,y0=[0 0 1 0 0 0 0];[t,y]=ode15s('traffickinga', [0 2.88e4], y0);plot(t,y)

% Rsyn = 2 for standard model, or Rsyn = 3.4499 for revisited standard model
% At t = 0, Ri = 0 for standard model, or Ri = 3.445 for revisited standard model

global kf kr kec krec kdeg kprot n Rsyn y0 Ro Leo f1 f2
global keR f1 f2 k1 kr1 kcl rrel Nav

% Kd=100 pM

% Diffusion controlled-limit for kf is 10^8 or 10^9 (M sec)-1, Voet and Voet p338

kf=1e6;
```

```
kr=1e-4;
%kr=1e-10*kf;
%kf=kr/1e-10;
kec=0.005;                          % 0.3 min-1
keR=0.0005;                         % 0.03 min-1
krec=1.542e-3;%1e-4;                % Chu et al. 0.13 min-1 = 1e-3 for B82's.
                                    % krec = 1e-4 for base case model
                                    % krec = 1e-4 for standard revisted model
                                    % krec = 1.542e-3 for enhanced model
kdeg=1e-3;                          % FGF in SMC, s-1 Sperinde and Nugent, 98
n=1e9;                              % 1e9 is standard cell/L, Starbuck and DAL, 1992
Nav=6.023e23;                       % Avogadro's number #/mol
Rsyn=0.33;%3.4499;%2;               % Rs synthesis rate, [#/(cell*sec)] from Chu et al.
                                    % Rsyn = 2 for standard model
                                    % Rsyn = 3.4499 for revisited standard model
                                    % Rsyn = 0.33 for enhanced model
Leo=1e-9;                           % Intact ligand concentration for scaling [M]
f1=0.5;                             % fraction of complexes degraded
f2=0.05;                            % fraction of receptors degraded
Ro=2e4;                             % Initial surface receptor number

kprot=0;%6.66e-4;                   % Chu et al., 1996. 0.00015; %0.0001

k1=0;%1e-3;          % Suggested numbers might be 1e-3, 1e-4, 1e-4 respectively
kr1=0;%1e-4;         % For in vitro tissue culture, no clearance mechanism so neglect.
kc1=0;%1e-4;

% This is Chu's model for receptor mediated trafficking events.

% Species                                          Initial conditions, y0
%-------------------------------------------------------------
% y(1) = intact ligand, Li              [M]        = 0 for CR, =1 for bolus
% y(2) = degraded ligand, Ld            [M]        0
% y(3) = surface receptor, Rs           [#/cell]   1
% y(4) = surface complex, Cs            [#/cell]   0
% y(5) = internal complex, Ci           [#/cell]   0
% y(6) = internal Ri                    [#/cell]   0
% y(7) = compartment 2 for in vivo      [M]        0
% y(8) = cell number = f(Cs)            [#/L]      1

% Rate constants
%-------------------------------------------------------------
% kf = forward binding constant         [(M sec)^-1]
% kr = reverse binding constant         [sec-1]
% kec = internalization of complexes    [sec-1]
% keR = internalization of free Rs      [sec-1]
% krec = recycling                      [sec-1]
% kdeg = degradation                    [sec-1]
% rsyn = synthesis                      [#/(cell*sec)]
% kprot = proteolysis extracellular     [sec-1]

% f1= fraction degraded of complexes
% f2= fraction degraded of receptors

% k1 = in vivo distribution constant    [sec-1]
% kr1 = in vivo redistribution constant [sec-1]
```

```
% kcl = clearance rate constant                [sec-1]
% rrel = polymeric drug release rate           [M sec-1]

g=1;     % g= is a parameter for variable Rs synthesis.
                % where g=(1-Rs/Ro). It is thus equal to 1 when surface
                % receptors are low, giving maximal rsyn. When Rs is high or equal
                % to Ro, it will be zero. Not sure how to prevent it from going
                % negative on me. The default is simply g=1 where Rsyn is constant.
                % For g=1, Rsyn is constant, reference Carpenter 1987

%g=(1-(y(3)/Ro)); % For synthesis = f(surface receptor number)

%umax=1e-5; % Maximal growth rate [sec-1]
%ED50=0.1;      % Ave Cs at which half-maximal stimulation seen.

% Equations
%-------------------------------------------------------
yp=[(-kf*y(1)*y(3)+kr*y(4)/Leo)*n*Ro/Nav-kprot*y(1)-(k1+kcl)*y(1)+kr1*y(7)+rrel/Leo;
        (kdeg*f1*y(5))*n*Ro/(Nav*Leo)+kprot*y(1);
        -kf*y(1)*y(3)*Leo+kr*y(4)+g*Rsyn/Ro-keR*y(3)+(1-f2)*krec*y(6);
        kf*y(1)*y(3)*Leo-(kr+kec)*y(4)+krec*y(5)*(1-f1);
        kec*y(4)-(krec*(1-f1)+kdeg*f1)*y(5);
        keR*y(3)-(1-f2)*krec*y(6)-f2*kdeg*y(6);
        k1*y(1)-kr1*y(7);];
        %(umax/(1+ED50/y(4)))*y(8);];

% Equations have been scaled to Leo and Ro for ligand and receptor species
% Time is left as dimensional.

%*************************************************************************
%****  STEADY-STATE CONSIDERATIONS FOR L = 0 or kf = 0        ****
%*************************************************************************

% The steady-state response is determined by setting dRs/dt = dRi/dt = 0 with
% all L = Cs = Ci = 0.
%
% For steady-state:
%
%         Ri = Rsyn / (Rt*kdeg*f2)
%         Rs = Rsyn/(keR*Rtotl) * { [1 + (1-f2)*krec] / [f2*kdeg] }

%*************************************************************************
```

7.1.2 Traffickingc.m

```
% This m-file controls 'runsimc.m' and allows one to do loops of varying
% parameters. It calls 'runsimc.m' which then calls 'traffickingc.m' and can
% be called from the command line.

% THIS is to be used with HSPG sites for "natural" control-release.
clear global, clear all global
clear, clear all

global samedose tday kdeg kprot kec f1 krec Ro keR kf kr Rsyn Leo f2
global ratioLi ratioLd ratioRs ratioRi ratioCs ratioCi ratioCell
global deplete kf2 kr2
```

```
tday=5;          % turn off %tday in 'runsimc.m' (line 20) when using this m-file

%kf=1e2;
%kdeg=1e-8;
%kprot=1e-8;
%kec=1e-8;
%f1=0.0;
%f2=0.0;
%krec=1e-8;
%Ro=1;
%keR=1e-8;
%kr=1e-9;
%Rsyn=1e-4;
Leo=1e-10;
kf2=1e4;                 % ECM forward binding constant

for j=1:10,j
        %tday=j*0.05;
        runsimc;

        ratioLihold(j)=ratioLi;
        ratioLdhold(j)=ratioLd;
        ratioRshold(j)=ratioRs;
        ratioRihold(j)=ratioRi;
        ratioCshold(j)=ratioCs;
        ratioCihold(j)=ratioCi;
        %ratioCellhold(j)=ratioCell;

        samedosehold(j)=samedose;
        ratioarrayhold(:,j)=ratioarray';
        depletehold(j)=deplete;

        %tdayhold(j)=tday;
        %kdeghold(j)=kdeg;
        %kprothold(j)=kprot;
        %kechold(j)=kec;
        %f1hold(j)=f1;
        %f2hold(j)=f2;
        %krechold(j)=krec;
        %Rohold(j)=Ro;
        %keRhold(j)=keR;
        %kfhold(j)=kf;
        %krhold(j)=kr;
        %Rsynhold(j)=Rsyn;
        Leohold(j)=Leo;

        %kdeg=kdeg*10;
        %kprot=kprot*10;
        %kec=kec*10;
        %f1=f1+0.1;
        %f2=f2+0.1;
        %krec=krec*10;
        %Ro=Ro*10;
        %keR=keR*10;
        %kf=kf*10;
        %kr=kr*10;
```

```
        %Rsyn=Rsyn*10;
        Leo=Leo*2;%*10;

        clear global ratioLi ratioLd ratioRs ratioRi ratioCs ratioCi
        clear global samedose ratioCell ratioarray deplete
end

clear global ratioLi ratioLd ratioRs ratioRi ratioCs ratioCi samedose ratioarray
clear global f1 f2 Leo Ro Rsyn kf kr kdeg krec k1 kr1 kcl kec keR n Nav rrel kprot
clear bottm bottom bottmCR last i j ff last
clear bolusAveLi bolusAveLd bolusAveRs bolusAveRi bolusAveCs bolusAveCi
clear CRAveCi CRAveCs CRAveLd CRAveLi CRAveRi CRAveRs
clear CRIntCidt CRIntCsdt CRIntLddt CRIntLidt CRIntRsdt CRIntRidt
clear bolusIntCsdt bolusIntCidt bolusIntRsdt bolusIntRidt bolusIntLddt bolusIntLidt
clear ttmin t y y0 total totalCR ttempBolus ttempCR final
clear global tday tCR tbolus yCR ybolus T kf2 kr2
clear averageBolus averageCR thr ytempBolus ytempCR
-----------------------------------------------------------------------------------------
% This m-file is similar to runsima.m except that there is no spatial
% dependence for variables. Here, this m-file compares the results of
% bolus versus controlled-release by normalizing total amount delivered,
% assuming constant volume and clearance (k1,kr1,kcl) kinetics.

% ** THIS to be used for HSPG sites. Requires a longer initial condition
% vector specifying details of the HSPG stuff...

%clear global, clear all global
%clear, clear all

global T tday
global kf kr kdeg krec f1 f2 kec keR Leo Rsyn Ro n kprot
global k1 kr1 kcl kf2 kr2
global rrel
global tbolus ybolus tCR yCR

global samedose tday n
global ratioLi ratioLd ratioRs ratioRi ratioCs ratioCi ratioCell ratioarray

ff=2;           % ff=1 for conserved mass/moles added; ff=2 for conserved A.U.C.
                % 'ff' is a fudge-factor that varies the rate at which drug is released.
                % For comparisons between bolus and CR, one can use either equivalent
                % doses of growth factor, (ff=1), or equivalent time-averaged doses, (ff=2).
                % Since most people seem to compare total AUC, ff=2 is done in most cases.
tday=5;         % turn this off when using 'control.m' if the time-effect
                % is desired. tday is the length in days for the simulation.

thr=tday*24;
ttmin=thr*60;   % Time length of simulation in hours
T=ttmin*60;     % converted to seconds.

kftemp=kf;      % Temporary ariables to hold values while changes are made
kprottemp=kprot; % Temporary ariables to hold values while changes are made
kf2temp=kf2;    % kf2 value is set in controlc.m

ECM=100;        % Scaled number of low affinity binding sites per cell [#/cell] wrt Rt
```

```
% Determines the in vivo profile without cellular pharmacology to get AUC
                y0=[1 0 1 0 0 0 0 ECM 0];
                rrel=0;kprot=0;kf=0;
                [ttempBolus,ytempBolus]=ode15s('traffickingc', [0 T], y0);

                total=cumtrapz(ttempBolus,ytempBolus(:,1));
                bottm=size(total);
                averageBolus=total(bottm(1,1))/T;

% Using AUC, determines rrel, and runs CR simulation
                y0=[0 0 1 0 0 0 0 ECM 0];rrel=Leo/T*ff;kprot=0;kf=0;
                [ttempCR,ytempCR]=ode15s('traffickingc', [0 T], y0);

                totalCR=cumtrapz(ttempCR,ytempCR(:,1));
                bottmCR=size(totalCR);
                averageCR=totalCR(bottmCR(1,1))/T;

% Compares dosage of bolus and CR without cellular pharmacology
%plot(ttempBolus/(24*3600),ytempBolus(:,1),ttempCR/(24*3600),ytempCR(:,1)), pause, pause
%xlabel('Time [days]'), ylabel('L/Leo'),title('Ligand Concentration = f(dosing)')
%will need to also set kprot, kdeg = 0 for ligand profile = f(t)

samedose=averageBolus/averageCR;  % Tests to see if the integrated doses are the same

% Actual computational/simulation part:

kprot=kprottemp; clear kprottemp
kf=kftemp; clear kftemp

for i=1:2
        if i==1
                % Runs bolus simulation
                y0=[1 0 1 0 0 0 0 ECM 0];
                rrel=0;

                kf2=0;   % **** Removes ECM interaction, thus no "natural" controlled-release

                [tbolus,ybolus]=ode15s('traffickingc', [0 T], y0);

                % Calculates integrated values = f(time)
                bolusIntLidt=cumtrapz(tbolus,ybolus(:,1));
                bolusIntLddt=cumtrapz(tbolus,ybolus(:,2));
                bolusIntRsdt=cumtrapz(tbolus,ybolus(:,3));
                bolusIntCsdt=cumtrapz(tbolus,ybolus(:,4));
                bolusIntCidt=cumtrapz(tbolus,ybolus(:,5));
                bolusIntRidt=cumtrapz(tbolus,ybolus(:,6));
                last=size(tbolus);

                % Calculates average values
                bolusAveLi=bolusIntLidt(last(1,1))/T;       % gives ave Li = [M]
                bolusAveLd=bolusIntLddt(last(1,1))/T;       % gives ave Ld = [M]
                bolusAveRs=bolusIntRsdt(last(1,1))/T;       % gives ave Rs = [#/cell]
                bolusAveCs=bolusIntCsdt(last(1,1))/T;       % gives ave Cs = [#/cell]
                bolusAveCi=bolusIntCidt(last(1,1))/T;       % gives ave Ci = [#/cell]
                bolusAveRi=bolusIntRidt(last(1,1))/T;       % gives ave Ri = [#/cell]
```

```
    else

        % Runs controlled-release simulation ("natural" control release via ECM)

        y0=[1 0 1 0 0 0 0 ECM 0]; % *** gives as a bolus and lets ECM do the release
        kf2=kf2temp;              % *** restores "natural" controlled-release
        rrel=0;                   % *** no need for release as ECM will do it "naturally".

        [tCR,yCR]=ode15s('traffickingc', [0 T], y0);

        % Calculates integrated values = f(time)

        CRIntLidt=cumtrapz(tCR,yCR(:,1));
        CRIntLddt=cumtrapz(tCR,yCR(:,2));
        CRIntRsdt=cumtrapz(tCR,yCR(:,3));
        CRIntCsdt=cumtrapz(tCR,yCR(:,4));
        CRIntCidt=cumtrapz(tCR,yCR(:,5));
        CRIntRidt=cumtrapz(tCR,yCR(:,6));
        bottom=size(tCR);

        % Calculates average values
        CRAveLi=CRIntLidt(bottom(1,1))/T;          % gives ave Li = [M]
        CRAveLd=CRIntLddt(bottom(1,1))/T;          % gives ave Ld = [M]
        CRAveRs=CRIntRsdt(bottom(1,1))/T;          % gives ave Rs = [#/cell]
        CRAveCs=CRIntCsdt(bottom(1,1))/T;          % gives ave Cs = [#/cell]
        CRAveCi=CRIntCidt(bottom(1,1))/T;          % gives ave Ci = [#/cell]
        CRAveRi=CRIntRidt(bottom(1,1))/T;          % gives ave Ri = [#/cell]
    end
end

% Calculates ratio of Bolus:CR for efficacy determination

ratioLi=CRAveLi/bolusAveLi;ratioLd=CRAveLd/bolusAveLd;
ratioRs=CRAveRs/bolusAveRs;ratioRi=CRAveRi/bolusAveRi;
ratioCs=CRAveCs/bolusAveCs;ratioCi=CRAveCi/bolusAveCi;

%ratioCell=yCR(bottom(1,1),8)/ybolus(last(1,1),8);
ratioarray(1)=ratioLi;ratioarray(2)=ratioLd;ratioarray(3)=ratioRs;
ratioarray(4)=ratioCs;ratioarray(5)=ratioCi;ratioarray(6)=ratioRi;
%plotcompare

giobal deplete    % This variable holds the amount of degraded ligand
                  % present at the end of the simulation and includes
                  % contributions from cellular metabolism and lumped
                  % extracellular proteolysis.
final=size(tbolus);deplete=ybolus(final(1,1),2);

clear kf2temp ECM

-------------------------------------------------------------------------------------------
function yp=traffickingc(t,y)

% This m-file is based on the model of Chu and Lauffenburger from Tissue Eng.
% Its purpose is to compare the bolus versus controlled-release response of
% growth factor on averaged Cs or averaged Ci over time. It is not spatially
% varying as there is no "tissue" invovled. It is simply a model of cells
```

```
% in suspension and the goal is to determine if the saturation of receptors is
% potentially a limiting factor for the delivery of growth factors and the uptake
% of such.
%
% It incorporates both "in vivo" clearance kinetics with constants k1, kr1, kcl
% and also a potential to release drug at rate constant rrel = molar/time
%
% It is called out of the command line with no other m-files within.
% The initial condition vector y0 needs to be included each time. Sample command is:
%
% clear all, clear all global,y0=[0 0 1 0 0 0 0];[t,y]=ode15s('traffickinga', [0 2.88e4], y0);plot(t,y)
%
% *** IT is different from traffickinga.m in that it has low-affinity binding
% that should simulate a storage depot for "natural" controlled-release. The goal
% is to compare the response of these cells when given a bolus of GF versus
% those same cells but without the HSPGs. ***

global kf kr kec krec kdeg kprot n Rsyn y0 Ro Leo f1 f2 kf2 kr2
global keR f1 f2 k1 kr1 kcl rrel

% Kd=100 pM

% Diffusion controlled-limit for kf is 10^8 or 10^9 (M sec)-1, Voet and Voet p338

kf=1e6;
kr=1e-4;
%kr=1e-10*kf;
%kf=kr/1e-10;
kec=0.005;          % 0.3 min-1
keR=0.0005;         % 0.03 min-1
krec=1e-4;          % Chu et al. 0.13 min-1 = 1e-3 for B82's.
kdeg=1e-3;          % FGF in SMC, s-1  Sperinde Nugent, 1998
n=1e9;              % cell/L from Starbuck Lauffenburger, 1992
Nav=6.023e23;       % Avogadro's number #/mol
Rsyn=2;             % Rs synthesis rate, [#/(cell*sec)] Chu et al.
Leo=1e-9;           % Intact ligand concentration for scaling [M]
f1=0.5;             % fraction of complexes degraded
f2=0.05;            % fraction of receptors degraded
Ro=2e4;             % Initial surface receptor number

%kf2=1e8;           % Forward binding to HSPG, "natural" controlled-release effect
                    % The value for kf2 is set in controlc.m
kr2=0.5;            % Reverse un-binding from HPSG, "natural" controlled-release effect

%kprot=6.66e-4;     % Chu et al., 1996. 0.00015; %0.0001

k1=0;%1e-3;         % Suggested numbers might be 1e-3, 1e-4, 1e-4 respectively
kr1=0;%1e-4;        % For in vitro tissue culture, no clearance mechanism so neglect.
kcl=0;%1e-4;

% This is Chu's model for receptor mediated trafficking events.

% Species                                       Initial conditions, y0
%-------------------------------------------------------
% y(1) = intact ligand, Li              [M]     = 0 for CR, =1 for bolus
% y(2) = degraded ligand, Ld            [M]             0
```

```
% y(3) = surface receptor, Rs                    [#/cell]          1
% y(4) = surface complex, Cs                     [#/cell]          0
% y(5) = internal complex, Ci                    [#/cell]          0
% y(6) = internal Ri                             [#/cell]          0
% y(7) = compartment 2 for in vivo               [M]               0
% y(10) = cell number = f(Cs)                    [#/L]             1
% y(8) = free HSPG                               [#/cell]          10-100
% y(9) = bound HSPG, 1:1 ratio                   [#/cell]          0

% Rate constants
%-------------------------------------------------------------
% kf = forward binding constant                  [(M sec)^-1]
% kr = reverse binding constant                  [sec-1]
% kec = internalization     of complexes         [sec-1]
% keR = internalization of free Rs               [sec-1]
% krec = recycling                               [sec-1]
% kdeg = degradation                             [sec-1]
% Rsyn = synthesis                               [#/(cell*sec)]
% kprot = proteolysis extracellular              [sec-1]
% kf2 = forward binding to HSPG                  [(M sec)^-1]
% kr2 = reverse binding from HSPG-gf complex     [sec-1]

% f1= fraction degraded of complexes
% f2= fraction degraded of receptors

% k1 = in vivo distribution constant             [sec-1]
% kr1 = in vivo redistribution constant          [sec-1]
% kcl = clearance rate constant                  [sec-1]

% rrel = polymeric drug release rate             [M sec-1]

g=1;    % g= is a parameter for variable Rs synthesis.
        % where g=(1-Rs/Ro). It is thus equal to 1 when surface
        % receptors are low, giving maximal Rsyn. When Rs is high or equal
        % to Ro, it will be zero. Not sure how to prevent it from going
        % negative on me. The default is simply g=1 where Rsyn is constant.
        % For g=1, Rsyn is constant, reference Carpenter 1987

%g=(1-(y(3)/Ro)); % For synthesis = f(surface receptor number)

%umax=1e-5; % Maximal growth rate [sec-1]
%ED50=0.1;      % Ave Cs at which half-maximal stimulation seen.

% Equations
%-------------------------------------------------------------
        yp=[(-kf*y(1)*y(3)+kr*y(4)/Leo-kf2*y(1)*y(8)+kr2*y(9)/Leo)*n*Ro/Nav-kprot*y(1)-
                (k1+kcl)*y(1)+kr1*y(7)+rrel/Leo;
        (kdeg*f1*y(5))*n*Ro/(Nav*Leo)+kprot*y(1);
        -kf*y(1)*y(3)*Leo+kr*y(4)+g*Rsyn/Ro-keR*y(3)+(1-f2)*krec*y(6);
        kf*y(1)*y(3)*Leo-(kr+kec)*y(4)+krec*y(5)*(1-f1);
        kec*y(4)-(krec*(1-f1)+kdeg*f1)*y(5);
        keR*y(3)-(1-f2)*krec*y(6)-f2*kdeg*y(6);
        k1*y(1)-kr1*y(7);
        -kf2*y(1)*y(8)+kr2*y(9);
        kf2*y(1)*y(8)-kr2*y(9);];
        %(umax/(1+ED50/y(4)))*y(10);];
```

```
% Equations have been scaled to Leo and Ro for ligand and receptor species
% Time is left as dimensional.
```

7.1.3 Interleukin-2 trafficking

```
% This m-file controls 'runil2.m' and allows one to do loops of varying
% parameters. It calls 'runil2.m' which then calls 'traffickingil2.m' and can
% be called from the command line.

clear global, clear all global
clear, clear all

global samedose tday kdeg kprot kec f1 krec Ro keR kf kr Rsyn Leo f2
global ratioLi ratioLd ratioRs ratioRi ratioCs ratioCi ratioCell
global deplete Nav leftover CsCi cellCR cellBolus depleteBolus depleteCR

%kf=1e2;
%kdeg=1e-12;%8;
%kprot=1e-8;
%kec=1e-8;
%krec=1e-6;
%Ro=1;
%keR=1e-8;
%kr=1e-9;
%Rsyn=1e-6;
Leo=0.1;                    % [pM]

for j=1:7,j
        runsimil2;

        ratioLihold(j)=ratioLi;
        ratioLdhold(j)=ratioLd;
        ratioRshold(j)=ratioRs;
        ratioRihold(j)=ratioRi;
        ratioCshold(j)=ratioCs;
        ratioCihold(j)=ratioCi;
        ratioCellhold(j)=ratioCell;

        samedosehold(j)=samedose;
        ratioarrayhold(:,j)=ratioarray';

        %tdayhold(j)=tday;
        %kdeghold(j)=kdeg;
        %kprothold(j)=kprot;
        %kechold(j)=kec;
        %krechold(j)=krec;
        %Rohold(j)=Ro;
        %keRhold(j)=keR;
        %kfhold(j)=kf;
        %krhold(j)=kr;
        %Rsynhold(j)=Rsyn;
        Leohold(j)=Leo;

        %kdeg=kdeg*10
        %kprot=kprot*10;
```

```
        %kec=kec*10;
        %krec=krec*2;
        %Ro=Ro*10;
        %keR=keR*10;
        %kf=kf*10;
        %kr=kr*10;
        %Rsyn=Rsyn*10;
        Leo=Leo*10;

% new added section

        bolusAveCshold(j)=bolusAveCs;
        CRAveCshold(j)=CRAveCs;

        cellCRhold(j)=cellCR;
        cellBolushold(j)=cellBolus;

        depleteBolushold(j)=depleteBolus;
        depleteCRhold(j)=depleteCR;

        clear global ratioLi ratioLd ratioRs ratioRi ratioCs ratioCi
        clear global samedose ratioCell ratioarray deplete leftover CsCi
end

clear global ratioLi ratioLd ratioRs ratioRi ratioCs ratioCi samedose ratioarray
clear global f1 f2 Leo Ro Rsyn kf kr kdeg krec k1 kr1 kcl kec keR n Nav rrel kprot
clear bottm bottom bottmCR last i j ff last ceilCR cellBolus depleteBolus depleteCR
clear bolusAveLi bolusAveLd bolusAveRs bolusAveRi bolusAveCs bolusAveCi
clear CRAveCi CRAveCs CRAveLd CRAveLi CRAveRi CRAveRs
clear CRIntCidt CRIntCsdt CRIntLddt CRIntLidt CRIntRsdt CRIntRidt
clear bolusIntCsdt bolusIntCidt bolusIntRsdt bolusIntRidt bolusIntLddt bolusIntLidt
clear ttmin t y y0 total totalCR ttempBolus ttempCR final
clear global tday tCR tbolus yCR ybolus T
clear averageBolus averageCR thr ytempBolus ytempCR

-------------------------------------------------------------------------------
% This m-file runs trafficking model for IL-2 and Fallon's work and calls the m-file6
% traffickingil2.m.  It can be called by the m-file controlil2.m.

%clear global, clear all global
%clear, clear all

global T tday
global kf kr kdeg krec kec keR Rsyn kprot
global kfe kre Ve rsyn Leo
global rrel Rso
global tbolus ybolus tCR yCR cellBolus cellCR

global samedose tday n Nav depleteBolus depleteCR
global ratioLi ratioLd ratioRs ratioRi ratioCs ratioCi ratioCell ratioarray

Rso=1500;%1500;          % Fallon measures 1500 #/cell
%Leo=10;                 % in [pM]
kprot=1e-4;

ff=1;              % ff=1 for conserved mass/moles added; ff=2 for conserved A.U.C.
```

```
                % 'ff' is a fudge-factor that varies the rate at which drug is released.
                % For comparisons between bolus and CR, one can use either equivalent
                % doses of growth factor, (ff=1), or equivalent time-averaged doses, (ff=2).
                % Since most people seem to compare total AUC, ff=2 is done in most cases.

tday=5;         % turn this off when using 'control.m' if the time-effect
                % is desired.  tday is the length in days for the simulation.

T=7200;         % Time simulation in minutes

kftemp=kf;      % Temporary ariables to hold values while changes are made
kprottemp=kprot; % Temporary ariables to hold values while changes are made

% Determines the in vivo profile without cellular pharmacology to get AUC
                y0=[Leo;0;Rso;0;0;300;0;2.5e8];
                rrel=0;kprot=0;kf=0;
                [ttempBolus,ytempBolus]=ode15s('traffickingil2',[0 T],y0);

                total=cumtrapz(ttempBolus,ytempBolus(:,1));
                bottm=size(total);
                averageBolus=total(bottm(1,1))/T;

% Using AUC, determines rrel, and runs CR simulation
                y0=[Leo;0;Rso;0;0;300;0;2.5e8];
                rrel=Leo/T*f  'prot=0;kf=0;
                [ttempCR,ytempCR]=ode15s('traffickingil2',[0 T],y0);

                totalCR=cumtrapz(ttempCR,ytempCR(:,1));
                bottmCR=size(totalCR);
                averageCR=totalCR(bottmCR(1,1))/T;

%plot(ttempBolus/(24*3600),ytempBolus(:,1),ttempCR/(24*3600),ytempCR(:,1)), pause, pause
%xlabel('Time [days]'), ylabel('L/Leo'),title('Ligand Concentration = f(dosing)')
%will need to also set kprot, kdeg = 0 for ligand profile = f(t)

samedose=averageBolus/averageCR;  % Tests to see if the integrated doses are the same

kprot=kprottemp; clear kprottemp
kf=kftemp; clear kftemp

for i=1:2
        if i==1
                % Runs bolus simulation
                y0=[Leo;0;Rso;0;0;300;0;2.5e8];
                rrel=0;
                [tbolus,ybolus]=ode15s('traffickingil2', [0 T], y0);

                % Calculates integrated values = f(time)
                bolusIntLidt=cumtrapz(tbolus,ybolus(:,1));
                bolusIntLddt=cumtrapz(tbolus,ybolus(:,2));
                bolusIntRsdt=cumtrapz(tbolus,ybolus(:,3));
                bolusIntCsdt=cumtrapz(tbolus,ybolus(:,4));
                bolusIntCidt=cumtrapz(tbolus,ybolus(:,5));
                bolusIntRidt=cumtrapz(tbolus,ybolus(:,6));
                last=size(tbolus);
```

```
        % Calculates average values
        bolusAveLi=bolusIntLidt(last(1,1))/T;        % gives ave Li = [M]
        bolusAveLd=bolusIntLddt(last(1,1))/T;        % gives ave Ld = [M]
        bolusAveRs=bolusIntRsdt(last(1,1))/T;        % gives ave Rs = [#/cell]
        bolusAveCs=bolusIntCsdt(last(1,1))/T;        % gives ave Cs = [#/cell]
        bolusAveCi=bolusIntCidt(last(1,1))/T;        % gives ave Ci = [#/cell]
        bolusAveRi=bolusIntRidt(last(1,1))/T;        % gives ave Ri = [#/cell]

    elseif i==2

        % Runs controlled-release simulation
        y0=[0;0;Rso;0;0;300;0;2.5e8];
        rrel=Leo/T*ff;
        [tCR,yCR]=ode15s('traffickingil2', [0 T], y0);

        % Calculates integrated values = f(time)

        CRIntLidt=cumtrapz(tCR,yCR(:,1));
        CRIntLddt=cumtrapz(tCR,yCR(:,2));
        CRIntRsdt=cumtrapz(tCR,yCR(:,3));
        CRIntCsdt=cumtrapz(tCR,yCR(:,4));
        CRIntCidt=cumtrapz(tCR,yCR(:,5));
        CRIntRidt=cumtrapz(tCR,yCR(:,6));
        bottom=size(tCR);

        % Calculates average values
        CRAveLi=CRIntLidt(bottom(1,1))/T;        % gives ave Li = [M]
        CRAveLd=CRIntLddt(bottom(1,1))/T;        % gives ave Ld = [M]
        CRAveRs=CRIntRsdt(bottom(1,1))/T;        % gives ave Rs = [#/cell]
        CRAveCs=CRIntCsdt(bottom(1,1))/T;        % gives ave Cs = [#/cell]
        CRAveCi=CRIntCidt(bottom(1,1))/T;        % gives ave Ci = [#/cell]
        CRAveRi=CRIntRidt(bottom(1,1))/T;        % gives ave Ri = [#/cell]
    end
end

% Calculates ratio of CR:Bolus for efficacy determination

ratioLi=CRAveLi/bolusAveLi;ratioLd=CRAveLd/bolusAveLd;
ratioRs=CRAveRs/bolusAveRs;ratioRi=CRAveRi/bolusAveRi;
ratioCs=CRAveCs/bolusAveCs;ratioCi=CRAveCi/bolusAveCi;

ratioCell=yCR(bottom(1,1),8)/ybolus(last(1,1),8);
ratioarray(1)=ratioLi;ratioarray(2)=ratioLd;ratioarray(3)=ratioRs;
ratioarray(4)=ratioCs;ratioarray(5)=ratioCi;ratioarray(6)=ratioRi;


global cellCR cellBolus

cellBolus=ybolus(last(1,1),8);cellCR=yCR(bottom(1,1),8);

global depleteCR depleteBolus

depleteBolus=ybolus(last(1,1),1)/Leo; depleteCR=yCR(bottom(1,1),1)/Leo;
```

```
function yp=traffickingil2(t,y)

% clear all global,y0=[10;0;1500;0;0;300;0;2.5e8];[t,y]=ode15s('traffickinga', [0 7500], y0);

% This m-file is based on the model of Fallon and Lauffenburger from Biotech Progress
% Its purpose is to compare the bolus versus controlled-release response of the
% growth factor IL-2 and 2D1 on averaged Cs or averaged Ci over time.
%
% It is called out of the command line with no other m-files within.
% The initial condition vector y0 needs to be included each time.  Sample command is:
%
% clear all, y0=[10;0;1500;0;0;300;0;2.5e8];  [t,y]=ode15s('traffickingil2', [0 7500], y0);

global kf kr kec krec kdeg kprot Rsyn kfe kre
global keR rrel Nav Ve Leo rrel kprot Leo T rsyn

kprot=0;%1e-2; %rrel=0;

% Diffusion controlled-limit for kf is 10^8 or 10^9 (M sec)-1, Voet and Voet p338

kr=0.0138;                      % dissociation rate constant [min-1]

kf=kr/11.1;                     % association rate constant for IL-2
%kf=kr/8.2;                     % association rate constant for 2D1

kre=8*kr;                       % dissociation rate constant, endosome for IL-2
%kre=5*kr;                      % dissociation rate constant, endosome for 2D1

kfe=kre/1000;                   % association rate constant, endosome for IL-2
%kfe=kre/3000;                  % association rate constant, endosome for 2D1

kec=0.04;                       % internalization rate constant [min-1]
keR=0.007;                      % constitutive internalization rate constant [min-1]
krec=0.15;                      % recycling rate constant [min-1]
kdeg=0.035;                     % degradation rate constant [min-1]
Nav=6.023e11;                   % Avogadro's number [#/picomol]
Rsyn=11;                        % Constitutive receptor synthesis rate [min-1]
rsyn=0.0011;                    % Induced receptor synthesis rate [min-1]
Ve=1e-14;                       % Total endosomal volume (L/cell)

% This is Fallon's model for receptor mediated trafficking events.

% Species
%-----------------------------------------------------------
% y(1) = intact ligand, L                   [pM]
% y(2) = degraded ligand, Ld                [pM]
% y(3) = surface receptor, Rs               [#/cell]
% y(4) = surface complex, Cs                [#/cell]
% y(5) = internal complex, Ci               [#/cell]
% y(6) = internal receptor, Ri              [#/cell]
% y(7) = internal ligand, Li                [#/cell]
% y(8) = cell number = f(Cs)                [#/L]

% Equations
%-----------------------------------------------------------
yp=[(-kf*y(1)*y(3)+kr*y(4)+krec*y(7)*Ve*Nav)*y(8)/Nav+rrel-kprot*y(1);
```

```
kdeg*y(5)+kprot*y(1);
-kf*y(1)*y(3)+(kr+rsyn)*y(4)-keR*y(3)+Rsyn;
kf*y(1)*y(3)-(kr+kec)*y(4);
kfe*y(7)*y(6)-(kre+kdeg)*y(5)+kec*y(4);
-kfe*y(7)*y(6)+kre*y(5)+keR*y(3)-kdeg*y(6);
(-kfe*y(7)*y(6)+kre*y(5))/(Ve*Nav)-krec*y(7);
max((600*y(4)/(250+y(4)))-200,0)*1e3;];
```

7.2 MATLAB files for tissue pharmacology simulations

7.2.1 IL-tissue

```
---------------------------------------------------------------------------------------------
---------------------------------------------------------------------------------------------
function [xf]=firstepil2

% This m-file takes the first step forward temporally from the initial conditions.

global boundary1 boundary2 initial N bc1xinit bc2xinit theta r A sp T t

%   -r*theta(1,x-1)+(2+2r)*theta(1,x)-r*theta(1,x+1)=
%                           =+r*theta(0,x-1)+(2-2r)*theta(0,x)+r*theta(0,x+1)

% g is a vector of size (N x sp) or N rows and sp columns

for q=1:sp
        for v=1:N
                if v==1
                        g(1,q)=r(q)*boundary1(1,q)+r(q)*bc1xinit(q)+(2-2*r(q))*initial(q,1)+r(q)*initial(q,2);
                elseif v==N
                        g(N,q)=r(q)*boundary2(1,q)+r(q)*initial(q,N-1)+(2-
2*r(q))*initial(q,N)+r(q)*bc2xinit(q);
                else
                        g(v,q)=r(q)*initial(q,v-1)+(2-2*r(q))*initial(q,v)+r(q)*initial(q,v+1);
                end
        end
end

for q=1:sp
        [L,U]=lu(A(:,:,q));
        xf(:,q)=U\(L\g(:,q));
end

clear L U

---------------------------------------------------------------------------------------------
---------------------------------------------------------------------------------------------

function [xn]=nextstepil2
global boundary1 boundary2 theta r A N xn sp t

% This m-file uses values for theta(t,x) and gives theta(t+1,x).
% The general recursion is

%   -r*theta(t+1,x-1)+(2+2r)*theta(t+1,x)-r*theta(t+1,x+1)
```

```
%                       =   +r*theta(t,x-1)+(2-2r)*theta(t,x)+r*theta(t,x+1)

% We can use the same coefficient matrix of size N x N, A.
% However, we need to re-write the g(x) vector...

clear xn
for q=1:sp
        for w=1:N
                if w==1
                        h(1,q)=r(q)*boundary1(t+1,q)+r(q)*boundary1(t,q)+(2-
2*r(q))*theta(t,1,q)+r(q)*theta(t,2,q);
                elseif w==N
                        h(N,q)=r(q)*boundary2(t+1,q)+r(q)*theta(t,N-1,q)+(2-
2*r(q))*theta(t,N,q)+r(q)*boundary2(t,q);
                else
                        h(w,q)=r(q)*theta(t,w-1,q)+(2-2*r(q))*theta(t,w,q)+r(q)*theta(t,w+1,q);
                end
        end
        [L,U]=lu(A(:,:,q));
        xn(:,q)=U\(L\h(:,q));
end
clear L U

-------------------------------------------------------------------------------
-------------------------------------------------------------------------------
function invariant4

global r N A sp
% Define the invariant coefficient matrix of size N x N to be solved.
% 'A' = is the invariant coefficient matrix

for q=1:sp
        for i=1:N
                if i == 1;
                        A(i,i,q) = (2+2*r(q));
                        A(i,i+1,q) = -r(q);
                elseif i == N
                        A(i,i-1,q) = -r(q);
                        A(i,i,q) = (2+2*r(q));
                else
                        A(i,i-1,q) = -r(q);
                        A(i,i,q) = (2+2*r(q));
                        A(i,i+1,q) = -r(q);
                end
        end
end

-------------------------------------------------------------------------------
-------------------------------------------------------------------------------
% David Wu

% Cellular Pharmacology Model for IL-2 created January 2001 using Scaled Fallon Model

% Method of Crank-Nicholson for implicit discretizing of parabolic partial
% differential equations for Fickian diffusion, referenced from J. Crank,
% 'The Mathematics of Diffusion'. Define a one-dimensional space along time, t.
```

```
% The discretized space is along the column axis and the temporal space is along
% the row axis of matrices used. Using scaled, dimensionless parameters, the
% diffusion equation is:

%                                   d(theta)/dt* = d^2(theta)/dx*^2

% where: theta(i) = C(i)/Co, t* = tD/L^2, here, D refers to a reference species, and
% x* = x/L.

% This m-file calls 'firstepil2.m', 'nextstepil2.m', 'invariantil2.m', 'traffickingil2.m', 'dosing.m'
% For plotting, 'sketchit.m', 'compareit.m', 'graphit.m', 'plotcells.m'
% It is called by 'runsim.m' which allows for variation in global variabes such as rate
% constants, kf, etc.

tic
global boundary1 boundary2 initial theta T bc1xinit bc2xinit    % variables for calculations
global r A N xn sp theta xf t ndsp                              % variables for calculations
global dx dt D                                                  % variables for plotting
global cells Leo cellinitial Rso y0 kf cDo                      % variables for cell pk
global administer
%-------------------------------------------------------------------------------
% Define constants:

Leo = 10e-12;     % intial ligand concentration = 10 picomolar for IL-2
Rso = 1500;       % initial cell receptor number [#/cell]
cDo = 2.5e8       % initial cell density at each node [#/L]
%-------------------------------------------------------------------------------
% Define size of domains:

sp=2;    % Number of DIFFUSING chemical species...(eg.) L intact & L degraded .
N=99;    % 99 Number of internal mesh/grid points along each time row for spatial variable.
T=1008; % 1008 Number of time steps of dt for temporal variable.
ndsp=6; % Number of NON-diffusing species...(eg.) Rs1, Cs1, Ci, Rs2, Cs2. Excludes Li, Ldeg.
%-------------------------------------------------------------------------------
% Define working domains:

theta=zeros(T,N,sp);              % the dimensionless concentration profile = f(t,x)
A=zeros(N,N,sp);                  % the invariant matrix
r=zeros([1,sp]);                  % ratio of time-step/distance step as dt/(dx)^2
cells=zeros(T,N,sp+ndsp);         % size [TxNx(sp+ndsp)]
cellinitial=zeros(N,sp+ndsp);% size [Nx(sp+ndsp)] with first two columns for Lintact and Ldegraded resp.

cellinitial(:,3)=ones;            % sets initial Rs= y(3)= 1 for Rs/Rso=1 for 1500 #/cell
cellinitial(:,6)=ones./5;         % sets initial Ri= y(6)= 0.2 for Ri/Rso= 300 #/cell
cellinitial(:,8)=ones;            % sets initial cell density, cDo y(8)= 1 for 2.5e8 cell#/L
%-------------------------------------------------------------------------------
% Absolute values of distance step, time step and diffusivities:

dx=10e-4;                         % in [cm]. Distance step = 10 um, or one cell distance.
dt=10;                            % in [min].
D=[1e-9*60;1e-9*60];              % Diffusivities in cm^2/sec converted to cm^2/min. Add Di here for sp>1.

totl_TIME_in_days=dt*T/60/24, totl_TIME_in_hours=dt*T/60,
totl_DISTANCE_in_cm=dx*(N+1), totl_DISTANCE_in_microns=dx*(N+1)*1e4, pause  % fyi

r=D*dt/dx^2;% Calculate r, = D*dt/dx^2:
```

```
%-------------------------------------------------------------------------
% ** GENERAL ** boundary conditions1,2 and intial conditions for each species where
% size(initial) = sp x N and size(boundary1) = size(boundary2) = T x sp.  Also define
% two corner pieces, bc1,2xinit(sp):

initial=ones([sp,N])*100; boundary1=zeros([T,sp]);boundary2=zeros([T,sp]);
for q=1:sp, bc1xinit(q) = 0; bc2xinit(q) = 0; end
%-------------------------------------------------------------------------
% ** SPECIFIC ** conditions, modify the available, general matrices of initial
% and boundary1,2 with zeroes or ones for sinks/source respectively.  Can also have the
% boundary conditions change = f(t), as in a bolus pulse using a double exponential
% or a continously releasing source for controlled release.

for q=1:sp
        if q==1
                %boundary1(:,q)=ones(T,1); boundary2(:,q)=zeros(T,1);          % source of 10 pM Lintact on left
                %boundary1(:,q)=ones(T,1)*100; boundary2(:,q)=zeros(T,1);  % source of 100 pM Lintact on left
        % for IL-2 concentration = 10 pM, use a boundary condition set to 1
                % for IL-2 concentration = 100 pM, use a boundary condition set to 10
        else
                boundary1(:,q)=zeros(T,1); boundary2(:,q)=zeros(T,1);          % no source of Ldeg anywhere
        end
end
%administer =0;  % for bolus, adminster = 0, for CR, administer = 1
%dosingil2;              % This m-file determines if a bolus or controlled-release method is used.
%-------------------------------------------------------------------------
% Begin first time-step for diffusion step...

t=0
invariantil2            % Define the invariant matrix of size [N x N x sp] for implicit solving.
xf=firstepil2;          % First calculate theta(t=1,x) from initial and boundary conditions.
                        % 'xf' is an array of size [N x sp] that holds the solution to the system
                        % of linear eqs.
%-------------------------------------------------------------------------
% Begin first reaction step...

for n=1:N
        for q=1:sp              % This writes Lintact and Ldegraded from xf into columns 1,2 of
                cellinitial(:,q)=xf(:,q);       % 'cellinitial' which is needed for pharmacology.
        end
        y0=cellinitial(n,:);            % For this and each 'n', writes 'y0' by taking all sp and ndsp.

        [tT,yY]=ode15s('traffickingil2',[t*dt (t+1)*dt],y0);
        last=size(tT);                  % 'last' is a vector of size [??x1], thus choose Last(1,1)

        for k=1:(sp+ndsp)
                if k<=sp
                        xf(n,k)=yY(last(1,1),k);cells(1,n,k)=yY(last(1,1),k);
                else
                        cells(1,n,k)=yY(last(1,1),k);
                        % Writes new receptor distribution profile to 'cell'
                end
        end
end
```

```
clear y0 last tT yY

for q=1:sp                              % For each species, calculate first approximation
        theta(1,:,q)=xf(:,q)';          % and copy data into theta matrix for q=1:sp.
end                                     % This gives the inital concentrations at each
                                        % position, x, for each species, sp.
%-------------------------------------------------------------------------
% For every other step after first... use the same m-file, 'nextstep4.m'
% Each time, 'theta' and 't' will be passed in with 'xn' and 't' being passed out.
% Will calculate each time point for each species before moving on to the next time point.

t=1             % This t=1 has to be here, otherwise, 'nextstep' won't work.
for p=1:T-1     % For each time step, we will calculate concentrations for all species at all points:

        [xn]=nextstepil2; % Returns 'xn' a vector of N rows and sp columns [N x sp]

        for q=1:sp              % This writes Lintact and Ldegraded from 'xn' into columns 1,2 of
                cells(p,:,q)=xn(:,q);
                                % 'cell' which is needed for pharmacology. Need p here, not p+1.
        end
        clear xn
        for n=1:N
                y0diag=cells(p,n,:);
                                % For this and each 'n', writes 'y0' by taking all sp and ndsp.
                for b=1:(sp+ndsp), y0(1,b)=y0diag(1,1,b); end
                                % Rotates y0diag into a vector instead of 1x1x3 matrix

                        [Tt,Yy]=ode15s('traffickingil2',[p*dt (p+1)*dt], y0);
                        bottom=size(Tt);

                        for g=1:(sp+ndsp)
                                if g<=sp
                                        xn(n,g)=Yy(bottom(1,1),g);cells(p+1,n,g)=Yy(bottom(1,1),g);
                                else
                                        cells(p+1,n,g)=Yy(bottom(1,1),g);
                                        % Writes new receptor distribution profile to 'cell'
                                end
                        end

                        clear y0 y0diag bottom Tt Yy last yY tT
                end

                for q=1:sp              % For each species, calculate the next approximation
                        theta(p+1,:,q)=xn(:,q)';
                                        % and copy data into theta matrix for q=1:sp.
                end                     % This gives the subsequent concentration at each
                t=t+1                   % position, x, for each species, sp.
                clear xn
        end
%-------------------------------------------------------------------------
% Animate the data
toc
%pause
%sketchit  % Calls 'sketchit.m' to sketch theta = f(x,t) in dimensionLESS variables
%graphit4  % Calls 'graphit.m' to graph theta = f(x,t) in dimensionAL coordinates
%compareit
```

```
clear global xf tinit time tfin r q p A D Leo Ro t b bc1xinit bc2xinit
clear global boundary1 boundary2 cellinitial distance g initial k n p q p r

clear xf tinit time tfin r q p A D Leo Ro t b bc1xinit bc2xinit
clear boundary1 boundary2 cellinitial distance g initial k n p q p r

-------------------------------------------------------------------------------------
-------------------------------------------------------------------------------------
function plotcells

global cellshold thetahold N T cells theta dt cells10

% This file can be called out of the command-line workspace
% which requires the global parameters cells and theta. It
% animates Li, Ld, Rs, Cs, Ci = f(t,x).
% Use 'plotcells1.m' in order to compare between bolus and
% controlled-release as subplots.

%hold on

figure(1)
for u=1:T
%for u=7*24*60/10

%plot([1:N],cellshold(u,:,4,1),[1:N],cellshold(u,:,4,2));
%plot([1:N],theta(u,:,1),'m',[1:N],theta(u,:,2),'r:');
%plot([1:N],cells(u,:,1),[1:N],cells(u,:,2),[1:N],cells(u,:,3),[1:N],cells(u,:,4),[1:N],cells(u,:,5))

        plot([1:N],cells(u,:,1)./100,'b',[1:N],cells(u,:,8),'g',[1:N],cells(u,:,4),'r',[1:N],cells10(u,:,1)./100,'b--
        ',[1:N],cells10(u,:,8),'g--',[1:N],cells10(u,:,4),'r--')
%plot([1:N],cells(u,:,1)./100,'b',[1:N],cells(u,:,8),'g',[1:N],cells(u,:,3),'r')
axis([0 N+1 0 6])

                title(floor(u*dt/60))
                ylabel('Scaled value, blue = L, green = cell#')
                xlabel('Dimensionless distance')
                pause(0.25);

                if u*dt/60/24==1
                        figure(2)
                elseif u*dt/60/24==2
                        figure(3)
                elseif u*dt/60/24==3
                        figure(4)
                elseif u*dt/60/24==4
                        figure(5)
                elseif u*dt/60/24==5
                        figure(6)
                elseif u*dt/60/24==6
                        figure(7)
                end

end

-------------------------------------------------------------------------------------
```

```
---------------------------------------------------------------------------------------------
function yp=traffickingil2(t,y)

% THIS IS THE DIMENSIONLESS FORM OF FALLON'S EQUATIONS WITH THE VARIABLES ALL
SCALED AS:

% L/Leo, Ld/Leo, Li/Leo
% Rs/Rso, Ri/Rso, Ci/Rso, Cs/Rso
% Y/cDo

% clear all global,y0=[10;0;1500;0;0;300;0;2.5e8];[t,y]=ode15s('traffickinga', [0 7500], y0);

% This m-file is based on the model of Fallon and Lauffenburger from Biotech Progress
% Its purpose is to compare the bolus versus controlled-release response of the
% growth factor IL-2 and 2D1 on averaged Cs or averaged Ci over time.
%
% It is called out of the command line with no other m-files within.
% The initial condition vector y0 needs to be included each time. Sample command is:
%
% clear all, y0=[10;0;1500;0;0;300;0;2.5e8]; [t,y]=ode15s('traffickingil2', [0 7500], y0);

global kf kr kec krec kdeg kprot Rsyn kfe kre
global keR rrel Nav Ve Leo rrel kprot Leo rsyn Rso cDo

Leo=10;                 % initial ligand concentration [picoMol]
Rso=1500;               % receptor number [#/cell]
cDo=2.5e8;              % cell density [#/L]

rrel=0;
kprot=0;

kr=0.0138;              % dissociation rate constant [min-1]
kf=kr/11.1;             % association rate constant for IL-2 in [min/picoMol]
kre=8*kr;               % dissociation rate constant, endosome for IL-2
kfe=kre/1000;           % association rate constant, endosome for IL-2 in [min/picoMol]

kec=0.04;               % internalization rate constant [min-1]
keR=0.007;              % constitutive internalization rate constant [min-1]
krec=0.15;              % recycling rate constant [min-1]
kdeg=0.035;             % degradation rate constant [min-1]
Nav=6.023e11;           % Avogadro's number [#/picomol]
Rsyn=11;                % Constitutive receptor synthesis rate [min-1]
rsyn=0.0011;            % Induced receptor synthesis rate [min-1]
Ve=1e-14;               % Total endosomal volume (L/cell)

% This is Fallon's model for receptor mediated trafficking events.

% Species
%-------------------------------------------------------------
% y(1) = intact ligand, L                    [pM]
% y(2) = degraded ligand, Ld                 [pM]
% y(3) = surface receptor, Rs                [#/cell]
% y(4) = surface complex, Cs                 [#/cell]
% y(5) = internal complex, Ci                [#/cell]
% y(6) = internal receptor, Ri               [#/cell]
% y(7) = internal ligand, Li                 [#/cell]
```

```
% y(8) = cell number = f(Cs)                    [#/L]

% Equations
%-------------------------------------------------------------
yp=[(-kf*y(1)*y(3)*Rso+kr*y(4)*Rso/Leo+krec*y(7)*Ve*Nav)*y(8)*cDo/Nav-kprot*y(1);
        kdeg*y(5)*Rso/Leo+kprot*y(1);
        -kf*y(1)*y(3)*Leo+(kr+rsyn)*y(4)-keR*y(3)+Rsyn/Rso;
        kf*y(1)*y(3)*Leo-(kr+kec)*y(4);
        kfe*y(7)*y(6)*Leo-(kre+kdeg)*y(5)+kec*y(4);
        -kfe*y(7)*y(6)*Leo+kre*y(5)+keR*y(3)-kdeg*y(6);
        (-kfe*y(7)*y(6)*Rso+kre*y(5)*Rso/Leo)/(Ve*Nav)-krec*y(7);
        max((600*y(4)*Rso/(250+y(4)*Rso))-200,0)*1e3/cDo;];
```

8 NOMENCLATURE

AS	Acid strip
A.U.C.	Total area under the curve
BMP4	Bone morphogenic protein
BSA	Bovine serum albumin
C_{eq}	Equilibrium surface bound complexes
ChAT	Choline acetyltransferase
CR	Controlled release
Da	Damkohler number
DMEM	Dulbecco Modified Eagle's Medium
ECM	Extracellular matrix
EGF	Epidermal growth factor
EVAc	poly-Ethylene-vinyl acetate
FBS	Fetal bovine serum
FGF-2	Fibroblast growth factor, basic
FPLC	Fast protein liquid chromatography
FRET	Fluorescence resonance energy transfer
G418	Geneticin
HPLC	High pressure liquid chromatography
IFQ	Intramolecular fluorescence quenching
IL-2	Interleukin-2
K_d	Equilibrium binding constant
L	Ligand concentration
NGF	Nerve growth factor
N.S.	Not significant, $p > 0.05$
PDGF	Platelet derived growth factor
Pe	Peclet number
PBS	Phosphate buffered saline
PBS^{++}	Phosphate buffered saline with calcium and magnesium
RA	Retinoic acid
TGFα	Transforming growth factor-α
TGFβ	Transforming growth factor-β
VEGF	Vascular endothelial growth factor
WHIPS	Wash buffer

9 REFERENCES

1. Daemen, M.J.A.P., H.H.W. Thijssen, and H.A.J. Struyker-Boudier, *Pharmacokinetic considerations in local drug delivery.* Adv Drug Del Rev, 1991. **6**: p. 1-18.
2. Eriksson, U.G. and T.N. Tozer, *Pharmacokinetic evaluation of regional drug delivery.* Acta Pharm Jugosl, 1987. **37**: p. 331-44.
3. Hoffman, A., *Pharmacodynamic aspects of sustained release preparations.* Adv Drug Del Rev, 1998. **33**: p. 185-99.
4. Suzuki, H., *et al.*, *Design of a drug delivery system for targeting based on pharmacokinetic consideration.* Adv Drug Del Rev, 1996. **19**: p. 335-7.
5. Charnick, S.B., *et al.*, *Perspectives in pharmacokinetics. Physiologically based pharmacokinetic modeling as a tool for drug development [see comments].* J Pharmacokinet Biopharm, 1995. **23**(2): p. 217-29.
6. Kornowski, R., *et al.*, *Delivery strategies to achieve therapeutic myocardial angiogenesis.* Circulation, 2000. **101**(4): p. 454-8.
7. Koch-Weser, J., *Clinical importance of pharmacokinetic and pharmacodynamic drug interactions.* Neth J Med, 1977. **20**(2): p. 59-70.
8. Greenblatt, D.J. and J. Koch-Weser, *Clinical pharmacokinetics (second of two parts).* N Engl J Med, 1975. **293**(19): p. 964-70.
9. Koch-Weser, J., *Bioavailability of drugs (second of two parts).* N Engl J Med, 1974. **291**(10): p. 503-6.
10. Koch-Weser, J., *Bioavailability of drugs (first of two parts).* N Engl J Med, 1974. **291**(5): p. 233-7.
11. Edelman, E.R. and M. Lovich, *Drug delivery models transported to a new level [news; comment].* Nat Biotechnol, 1998. **16**(2): p. 136-7.
12. Chu, L., H.S. Wiley, and D.A. Lauffenburger, *Endocytic Relay as a Potential Means for Enhancing Ligand Transport through Cellular Tissue Matrices: Analysis and Possible Implications for Drug Delivery.* Tissue Eng, 1996. **2**(1): p. 17-38.
13. Rippley, R.K. and C.L. Stokes, *Effects of cellular pharmacology on drug distribution in tissues.* Biophys J, 1995. **69**(3): p. 825-39.
14. Lauffenburger, D.A. and J.J. Linderman, *Receptors: Models for binding, trafficking, and signaling.* 1993, New York: Oxford University Press. 365.
15. Wilson, P.A., *et al.*, *Concentration-dependent patterning of the Xenopus ectoderm by BMP4 and its signal transducer Smad1.* Development, 1997. **124**(16): p. 3177-84.
16. Neumann, C. and S. Cohen, *Morphogens and pattern formation.* Bioessays, 1997. **19**(8): p. 721-9.
17. Zecca, M., K. Basler, and G. Struhl, *Direct and long-range action of a wingless morphogen gradient.* Cell, 1996. **87**(5): p. 833-44.
18. Gurdon, J.B., A. Mitchell, and K. Ryan, *An experimental system for analyzing response to a morphogen gradient.* Proc Natl Acad Sci U S A, 1996. **93**(18): p. 9334-8.
19. Strigini, M. and S.M. Cohen, *A Hedgehog activity gradient contributes to AP axial patterning of the Drosophila wing.* Development, 1997. **124**(22): p. 4697-705.
20. McDowell, N., *et al.*, *Activin has direct long-range signalling activity and can form a concentration gradient by diffusion.* Curr Biol, 1997. **7**(9): p. 671-81.
21. Gurdon, J.B., A. Mitchell, and D. Mahony, *Direct and continuous assessment by cells of their position in a morphogen gradient.* Nature, 1995. **376**(6540): p. 520-1.
22. Cooke, J., *Morphogens in vertebrate development: how do they work?* Bioessays, 1995. **17**(2): p. 93-6.
23. Kengaku, M. and H. Okamoto, *bFGF as a possible morphogen for the anteroposterior axis of the central nervous system in Xenopus.* Development, 1995. **121**(9): p. 3121-30.
24. Roth, S., D. Stein, and C. Nusslein-Volhard, *A gradient of nuclear localization of the dorsal protein determines dorsoventral pattern in the Drosophila embryo.* Cell, 1989. **59**(6): p. 1189-202.
25. Tickle, C., J. Lee, and G. Eichele, *A quantitative analysis of the effect of all-trans-retinoic acid on the pattern of chick wing development.* Dev Biol, 1985. **109**(1): p. 82-95.
26. Scadding, S.R. and M. Maden, *Retinoic acid gradients during limb regeneration.* Dev Biol, 1994. **162**(2): p. 608-17.
27. Zheng, M. and D.P. Kuffler, *Guidance of regenerating motor axons in vivo by gradients of diffusible peripheral nerve-derived factors.* J Neurobiol, 2000. **42**(2): p. 212-9.
28. Allavena, P., *et al.*, *Interleukin-12 is chemotactic for natural killer cells and stimulates their interaction with vascular endothelium.* Blood, 1994. **84**(7): p. 2261-8.

29. Shahabuddin, S., P. Ponath, and R.P. Schleimer, *Migration of eosinophils across endothelial cell monolayers: interactions among IL-5, endothelial-activating cytokines, and C-C chemokines.* J Immunol, 2000. **164**(7): p. 3847-54.
30. Laan, M., *et al.*, *Neutrophil recruitment by human IL-17 via C-X-C chemokine release in the airways.* J Immunol, 1999. **162**(4): p. 2347-52.
31. Wang, J.M., *et al.*, *Chemotactic activity of recombinant human granulocyte colony- stimulating factor.* Blood, 1988. 72(5): p. 1456-60.
32. Bochner, B.S., *et al.*, *IL-3 augments adhesiveness for endothelium and CD11b expression in human basophils but not neutrophils.* J Immunol, 1990. **145**(6): p. 1832-7.
33. Komjati, M., P. Bratusch-Marrain, and W. Waldhausl, *Superior efficacy of pulsatile versus continuous hormone exposure on hepatic glucose production in vitro.* Endocrinology, 1986. **118**(1): p. 312-9.
34. Schmitz, O., *et al.*, *Augmented effect of short-term pulsatile versus continuous insulin delivery on lipid metabolism but similar effect on whole-body glucose metabolism in obese subjects.* Metabolism, 1994. **43**(7): p. 842-6.
35. Chou, H.F. and E. Ipp, *Pulsatile insulin secretion in isolated rat islets.* Diabetes, 1990. **39**(1): p. 112-7.
36. Matthews, D.R., *et al.*, *Pulsatile insulin has greater hypoglycemic effect than continuous delivery.* Diabetes, 1983. **32**(7): p. 617-21.
37. Paolisso, G., *et al.*, *Effects of pulsatile delivery of insulin and glucagon in humans.* Am J Physiol, 1989. **257**(5 Pt 1): p. E686-96.
38. Laursen, T., *et al.*, *Serum concentrations of growth hormone (GH) binding protein in GH-deficient patients: Impact of mode of GH administration.* Endo Met, 1997. **4**(4): p. 281-7.
39. Clark, R.G., *et al.*, *Growth Responses to Patterned GH Delivery.* Endocrine, 1995. **3**(10): p. 717-23.
40. Hochberg, Z., T. Bick, and T. Amit, *Stoichiometry of the pulsating growth hormone (GH) binding to the GH-binding protein and the turnover GH-receptor.* Proc Soc Exp Biol Med, 1994. **206**(3): p. 249-53.
41. Hoffmann, H., *et al.*, *Evaluation of an oral pulsatile delivery system for melatonin in humans.* Pharmazie, 1998. **53**(7): p. 462-6.
42. Benghuzzi, H., R. Possley, and B. England, *Pulsatile delivery of progesterone and estradiol to mimic the ovulatory surge in adult ewes by means of TCPL implants.* Biomed Sci Instrum, 1994. **30**: p. 187-95.
43. Weigle, D.S. and C.J. Goodner, *Evidence that the physiological pulse frequency of glucagon secretion optimizes glucose production by perifused rat hepatocytes.* Endocrinology, 1986. **118**(4): p. 1606-13.
44. Randolph, G.W. and A.R. Fuchs, *Pulsatile administration enhances the effect and reduces the dose of oxytocin required for induction of labor.* Am J Perinatol, 1989. **6**(2): p. 159-66.
45. Reid, G.J. and M.E. Helewa, *A trial of pulsatile versus continuous oxytocin administration for the induction of labor.* J Perinatol, 1995. **15**(5): p. 364-6; quiz 367-8.
46. Apostolakis, E.M., *et al.*, *Dissociation of pulsatile cortisol and adrenocorticotropin secretion in fetal sheep during late gestation.* Endocrinology, 1992. **130**(5): p. 2571-8.
47. Wetsel, W.C., *et al.*, *Intrinsic pulsatile secretory activity of immortalized luteinizing hormone-releasing hormone-secreting neurons.* Proc Natl Acad Sci U S A, 1992. **89**(9): p. 4149-53.
48. Bick, T., *et al.*, *The interrelationship of growth hormone (GH), liver membrane GH receptor, serum GH-binding protein activity, and insulin-like growth factor I in the male rat.* Endocrinology, 1990. **126**(4): p. 1914-20.
49. Paolisso, G., *et al.*, *Pulsatile rather than continuous glucagon infusion leads to greater metabolic derangements in insulin-dependent diabetic subjects.* Diabete Metab, 1990. **16**(1): p. 42-7.
50. Lovich, M.A. and E.R. Edelman, *Tissue concentration of heparin, not administered dose, correlates with the biological response of injured arteries in vivo.* Proc Natl Acad Sci U S A, 1999. **96**(20): p. 11111-6.
51. Mahoney, M.J. and W.M. Saltzman, *Millimeter-scale positioning of a nerve-growth-factor source and biological activity in the brain.* Proc Natl Acad Sci U S A, 1999. **96**(8): p. 4536-9.
52. Beaty, C.E. and W.M. Saltzman, *Controlled growth factor delivery induces differentiatial neurite outgrowth in three-dimensional cell cultures.* J Controlled Rel, 1993. **24**: p. 15-23.
53. Flaumenhaft, R., D. Moscatelli, and D.B. Rifkin, *Heparin and heparan sulfate increase the radius of diffusion and action of basic fibroblast growth factor.* J Cell Biol, 1990. **111**(4): p. 1651-9.
54. Bratusch-Marrain, P.R., M. Komjati, and W.K. Waldhausl, *Efficacy of pulsatile versus continuous insulin administration on hepatic glucose production and glucose utilization in type I diabetic humans.* Diabetes, 1986. **35**(8): p. 922-6.
55. Paolisso, G., *et al.*, *Pulsatile insulin delivery has greater metabolic effects than continuous hormone administration in man: importance of pulse frequency.* J Clin Endocrinol Metab, 1991. 72(3): p. 607-15.

56. Paolisso, G., *et al.*, *Pulsatile glucagon has greater hyperglycaemic, lipolytic and ketogenic effects than continuous hormone delivery in man: effect of age.* Diabetologia, 1990. **33**(5): p. 272-7.
57. Johansson, J.O., *et al.*, *Two weeks of daily injections and continuous infusion of recombinant human growth hormone (GH) in GH-deficient adults. 1. Effects of insulin-like growth factor-I (IGF-I), GH and IGF binding proteins, and glucose homeostasis.* Metab-Clin Expt, 1996. **45**(3): p. 362-9.
58. Odem, R.R., B.A. Work, Jr., and M.Y. Dawood, *Pulsatile oxytocin for induction of labor: a randomized prospective controlled study.* J Perinat Med, 1988. **16**(1): p. 31-7.
59. McFadden, R. and C.S. Kwok, *Mathematical model of simultaneous diffusion and binding of antitumor antibodies in multicellular human tumor spheroids.* Cancer Res, 1988. **48**(14): p. 4032-7.
60. Thomas, G.D., *et al.*, *Effect of dose, molecular size, affinity, and protein binding on tumor uptake of antibody or ligand: a biomathematical model.* Cancer Res, 1989. **49**(12): p. 3290-6.
61. Thomas, G.D., *et al.*, *Theoretical considerations for improving tumour targeting.* Br J Cancer Suppl, 1990. **10**: p. 70-3.
62. Baxter, L.T. and R.K. Jain, *Transport of fluid and macromolecules in tumors. III. Role of binding and metabolism.* Microvasc Res, 1991. **41**(1): p. 5-23.
63. Baxter, L.T. and R.K. Jain, *Transport of fluid and macromolecules in tumors. IV. A microscopic model of the perivascular distribution.* Microvasc Res, 1991. **41**(2): p. 252-72.
64. Bratzler, R.L., C.K. Colton, and K.A. Smith, *Theoretical models for transport of low-density lipoproteins in the arterial wall.* Adv Exp Med Biol, 1977. **82**: p. 943-51.
65. Bratzler, R.L., *et al.*, *The distribution of labeled low-density lipoproteins across the rabbit thoracic aorta in vivo.* Atherosclerosis, 1977. **28**(3): p. 289-307.
66. Bratzler, R.L., *et al.*, *The distribution of labeled albumin across the rabbit thoracic aorta in vivo.* Circ Res, 1977. **40**(2): p. 182-90.
67. Karel, S.F., L. S.B., and C.R. Robertson, *The Immobilization of Whole Cells: Engineering Principles.* Chem Eng Sci, 1985. **40**(8): p. 1321-54.
68. Saltzman, W.M. and M.L. Radomsky, *Drugs Released from Polymers: Diffusion and Elimination in Brain Tissue.* Chem Eng Sci, 1991. **46**(10): p. 2429-44.
69. Lovich, M.A. and E.R. Edelman, *Computational simulations of local vascular heparin deposition and distribution.* Am J Physiol, 1996. **271**(5 Pt 2): p. H2014-24.
70. Juweid, M., *et al.*, *Micropharmacology of monoclonal antibodies in solid tumors: direct experimental evidence for a binding site barrier.* Cancer Res, 1992. **52**(19): p. 5144-53.
71. Fujimori, K., *et al.*, *Modeling analysis of the global and microscopic distribution of immunoglobulin G, F(ab')2, and Fab in tumors.* Cancer Res, 1989. **49**(20): p. 5656-63.
72. Shockley, T.R., *et al.*, *Spatial distribution of tumor-specific monoclonal antibodies in human melanoma xenografts.* Cancer Res, 1992. **52**(2): p. 367-76.
73. Chu, L., *Ligand transport through cellular matrices and the role of receptor-mediated trafficking*, in *Dept. of Chemical Engineering*. 1998, Massachusetts Institute of Technology: Cambridge.
74. Topp, E.M., *et al.*, *Antibody transport in cultured tumor cell layers.* J Controlled Release, 1998. **53**(1-3): p. 15-23.
75. King, G.L. and S.M. Johnson, *Receptor-mediated transport of insulin across endothelial cells.* Science, 1985. **227**(4694): p. 1583-6.
76. Okamoto, C.T., *Endocytosis and Transcytosis.* Adv Drug Del Rev, 1998. **29**: p. 215-28.
77. Ghinea, N., *et al.*, *How protein hormones reach their target cells. Receptor-mediated transcytosis of hCG through endothelial cells.* J Cell Biol, 1994. **125**(1): p. 87-97.
78. Fillebeen, C., *et al.*, *Receptor-mediated transcytosis of lactoferrin through the blood-brain barrier.* J Biol Chem, 1999. **274**(11): p. 7011-7.
79. Dehouck, B., *et al.*, *A new function for the LDL receptor: transcytosis of LDL across the blood-brain barrier.* J Cell Biol, 1997. **138**(4): p. 877-89.
80. De Angelis, E., S.H. Moss, and C.W. Pouton, *Endothelial cell biology and culture methods for drug transport studies.* Adv Drug Del Rev, 1995. **18**: p. 193-218.
81. Edelman, E.R. and M.J. Karnovsky, *Contrasting effects of the intermittent and continuous administration of heparin in experimental restenosis.* Circulation, 1994. **89**(2): p. 770-6.
82. Rogers, C., M.J. Karnovsky, and E.R. Edelman, *Inhibition of experimental neointimal hyperplasia and thrombosis depends on the type of vascular injury and the site of drug administration.* Circulation, 1993. **88**(3): p. 1215-21.

83. Edelman, E.R., D.H. Adams, and M.J. Karnovsky, *Effect of controlled adventitial heparin delivery on smooth muscle cell proliferation following endothelial injury.* Proc Natl Acad Sci U S A, 1990. **87**(10): p. 3773-7.
84. Lovich, M.A., *et al.*, *Arterial heparin deposition: role of diffusion, convection, and extravascular space.* Am J Physiol, 1998. **275**(6 Pt 2): p. H2236-42.
85. Lovich, M.A., L. Brown, and E.R. Edelman, *Drug clearance and arterial uptake after local perivascular delivery to the rat carotid artery.* J Am Coll Cardiol, 1997. **29**(7): p. 1645-50.
86. Lovich, M.A. and E.R. Edelman, *Mechanisms of transmural heparin transport in the rat abdominal aorta after local vascular delivery.* Circ Res, 1995. **77**(6): p. 1143-50.
87. Simons, M., *et al.*, *Antisense c-myb oligonucleotides inhibit intimal arterial smooth muscle cell accumulation in vivo.* Nature, 1992. **359**(6390): p. 67-70.
88. Edelman, E.R., *et al.*, *c-myc in vasculoproliferative disease.* Circ Res, 1995. **76**(2): p. 176-82.
89. Simons, M., E.R. Edelman, and R.D. Rosenberg, *Antisense proliferating cell nuclear antigen oligonucleotides inhibit intimal hyperplasia in a rat carotid artery injury model.* J Clin Invest, 1994. **93**(6): p. 2351-6.
90. Koo, E.W.Y. and E.R. Edelman, *Cellular Effects of Antisense c-myc Oligonucleotides Are Delivery Dependent.* Drug Del, 1996. **3**(3): p. 149-54.
91. Arai, K.I., *et al.*, *Peptide growth factors and their receptors.* Handbook of experimental pharmacology. Vol. 95. 1990: Springer-Verlag.
92. Sporn, M.B. and A.B. Roberts, *Peptide growth factors are multifunctional.* Nature, 1988. **332**(6161): p. 217-9.
93. Lopez, J.J., *et al.*, *Hemodynamic effects of intracoronary VEGF delivery: evidence of tachyphylaxis and NO dependence of response.* Am J Physiol, 1997. **273**(3 Pt 2): p. H1317-23.
94. Heldin, C.H., B. Westermark, and A. Wasteson, *Desensitisation of cultured glial cells to epidermal growth factor by receptor down-regulation.* Nature, 1979. **282**(5737): p. 419-20.
95. Blackard, W.G., P.S. Guzelian, and E.E. Small, *Down regulation of insulin receptors.* Trans Am Clin Climatol Assoc, 1979. **90**: p. 94-101.
96. Stoscheck, C.M. and G. Carpenter, *Characterization of the metabolic turnover of epidermal growth factor receptor protein in A-431 cells.* J Cell Physiol, 1984. **120**(3): p. 296-302.
97. Stoscheck, C.M. and G. Carpenter, *Down regulation of epidermal growth factor receptors: direct demonstration of receptor degradation in human fibroblasts.* J Cell Biol, 1984. **98**(3): p. 1048-53.
98. Masui, H., L. Castro, and J. Mendelsohn, *Consumption of EGF by A431 cells: evidence for receptor recycling.* J Cell Biol, 1993. **120**(1): p. 85-93.
99. Lohse, M.J., *Molecular mechanisms of membrane receptor desensitization.* Biochim Biophys Acta, 1993. **1179**(2): p. 171-88.
100. Reddy, C.C., A. Wells, and D.A. Lauffenburger, *Proliferative response of fibroblasts expressing internalization- deficient epidermal growth factor (EGF) receptors is altered via differential EGF depletion effect.* Biotechnol Prog, 1994. **10**(4): p. 377-84.
101. Cohen, S., *et al.*, *Controlled delivery systems for proteins based on poly(lactic/glycolic acid) microspheres.* Pharm Res, 1991. **8**(6): p. 713-20.
102. Mitragotri, S., D. Blankschtein, and R. Langer, *Ultrasound-mediated transdermal protein delivery.* Science, 1995. **269**(5225): p. 850-3.
103. Edwards, D.A., *et al.*, *Large porous particles for pulmonary drug delivery.* Science, 1997. **276**(5320): p. 1868-71.
104. Langer, R., *Drug delivery and targeting.* Nature, 1998. **392**(6679 Suppl): p. 5-10.
105. Santini, J.T., Jr., M.J. Cima, and R. Langer, *A controlled-release microchip.* Nature, 1999. **397**(6717): p. 335-8.
106. Cullis, P.R., A. Chonn, and S.C. Semple, *Interactions of liposomes and lipid-based carrier systems with blood proteins: Relation to clearance behaviour in vivo.* Adv Drug Deliv Rev, 1998. **32**(1-2): p. 3-17.
107. Cullis, P.R. and A. Chonn, *Recent advances in liposome technologies and their applications for systemic gene delivery.* Adv Drug Deliv Rev, 1998. **30**(1-3): p. 73-83.
108. Nugent, H.M., C. Rogers, and E.R. Edelman, *Endothelial implants inhibit intimal hyperplasia after porcine angioplasty.* Circ Res, 1999. **84**(4): p. 384-91.
109. Nugent, M.A., *et al.*, *Perlecan is required to inhibit thrombosis after deep vascular injury and contributes to endothelial cell-mediated inhibition of intimal hyperplasia.* Proc Natl Acad Sci U S A, 2000. **97**(12): p. 6722-7.

110. Nathan, A., M.A. Nugent, and E.R. Edelman, *Tissue engineered perivascular endothelial cell implants regulate vascular injury.* Proc Natl Acad Sci U S A, 1995. **92**(18): p. 8130-4.
111. Kuhl, P.R. and L.G. Griffith-Cima, *Tethered epidermal growth factor as a paradigm for growth factor-induced stimulation from the solid phase [published erratum appears in Nat Med 1997 Jan;3(1):93].* Nat Med, 1996. **2**(9): p. 1022-7.
112. Dinbergs, I.D., L. Brown, and E.R. Edelman, *Cellular response to transforming growth factor-beta1 and basic fibroblast growth factor depends on release kinetics and extracellular matrix interactions.* J Biol Chem, 1996. **271**(47): p. 29822-9.
113. Peters, M.C., *et al.*, *Release from alginate enhances the biological activity of vascular endothelial growth factor.* J Biomater Sci Polym Ed, 1998. **9**(12): p. 1267-1278.
114. Bick, T., *et al.*, *Roles of pulsatility and continuity of growth hormone (GH) administration in the regulation of hepatic GH-receptors, and circulating GH-binding protein and insulin-like growth factor-I.* Endocrinology, 1992. **131**(1): p. 423-9.
115. Aharonov, A., D.S. Passovoy, and H.R. Herschman, *Mitogenic response to epidermal growth factor: relationship to number, affinity, and down-regulation of EGF receptors in three murine embryo cell lines.* J Supramol Struct, 1978. **9**(1): p. 41-5.
116. Presta, M., *et al.*, *Basic fibroblast growth factor requires a long-lasting activation of protein kinase C to induce cell proliferation in transformed fetal bovine aortic endothelial cells.* Cell Regul, 1991. **2**(9): p. 719-26.
117. Zhan, X., *et al.*, *Long term growth factor exposure and differential tyrosine phosphorylation are required for DNA synthesis in BALB/c 3T3 cells.* J Biol Chem, 1993. **268**(13): p. 9611-20.
118. Sefton, M.V., L.R. Brown, and R.S. Langer, *Ethylene-vinyl acetate copolymer microspheres for controlled release of macromolecules.* J Pharm Sci, 1984. **73**(12): p. 1859-61.
119. Reddy, C.C., *et al.*, *Engineering epidermal growth factor for enhanced mitogenic potency [see comments].* Nat Biotechnol, 1996. **14**(13): p. 1696-1699.
120. Reddy, C.C., A. Wells, and D.A. Lauffenburger, *Receptor-mediated effects on ligand availability influence relative mitogenic potencies of epidermal growth factor and transforming growth factor alpha.* J Cell Physiol, 1996. **166**(3): p. 512-22.
121. Edelman, E.R., *et al.*, *Controlled and modulated release of basic fibroblast growth factor.* Biomaterials, 1991. **12**(7): p. 619-26.
122. Ebner, R. and R. Derynck, *Epidermal growth factor and transforming growth factor-alpha: differential intracellular routing and processing of ligand-receptor complexes.* Cell Regul, 1991. **2**(8): p. 599-612.
123. French, A.R., *et al.*, *Intracellular trafficking of epidermal growth factor family ligands is directly influenced by the pH sensitivity of the receptor/ligand interaction.* J Biol Chem, 1995. **270**(9): p. 4334-40.
124. Korc, M. and J.E. Finman, *Attenuated processing of epidermal growth factor in the face of marked degradation of transforming growth factor-alpha.* J Biol Chem, 1989. **264**(25): p. 14990-9.
125. Ouyang, X., *et al.*, *Transforming growth factor-alpha short-circuits downregulation of the epidermal growth factor receptor.* J Cell Physiol, 1999. **179**(1): p. 52-7.
126. Wells, A., *et al.*, *Ligand-induced transformation by a noninternalizing epidermal growth factor receptor.* Science, 1990. **247**(4945): p. 962-4.
127. Knauer, D.J., H.S. Wiley, and D.D. Cunningham, *Relationship between epidermal growth factor receptor occupancy and mitogenic response. Quantitative analysis using a steady state model system.* J Biol Chem, 1984. **259**(9): p. 5623-31.
128. Nugent, M.A., M.J. Karnovsky, and E.R. Edelman, *Vascular cell-derived heparan sulfate shows coupled inhibition of basic fibroblast growth factor binding and mitogenesis in vascular smooth muscle cells.* Circ Res, 1993. **73**(6): p. 1051-60.
129. Fannon, M. and M.A. Nugent, *Basic fibroblast growth factor binds its receptors, is internalized, and stimulates DNA synthesis in Balb/c3T3 cells in the absence of heparan sulfate.* J Biol Chem, 1996. **271**(30): p. 17949-56.
130. Banai, S., *et al.*, *Angiogenic-induced enhancement of collateral blood flow to ischemic myocardium by vascular endothelial growth factor in dogs.* Circulation, 1994. **89**(5): p. 2183-9.
131. Kuo, P.Y., J.K. Sherwood, and W.M. Saltzman, *Topical antibody delivery systems produce sustained levels in mucosal tissue and blood [see comments].* Nat Biotechnol, 1998. **16**(2): p. 163-7.
132. Creel, C.J., M.A. Lovich, and E.R. Edelman, *Arterial paclitaxel distribution and deposition [In Process Citation].* Circ Res, 2000. **86**(8): p. 879-84.

133. Lambert, T.L., *et al.*, *Localized arterial wall drug delivery from a polymer-coated removable metallic stent. Kinetics, distribution, and bioactivity of forskolin.* Circulation, 1994. **90**(2): p. 1003-11.
134. Vlodavsky, I., *et al.*, *Endothelial cell-derived basic fibroblast growth factor: synthesis and deposition into subendothelial extracellular matrix.* Proc Natl Acad Sci U S A, 1987. **84**(8): p. 2292-2296.
135. Bashkin, P., *et al.*, *Basic fibroblast growth factor binds to subendothelial extracellular matrix and is released by heparitinase and heparin-like molecules.* Biochemistry, 1989. **28**(4): p. 1737-1743.
136. Rifkin, D.B., *et al.*, *Growth factor control of extracellular proteolysis.* Cell Differ Dev, 1990. **32**(3): p. 313-8.
137. Moscatelli, D., R. Flaumenhaft, and O. Saksela, *Interaction of basic fibroblast growth factor with extracellular matrix and receptors.* Ann N Y Acad Sci, 1991. **638**: p. 177-81.
138. Moscatelli, D., *Basic fibroblast growth factor (bFGF) dissociates rapidly from heparan sulfates but slowly from receptors. Implications for mechanisms of bFGF release from pericellular matrix.* J Biol Chem, 1992. **267**(36): p. 25803-9.
139. Flaumenhaft, R., *et al.*, *Role of extracellular matrix in the action of basic fibroblast growth factor: matrix as a source of growth factor for long-term stimulation of plasminogen activator production and DNA synthesis.* J Cell Physiol, 1989. **140**(1): p. 75-81.
140. Rifkin, D.B., *et al.*, *Mechanisms controlling the extracellular activity of basic fibroblast growth factor and transforming growth factor.* Ann N Y Acad Sci, 1991. **614**: p. 250-8.
141. Starbuck, C. and D.A. Lauffenburger, *Mathematical model for the effects of epidermal growth factor receptor trafficking dynamics on fibroblast proliferation responses.* Biotechnol Prog, 1992. **8**(2): p. 132-43.
142. Starbuck, C., H.S. Wiley, and D.A. Lauffenburger, *Epidermal growth factor binding and trafficking dynamics in fibroblasts: Relationship to cell proliferation.* Chem Eng Sci, 1990. **45**: p. 2367.
143. Fallon, E.M. and D.A. Lauffenburger, *Computational model for effects of ligand/receptor binding properties on interleukin-2 trafficking dynamics and T cell proliferation response.* Biotechnol Prog, 2000. **16**(5): p. 905-16.
144. Wiley, H.S. and D.D. Cunningham, *A steady state model for analyzing the cellular binding, internalization and degradation of polypeptide ligands.* Cell, 1981. **25**(2): p. 433-40.
145. Lund, K.A., *et al.*, *Quantitative analysis of the endocytic system involved in hormone- induced receptor internalization.* J Biol Chem, 1990. **265**(26): p. 15713-23.
146. Nugent, M.A. and E.R. Edelman, *Kinetics of basic fibroblast growth factor binding to its receptor and heparan sulfate proteoglycan: a mechanism for cooperactivity.* Biochemistry, 1992. **31**(37): p. 8876-83.
147. Crank, J., *The Mathematics of Diffusion.* 2nd ed. 1997, New York: Oxford University Press, Inc. 411.
148. Bohley, P. and P.O. Seglen, *Proteases and proteolysis in the lysosome.* Experientia, 1992. **48**(2): p. 151-7.
149. Moscatelli, D., *High and low affinity binding sites for basic fibroblast growth factor on cultured cells: absence of a role for low affinity binding in the stimulation of plasminogen activator production by bovine capillary endothelial cells.* J Cell Physiol, 1987. **131**(1): p. 123-30.
150. Chen, S.A., *et al.*, *Plasma and lymph pharmacokinetics of recombinant human interleukin-2 and polyethylene glycol-modified interleukin-2 in pigs.* J Pharmacol Exp Ther, 2000. **293**(1): p. 248-59.
151. Sellke, F.W., *et al.*, *Therapeutic angiogenesis with basic fibroblast growth factor: technique and early results.* Ann Thorac Surg, 1998. **65**(6): p. 1540-4.
152. Sellke, F.W., *et al.*, *Angiogenesis induced by acidic fibroblast growth factor as an alternative method of revascularization for chronic myocardial ischemia.* Surgery, 1996. **120**(2): p. 182-8.
153. Pearlman, J.D., *et al.*, *Magnetic resonance mapping demonstrates benefits of VEGF-induced myocardial angiogenesis [see comments].* Nat Med, 1995. **1**(10): p. 1085-9.
154. Lopez, J.J., *et al.*, *VEGF administration in chronic myocardial ischemia in pigs.* Cardiovasc Res, 1998. **40**(2): p. 272-81.
155. Lopez, J.J., *et al.*, *Basic fibroblast growth factor in a porcine model of chronic myocardial ischemia: a comparison of angiographic, echocardiographic and coronary flow parameters.* J Pharmacol Exp Ther, 1997. **282**(1): p. 385-90.
156. Laham, R.J., *et al.*, *Local perivascular delivery of basic fibroblast growth factor in patients undergoing coronary bypass surgery: results of a phase I randomized, double-blind, placebo-controlled trial.* Circulation, 1999. **100**(18): p. 1865-71.
157. Harada, K., *et al.*, *Vascular endothelial growth factor administration in chronic myocardial ischemia.* Am J Physiol, 1996. **270**(5 Pt 2): p. H1791-802.
158. Schaffer, D.V. and D.A. Lauffenburger, *Optimization of cell surface binding enhances efficiency and specificity of molecular conjugate gene delivery.* J Biol Chem, 1998. **273**(43): p. 28004-9.

159. Yu, C., *et al.*, *The biologic effects of growth factor-toxin conjugates in models of vascular injury depend on dose, mode of delivery, and animal species.* J Pharm Sci, 1998. **87**(11): p. 1300-4.
160. Dowd, C.J., C.L. Cooney, and M.A. Nugent, *Heparan sulfate mediates bFGF transport through basement membrane by diffusion with rapid reversible binding.* J Biol Chem, 1999. **274**(8): p. 5236-44.
161. Lovich, M.A. and E.R. Edelman, *Tissue average binding and equilibrium distribution: an example with heparin in arterial tissues.* Biophys J, 1996. **70**(3): p. 1553-9.
162. Lambert, T.L., *et al.*, *Localized arterial wall drug delivery from a polymer-coated removable metallic stent. Kinetics, distribution, and bioactivity of forskolin.* Circulation, 1994. **90**(2): p. 1003-11.
163. Alt, E. and C. Seliger, *Antithrombotic stent coatings: hirudin/iloprost combination.* Semin Interv Cardiol, 1998. **3**(3-4): p. 177-83.
164. Ahn, Y.K., *et al.*, *Preventive effects of the heparin-coated stent on restenosis in the porcine model.* Catheter Cardiovasc Interv, 1999. **48**(3): p. 374-30.
165. Muller, D.W., *et al.*, *Sustained-release local hirulog therapy decreases early thrombosis but not neointimal thickening after arterial stenting.* Am Heart J, 1996. **131**(2): p. 211-8.
166. Alt, E., *et al.*, *Inhibition of neointima formation after experimental coronary artery stenting: a new biodegradable stent coating releasing hirudin and the prostacyclin analogue iloprost.* Circulation, 2000. **101**(12): p. 1453-8.
167. Drachman, D.E., *et al.*, *Neointimal thickening after stent delivery of paclitaxel: change in composition and arrest of growth over six months.* J Am Coll Cardiol, 2000. **36**(7): p. 2325-32.
168. Clegg, R.M., *Fluorescence resonance energy transfer.* Curr Opin Biotechnol, 1995. **6**(1): p. 103-10.
169. Wu, P. and L. Brand, *Resonance Energy Transfer: Method and Applications.* Anal Bioch, 1994. **218**: p. 1-13.
170. Selvin, P.R., *Fluorescence resonance energy transfer.* Methods Enzymol, 1995. **246**: p. 300-34.
171. Uchiyama, H., *et al.*, *Detection of undegraded oligonucleotides in vivo by fluorescence resonance energy transfer. Nuclease activities in living sea urchin eggs.* J Biol Chem, 1996. **271**(1): p. 380-4.
172. Bastiaens, P.I., *et al.*, *Imaging the intracellular trafficking and state of the AB5 quaternary structure of cholera toxin.* Embo J, 1996. **15**(16): p. 4246-53.
173. Bastiaens, P.I. and T.M. Jovin, *Microspectroscopic imaging tracks the intracellular processing of a signal transduction protein: fluorescent-labeled protein kinase C beta I.* Proc Natl Acad Sci U S A, 1996. **93**(16): p. 8407-12.
174. Ng, T., *et al.*, *Imaging protein kinase Calpha activation in cells.* Science, 1999. **283**(5410): p. 2085-9.
175. Yaron, A., A. Carmel, and E. Katchalski-Katzir, *Intramolecularly Quenched Fluorogenic Substrates for Hydrolytic Enzymes.* Anal Biochem, 1979. **95**: p. 228-35.
176. Reis, R.C., M.H. Sorgine, and T. Coelho-Sampaio, *A novel methodology for the investigation of intracellular proteolytic processing in intact cells.* Eur J Cell Biol, 1998. **75**(2): p. 192-7.
177. Wan, W.K., *et al.*, *Measurement of drug distribution in vascular tissue using quantitative fluorescence microscopy.* J Pharm Sci, 1999. **88**(8): p. 822-9.
178. Creel, C.J., M.A. Lovich, and E.R. Edelman, *Arterial paclitaxel distribution and deposition.* Circ Res, 2000. **86**(8): p. 879-84.
179. Healy, A.M. and I.M. Herman, *Preparation of fluorescent basic fibroblast growth factor: localization in living retinal microvascular endothelial cells.* Exp Eye Res, 1992. **55**(5): p. 663-9.
180. Rosengart, T.K., *et al.*, *Heparin protects heparin-binding growth factor-1 from proteolytic inactivation in vitro.* Biochem Biophys Res Commun, 1988. **152**(1): p. 432-40.
181. Saksela, O., *et al.*, *Endothelial cell-derived heparan sulfate binds basic fibroblast growth factor and protects it from proteolytic degradation.* J Cell Biol, 1988. **107**(2): p. 743-51.
182. Koo, E.W. and A.I. Gotlieb, *Endothelial stimulation of intimal cell proliferation in a porcine aortic organ culture.* Am J Pathol, 1989. **134**(3): p. 497-503.
183. Koo, E.W. and A.I. Gotlieb, *Neointimal formation in the porcine aortic organ culture. I. Cellular dynamics over 1 month.* Lab Invest, 1991. **64**(6): p. 743-53.
184. Koo, E.W. and A.I. Gotlieb, *The use of organ cultures to study vessel wall pathobiology.* Scanning Microsc, 1992. **6**(3): p. 827-34; discussion 835.
185. Lobb, R.R., *Thrombin inactivates acidic fibroblast growth factor but not basic fibroblast growth factor.* Biochemistry, 1988. **27**(7): p. 2572-8.
186. Raman, V.K. and E.R. Edelman, *Coated stents: local pharmacology.* Semin Interv Cardiol, 1998. **3**(3-4): p. 133-7.
187. Lincoff, A.M., *et al.*, *Sustained local delivery of dexamethasone by a novel intravascular eluting stent to prevent restenosis in the porcine coronary injury model.* J Am Coll Cardiol, 1997. **29**(4): p. 808-16.

188. Baumbach, A., *et al., Local drug delivery: impact of pressure, substance characteristics, and stenting on drug transfer into the arterial wall.* Catheter Cardiovasc Interv, 1999. **47**(1): p. 102-6.
189. Dev, V., *et al., Kinetics of drug delivery to the arterial wall via polyurethane-coated removable nitinol stent: comparative study of two drugs.* Cathet Cardiovasc Diagn, 1995. **34**(3): p. 272-8.
190. Elmalak, O., M.A. Lovich, and E. Edelman, *Correlation of transarterial transport of various dextrans with their physicochemical properties.* Biomaterials, 2000. **21**(22): p. 2263-72.
191. Herdeg, C., M. Oberhoff, and K.R. Karsch, *Antiproliferative stent coatings: Taxol and related compounds.* Semin Interv Cardiol, 1998. **3**(3-4): p. 197-9.

THESIS PROCESSING SLIP

FIXED FIELD: ill. _____ name _____

index _____ biblio _____

► **COPIES:** Archives Aero Dewey Barker Hum

Lindgren Music Rotch Science Sche-Plough

TITLE VARIES: ► ☐ _____

_____

_____

NAME VARIES: ► ☐ _____

_____

IMPRINT: **(COPYRIGHT)** _____

_____

► **COLLATION:** _____

_____

► **ADD: DEGREE:** _____ ► **DEPT.:** _____

► **ADD: DEGREE:** _____ ► **DEPT.:** _____

SUPERVISORS: _____

_____

NOTES:

cat'r: date:

page: 205

► **DEPT:** _____

► **YEAR:** _____ ► **DEGREE:** _____

► **NAME:** _____

_____